HYPOXIA-INDUCED MODULATION OF IMMUNOTHERAPY EFFICACY IN HEPATOCELLULAR CARCINOMA

HUANG MOHAN

PhD

The Hong Kong Polytechnic University

2025

The Hong Kong Polytechnic University

Department of Health Technology and Informatics

Hypoxia-Induced Modulation of Immunotherapy Efficacy in Hepatocellular Carcinoma

Huang Mohan

A thesis submitted in partial fulfillment of the requirements for the degree of Doctor of Philosophy

August 2024

CERTIFICATE OF ORIGINALITY

I hereby declare that this thesis is my own work and that, to the best of my knowledge and belief, it reproduces no material previously published or written, nor material that has been accepted for the award of any other degree or diploma except where due acknowledgment has been made in the text.

_____

Mohan Huang
3rd May 2025

Abstract

Background

Hepatocellular carcinoma (HCC) is a leading cause of cancer-related mortality, with most cases diagnosed at an advanced stage, making immunotherapy a key treatment strategy. However, the response rate to PD-L1 inhibitors remains low, necessitating further exploration of resistance mechanisms and predictive biomarkers. Hypoxia is a major contributor to immunotherapy resistance, as HIF-1α upregulates PD-L1 expression and activates genes that help tumor cells adapt to hypoxia, ultimately reducing immunotherapy efficacy.

This study integrated bioinformatics, machine learning, and deep learning to identify key hypoxia-associated genes and pathways contributing to PD-L1 expression. A hypoxia risk score model was developed to stratify cases by risk, and a Kolmogorov-Arnold Network (KAN) deep learning model was constructed to predict immunotherapy response. Additionally, an in vitro hypoxia-induced drug-resistant HepG2 cell model was established, and the role of NOXA in apoptosis regulation was examined through flow cytometry and AI-based image analysis.

Results and Conclusion

52 HCC-Hypoxia Overlap genes (HHOs) were identified, with 14 PD-L1 regulatory genes and 10 hub genes influencing immunotherapy response. PMAIP1 (NOXA) was significantly associated with immunotherapy response ($p < 0.001$). A hypoxia risk score model integrating PMAIP1 and 9 hypoxia risk-associated genes demonstrated high predictive accuracy (AUC = 0.815, 0.774, 0.771 for 1-, 2-, and 3-year survival, respectively). The KAN deep learning model incorporating 11 key genes achieved high predictive accuracy (AUC = 0.936 training, 0.7 test). SVM-based integration of hypoxia risk score and KAN model improved prediction performance (AUC = 0.725 test set).

Experimental validation demonstrated that hypoxia enhances drug resistance in HepG2 cells, while NOXA knockdown alters apoptosis patterns, potentially modulating treatment response. These findings highlight NOXA as a potential therapeutic target and establish a robust model for predicting immunotherapy response, advancing precision medicine in HCC treatment.

List of publications

International journal papers

Published journal papers:

1. **M. Huang**, X. Chen, Y. Jiang, L.W.C. Chan, Kolmogorov–Arnold Network Model Integrated with Hypoxia Risk for Predicting PD-L1 Inhibitor Responses in Hepatocellular Carcinoma, Bioengineering 12(3) (2025), 322.

2. **M. Huang**, S. Yang, W.C.S. Tai, L. Zhang, Y. Zhou, W.C.S. Cho, L.W.C. Chan, S.C.C. Wong, Bioinformatics Identification of Regulatory Genes and Mechanism Related to Hypoxia-Induced PD-L1 Inhibitor Resistance in Hepatocellular Carcinoma, Int J Mol Sci 24(10) (2023).

3. H. Lun, **M. Huang**, Y. Zhao, J. Huang, L. Li, H. Cheng, Y. Leung, H. So, Y. Wong, C. Cheung, C. So, L.W.C. Chan, Q. Hu, Contrast-enhanced ultrasound-based radiomics for the prediction of axillary lymph nodes status in breast cancer. Cancer Reports 7: e70011 (2024).

4. L. Kong, **M. Huang**, L. Zhang, L.W.C. Chan, Enhancing Diagnostic Images to Improve the Performance of the Segment Anything Model in Medical Image Segmentation, Bioengineering (Basel) 11(3) (2024).

5. L.W.C. Chan, S.C.C. Wong, W.C.S. Cho, **M. Huang**, F. Zhang, M.L. Chui, U.N.Y. Lai, T.Y.K. Chan, Z.H.C. Cheung, J.C.Y. Cheung, K.F. Tang, M.L. Tse, H.K. Wong, H.M.F. Kwok, X. Shen, S. Zhang, K.W.H. Chiu, Primary Tumor Radiomic Model for Identifying Extrahepatic Metastasis of Hepatocellular Carcinoma Based on Contrast Enhanced Computed Tomography, Diagnostics (Basel) 13(1) (2022).

6. L.W.C. Chan, T. Ding, H. Shao, **M. Huang**, W.F. Hui, W.C. Cho, S.C. Wong, K.W. Tong, K.W. Chiu, L. Huang, H. Zhou, Augmented Features Synergize Radiomics in Post-Operative Survival Prediction and Adjuvant Therapy Recommendation for Non-Small Cell Lung Cancer, Front Oncol 12 (2022).

International conference papers

7. **M. Huang**, L.W.C. Chan, Machine learning identification of hypoxia-related genes and prognostic risk-scoring model for effective survival stratification in hepatocellular carcinoma. American Society of Clinical Oncology (ASCO), 42, e16261-e16261(2024). Poster presentation.
DOI:10.1200/JCO.2024.42.16_suppl.e16261
Link:https://ascopubs.org/doi/10.1200/JCO.2024.42.16_suppl.e16261

8. **M. Huang**, L.W.C. Chan, Hypoxia-related genes and PD-L1 inhibitor resistance in hepatocellular carcinoma. American Society of Clinical Oncology (ASCO)Breakthrough,9,158-158(2023). Online publication.
DOI:10.1200/GO.2023.9.Supplement_1.158
Link: https://ascopubs.org/doi/10.1200/GO.2023.9.Supplement_1.158

Acknowledgments

First and foremost, I would like to express my deepest gratitude to my chief supervisor, Dr. Lawrence Chan Wing-Chi. Your sharp scientific insight, rigorous approach, and selfless dedication have profoundly influenced me, becoming a precious asset in my life that I will benefit from for years to come. During my doctoral studies, I experienced significant growth, developing strong habits of integrity and diligence in both life and work and meticulously completing each step of my research project according to plan. You have always been patient in teaching me how to conduct research and promptly corrected my mistakes. From my initial unfamiliarity with Python tools to eventually being able to use Python for research purposes, you invested a great deal of time and effort in my training. I am particularly grateful for the new methods you introduced when my research faced bottlenecks, helping me overcome the challenges smoothly. Additionally, I deeply appreciate your tremendous support in my personal life, easing the pressure of living in Hong Kong, which allowed me to dedicate more time and energy to my research.

I would also like to extend my thanks to the members of our research group! United, warm, supportive, and aspirational, we discussed and solved problems together. Because of you all, I have navigated this unforgettable journey. Special thanks to Chen Xinyue, Kong Luoyi, Zhang Lingfeng, and Zhou Yinuo for their significant assistance with the data and code aspects of my research!

I am grateful to my co-supervisors, Dr. William Tai and Prof. Zou Xiang, for their guidance and support.

Thanks to Dr. CM research group for providing the hepG2 cell line.

I also thank Liyue for patiently teaching me experimental techniques and providing immense support.

I am thankful to the Prof. Lan's research group of Guangdong Pharmaceutical University for their assistance in my in vitro verification experiments.

Finally, I want to express my heartfelt thanks to my parents, who have always supported and trusted me. Because of you, I have never had any worries, enabling me to pursue my dreams with a single-minded focus. You are forever my strongest backing and my warmest haven!

List of Abbreviations

HCC	Hepatocellular carcinoma
WHO	World Health Organization
MRI	Magnetic resonance imaging
PET	Positron emission tomography
AFP	Alpha-fetoprotein
PIVKA-II	Protein induced by vitamin K absence or antagonist-II
GPC3	Glypican-3
BCLC	Barcelona Clinic Liver Cancer
TACE	Transarterial chemoembolization
ICI	Immune Checkpoint Inhibitors
OS	Overall survival
FDA	Food and Drug Administration
ORR	Objective response rate
PD-L1	Programmed death-ligand 1
HIF-1α	Hypoxia-inducible factor 1-alpha
TME	Tumor microenvironment
PI3K	Phosphoinositide 3-kinase
EGFR	Epidermal growth factor receptor
MHC	Major histocompatibility complex
PD-1	Programmed death-1
TCR	T-cell receptor
CTL	Cytotoxic T lymphocyte

IFN-γ	Interferon-gamma
NSCLC	Non-small cell lung cancer
CRC	Colorectal cancer
HIFs	Hypoxia-inducible factors
PHD	Prolyl hydroxylase structural domain
EMT	Epithelial-to-mesenchymal transition
VEGF	Vascular endothelial growth factor
VSN	Variance stabilizing normalization
HSGs	HCC-signature genes
HRGs	Hypoxia-related genes
FC	Fold change
FDRs	False discovery rates
HHO	HCC-Hypoxia Overlap
PPI	Protein-Protein Interaction
KM	Kaplan Meier
ROC	Receiver Operating Characteristic
LASSO	Least absolute Shrinkage and Selection Operator
HR	Hazard ratio
ICGC	International Cancer Genome Consortium
GO	Gene Ontology
KEGG	Kyoto Encyclopedia of Genes and Genomes
EGA	European Genome-Phenome Archive
CPM	Counts-per-million
DEG	Differentially expressed gene

IRH	Immunotherapy Response to Hypoxia
HRH	Hypoxia-Regulated HIF-1α
mRMR	Minimum Redundancy Maximum Relevance
KAN	Kolmogorov-Arnold Network
SVM	Support Vector Machine
PMAIP1 (NOXA)	Phorbol-12-Myristate-13-Acetate-Induced Protein 1

Table of Contents

List of Figures and Tables

Chapter 1 Literature Review

1.1 Hepatocellular Carcinoma

Hepatocellular carcinoma (HCC), a disease known for its high aggression and heterogeneity, is the leading form of primary liver cancer, constituting 80-90% of all cases. From 2005 to 2015, HCC has risen to become the second largest cause of cancer-related years of life lost on a global scale and the second leading cause of malignant tumor deaths in Asia. The latest report from the World Health Organization (WHO) indicates that the incidence and mortality rates of liver cancer have increased over the last 20 years. In 2020, the global incidence and mortality rates of HCC were 906,000 and 830,000, respectively. The WHO also reported that nearly 70% of cases occur in the Asian region, with China having the top incidence rate among HCC patients. It is reported that the age-specific incidence rate is highest among individuals over 70 years old. Additionally, HCC is predominant in males (showing a male-to-female ratio ranging from 2 to 3:1), which may be connected to the higher prevalence of risk factors in males [1-3].

1.1.1 The Diagnosis of HCC

Currently, the guidelines for diagnosing HCC recommend the use of imaging characteristics, with ultrasound being widely utilized for HCC surveillance and early diagnosis due to its cost-effectiveness, non-invasiveness, and lack of excessive radiation exposure. Despite its widespread clinical application, the

sensitivity and specificity of ultrasound in diagnosing HCC, especially in its early stages, remain unsatisfactory. Magnetic resonance imaging (MRI) offers higher accuracy for early HCC detection with a sensitivity ranging from 66.7% to 73%. However, MRI is costly, time-consuming, and associated with high cumulative radiation doses. Positron emission tomography (PET) and other nuclear imaging techniques show a sensitivity of 30–70% in diagnosing primary HCC [4, 5].

In addition to imaging techniques, serum biomarkers hold significant value in HCC diagnosis. Traditionally, HCC has been screened and diagnosed based on the expression of molecular biomarkers, which also aid in predicting patient prognosis and monitoring treatment response. Over the past few decades, alpha-fetoprotein (AFP) has emerged as the most promising and extensively studied candidate biomarker. Abnormal plasma AFP levels are closely associated with the malignancy of HCC. However, approximately 20% of HCC patients do not produce AFP, 60% overexpress AFP, and 30-40% have normal AFP levels (≤ 20 ng/mL). Thus, the performance of AFP as a screening, diagnostic, and prognostic biomarker for HCC is suboptimal. AFP-L3, with its high specificity, was approved by the FDA as an HCC biomarker in 2015, but it only has a sensitivity of 48.3%. Protein induced by vitamin K absence or antagonist-II (PIVKA-II), also known as Des-γ-carboxy prothrombin, has been approved as a serum biomarker for HCC in East Asia, yet its sensitivity remains controversial. Glypican-3 (GPC3) is overexpressed in most HCC tumor tissues, but its diagnostic accuracy for early

HCC is still unsatisfactory. To date, no single protein biomarker has demonstrated sufficient accuracy to be used alone for early HCC diagnosis [6, 7]. Despite the potential of several biomarkers, their practicality in clinical practice requires further validation. Compounding the challenge is the lack of specific tumor symptoms in HCC, causing most patients to be diagnosed at a later stage.

1.1.2 Therapeutic Progression of HCC

Treatment strategies for HCC patients are contingent on the disease's clinical stage. According to the internationally accepted Barcelona Clinic Liver Cancer (BCLC) staging system, HCC patients are categorized into five stages: BCLC-0 (very early stage), BCLC-A (early stage), BCLC-B (intermediate stage), BCLC-C (advanced stage), and BCLC-D (terminal stage) [8]. The primary treatment options for HCC include liver resection, liver transplantation, ablation, or transarterial chemoembolization (TACE), which may offer curative potential for early-stage patients. For patients with intermediate-stage HCC, locoregional treatments such as TACE are preferred [9, 10]. However, for advanced-stage HCC patients, surgical options are unsuitable due to factors such as tumor size, location, lesion count, and comorbidities, making appropriate treatment options very limited. Advanced-stage HCC patients primarily benefit from systemic therapies. More than 50% of HCC patients are diagnosed at an advanced stage, significantly increasing the rate of patients undergoing systemic treatments. Initially,

chemotherapy drugs were the mainstay for advanced HCC treatment, but their efficacy was limited, and adverse effects were significant. In 2007, targeted inhibitors such as sorafenib and other multikinase inhibitors, along with immune checkpoint inhibitors (ICI), were approved for systemic therapy in advanced liver cancer [11-15]. Until the mid-2010s, sorafenib was the only drug available for systemic treatment of HCC.

1.1.3 The Immunological Classification of HCC

HCC can be categorized into inflamed and non-inflamed types based on their immune profiles. The inflamed type includes immune-active, immune-exhausted, and immune-like subclasses. The immune-active and immune-like subclasses share similar characteristics, such as high cytotoxic immune cell activity, elevated interferon signaling, and favorable prognosis, with the immune-like subclass showing enhanced Wnt–β-catenin signaling [16]. Recent research has demonstrated that patients with inflamed HCC have higher response rates to immunotherapy. The non-inflamed type includes immune-intermediate and immune-excluded subclasses. The immune-intermediate subclass is associated with a high frequency of TP53 mutations and significant chromosomal loss of immune-related genes. The immune-excluded subclass is distinguished by high-frequency CTNNB1 mutations, PTK2 overexpression, gene amplification, and promoter hypomethylation, usually exhibiting low immune infiltration[17, 18].

Additionally, HCC can be categorized into four unique immunovascular subtypes based on the interaction between immune-related and angiogenesis-driven tumor microenvironments: immune-high/vascular-suppressed, immune-medium / vascular-medium, immune-low/vascular-activated, and immune-low/vascular-low [18, 19]. This classification provides new insights into the efficacy of immunotherapy.

1.1.4 ICI Therapy in HCC

In recent years, significant progress has been made in the treatment of HCC with immune checkpoint inhibitors (ICIs). Tumor cells often evade immune system attacks by activating immune checkpoints. ICIs restore T-cell antitumor activity by blocking the signaling pathways between immune checkpoints. In HCC, the primary immune checkpoint targets are PD-1/PD-L1 and CTLA-4. In 2019, the atezolizumab and bevacizumab combination therapy demonstrated a significantly longer overall survival (OS) compared to sorafenib in the IMbrave150 trial [20-23]. In 2020, the U.S. FDA approved atezolizumab (Tecentriq) in combination with bevacizumab (Avastin) for the first-line option for treating advanced, unresectable, or metastatic HCC. Although these therapies have become the standard treatment for HCC patients, their widespread clinical application is limited by the frequency of adverse events, intolerance, lack of treatment response, and drug resistance. The objective response rate (ORR) for advanced HCC

patients receiving ICIs in combination therapy is only 36%, and even lower at under 20% for monotherapy [24, 25]. Consequently, new therapeutic strategies are being developed to enhance the efficacy of immunotherapy, improve cancer treatment safety, and expand available treatment options for HCC patients.

1.2 PD-L1

PD-L1 (B7-H1 or CD274) is a transmembrane protein that is a member of the B7 family. In various cancers, the expression levels of PD-L1 are significantly elevated, making it a crucial immune checkpoint. PD-L1 plays a vital immunoregulatory role by modulating the initiation and cessation of immunotherapy responses. Consequently, PD-L1 has become a significant target in anti-tumor immunotherapy [26].

1.2.1 PD-L1 Structure

PD-L1 is a type I transmembrane protein composed of 290 amino acids, belonging to the immunoglobulin superfamily with IgC and IgV domains. PD-L1 encompasses three primary domains: the extracellular domain (ED), the transmembrane domain (TM), and the intracellular domain (ID). The extracellular domain (ED) includes variable immunoglobulin regions, comprising both distal and proximal segments. The intracellular domain (ID) contains three conserved amino acid motifs: DTSSK, RMLD-VEKC, and QFEET. Promoting signal

transduction and signal transducer and activator of transcription 3 (STAT3) phosphorylation is the primary function of the RMLD-VEKC motif, in contrast to the DTSSK motif, which inhibits this phosphorylation process [26, 27].

The expression of PD-L1 on the surface of cancer cells is regulated by multiple signaling pathways and proteins, including PI3K/AKT/mTOR, COX2/mPGES1/PGE2, nuclear factor kappa B p105 subunit (NF-κB), hypoxia-inducible factor 1-alpha (HIF-1α), RAF/MEK/ERK/MAPK pathways, and STAT proteins [27-29]. These signaling pathways and proteins are frequently mutated or upregulated during malignant transformation, thereby influencing the expression levels and functions of PD-L1.

1.2.2 The Expression Level of PD-L1 in Cancers

PD-L1 is regulated by intrinsic oncogenic and adaptive signaling pathways, exhibiting high expression levels across various cancers, including hepatocellular carcinoma, non-small cell lung cancer, melanoma, and breast cancer. The aberrant expression of PD-L1 significantly reduces antitumor immunity in the tumor microenvironment (TME), thus closely correlating with tumor aggression, metastatic potential, and unfavorable patient outcomes. Elevated PD-L1 levels are often indicative of poorer prognosis and lower therapeutic response rates [30].

Recent studies have revealed that MYC is capable of binding to the PD-L1 promoter, thereby upregulating its expression across various cancer types. Furthermore, genetic or pharmacological inhibition of MYC can decrease PD-L1 mRNA levels and revive antitumor immunity in the TME. Anaplastic lymphoma kinase (ALK) also drives PD-L1 upregulation, with hyperactivation of the ALK signaling pathway, induced by NPM-ALK gene fusion, enhancing PD-L1 expression through STAT3. Besides MYC and ALK, other oncogenic pathways such as HIF1/2α, mitogen-activated protein kinase (MAPK), nuclear factor κB (NF-κB), phosphoinositide 3-kinase (PI3K)/phosphatase and tensin homolog (PTEN), and epidermal growth factor receptor (EGFR) also enhance PD-L1 mRNA expression when mutated or hyperactivated [31-33].

In the TME, cancer cells are subjected to the surveillance threats of innate and adaptive immunity. This region is rich in inflammatory cytokines that coordinate the stability of antitumor immunity. However, by exploiting inflammatory pathways (also known as adaptive signaling pathways), cancer cells can boost PD-L1 expression, leading to an environment conducive to tumor progression through the inhibition of antitumor immunity. In order to escape from T-cell attacks, cancer cells activate the IFN- γ /JAK/STAT1 pathway, leading to increased PD-L1 mRNA expression [30, 34]. IFN-γ, produced by natural killer (NK) cells and T cells, is an inflammation-promoting cytokine that boosts the expression of major histocompatibility complex (MHC) and promotes the presentation of neoantigens

on cancer cells [35]. By leveraging the IFN-γ/JAK/STAT1 pathways, PD-L1 on cancer cells can neutralize cytotoxic T cells and diminish immune surveillance within the TME [34].

Similarly, multiple inflammatory cytokines can stimulate PD-L1 mRNA expression within tumor cells or the stromal cells associated with tumors, including TNF-α, IFN-α/β, TLR3, IL-4/6/17/27 ,and transforming growth factor β (TGF-β) [30, 36-38]. These discoveries contribute to a better grasp of the mechanisms that could be regulating PD-L1 expression in tumor cells. Nonetheless, the specific role of oncogenic signaling pathways in modulating PD-L1 expression post-translationally to inhibit antitumor immunotherapy responses remains unclear and warrants further investigation.

1.2.3 The Role of PD-L1 in Cancer Progression

Programmed death-1 (PD-1) and programmed death-ligand 1 (PD-L1) are type I transmembrane proteins belonging to the immunoglobulin (Ig) superfamily. PD-L1 plays a critical role in cancer progression by inhibiting T-cell activation and promoting immune evasion. The PD-1 cytoplasmic domain features two tyrosine-based signaling motifs: ITIM (immunoreceptor tyrosine-based inhibitory motif) and ITSM (immunoreceptor tyrosine-based switch motif). During T cell activation, the binding of PD-1 to PD-L1 induces conformational changes that

recruit the phosphatase SHP-2 [32, 39]. The recruitment leads to a reduction in key proximal T-cell receptor (TCR) signaling events, such as LCK-induced phosphorylation of ZAP70, and decreases the activity of the RAS-MEK-ERK and PI3K-Akt-mTOR pathways. The inhibition of these signaling pathways results in suppressed T-cell proliferation and cytotoxic functions, altered metabolism, impaired cytotoxic T lymphocyte (CTL) killing activity, and ultimately leads to the apoptosis of activated T cells, leading to the protection of tumor cells from immune system attacks [40].

Furthermore, PD-L1 can enhance its immunosuppressive effects by engaging with B7-1 (CD80). B7-1 is another immune regulatory molecule that typically binds to CD28 to promote T-cell activation. However, when PD-L1 engages with B7-1, it inhibits B7-1 from interacting with CD28, thus inhibiting the co-stimulatory signals necessary for T-cell activation. This inhibition leads to a decrease in T-cell proliferation and cytotoxicity, while also compromising the immune systems effectiveness in recognizing and attacking tumor cells. The binding of PD-L1 to B7-1 within the tumor microenvironment exerts a dual inhibitory effect, reinforcing the mechanisms of immune evasion and allowing tumor cells to continue growing and spreading under the surveillance of the immune system [41, 42].

1.2.4 The Regulation of PD-L1 in Cancers

The expression of PD-L1 is regulated by multiple factors, including genetic mutations, signaling pathway activation, and microenvironmental influences. For instance, hypoxic conditions can upregulate PD-L1 expression via HIF-1α, while mutations in EGFR and ALK also promote its expression [43-45]. Additionally, cytokines in the tumor microenvironment, such as IFN-γ, can significantly increase PD-L1 expression levels [30, 45].The expression of PD-L1 is also significantly influenced by epigenetic factors like histone modifications and DNA methylation [44, 46].

The PI3K-Akt signaling pathway is critical for survival, metabolism, proliferation, and migration of cancer cells. Numerous studies have established a positive correlation between PI3K-Akt signaling and PD-L1 expression across various cancers, including colorectal cancer (CRC), non-small cell lung cancer (NSCLC), glioblastoma, breast cancer, and melanoma [32]. Moreover, the activation of the PI3K-Akt-mTOR cascade by both type I and type II interferons, which regulates interferon-dependent mRNA translation, points to a synergistic interaction between the Akt-mTOR pathway and interferon receptor signaling. [47, 48]. Consistently, pharmacological inhibition of PI3K-Akt signaling can suppress IFN-γ-induced PD-L1 expression [49].

The MEK-ERK pathway, typically activated by upstream receptor mutations such

as KRAS and EGFR, represents another common activation pathway in human cancers and plays a pivotal role in the upregulation of PD-L1 levels. Evidence suggests that hyperactivation of MEK-ERK signaling can directly enhance PD-L1 gene expression across various cancers, including lung cancer, breast cancer, multiple myeloma, bladder cancer, and lymphoma [32, 50, 51].

These findings elucidate the complex regulatory mechanisms governing PD-L1 expression and underscore the importance of these pathways in cancer immunology. Comprehending these mechanisms is essential for the development of targeted therapies aimed at modulating PD-L1 expression to enhance antitumor immunity.

1.3 Hypoxia

Hypoxia is frequently found in cells and tissues in the tumor microenvironment due to a lack of adequate vascularization. In normal tissues, the oxygen level of the liver cell is as high as 7.3%. Compared to the normal tissues, oxygenation levels in HCC are much lower, with O_2 ratios of only 0.8% [52]. Folkman's theory indicates that the growth of tissues (including cancer tissues) beyond 2-3mm^3 requires new blood vessels, and that optimal nutrients and oxygen are supplied within a 250μm radius of capillaries. But tumors beyond one mm3 can still survive in lack of new blood vessels [53]. Collectively, hypoxia is a common feature in

solid tumors of HCC and not only drives tumorigenesis and progression and is a significant cause of drug resistance to various therapeutic modalities. Thus, cancer progression is driven by intrinsic oncogenic mechanisms but not the presence of blood vessels. Hypoxia may induce a physiological response in tumor tissues, leading to genetic alterations in signaling pathways [54].

1.3.1 HIF structure

In recent years increasing evidence has indicated that hypoxia-inducible factors (HIFs) are commonly detected in solid tumors and have shown a strong association between hypoxia and adverse clinical outcomes in HCC [55]. HIFs mediate a series of responses of cells to adapt to hypoxia, which are three different subtypes consisting of the HIF-1α, HIF-2α and HIF-3α [56]. HIFs are heterodimeric proteins composed of a functional HIF-1α subunit and a stably expressed HIF-1β subunit. Prolyl hydroxylase structural domain (PHD) is a critical enzyme in the HIFs degradation process, and the PHD in an O_2-rich environment can hydroxylate the proline residues of HIF-1/2α. Hydroxylated HIF subtypes are recognized and bound by ubiquitin ligases and von Hippel-Lindau tumor suppressor protein (VHL). Ultimately, ubiquitinated HIF-1/-2α is degraded by the 26S proteasome [57]. Since both PHD and HIF are oxygen-dependent, in a hypoxic environment, stable HIF-1/2α translocate into the nucleus and activates a series of hypoxia-responsive element (HRE) genomic sequences [58]. In general,

HIFs are the shortest half-life proteins in normoxic conditions. In contrast, in hypoxic environments HIFs are stable and accumulate and translocate to the nucleus, activating the expression of some genes and adapting to the hypoxic environment [59].

1.3.2 The expression level of HIF in HCC

Numerous clinical studies have demonstrated the correlation between HIFs and the recurrence, prognosis, and survival of HCC patients. HIF-1α expression is higher in HCC tissues than adjacent tissues and is mainly involved in promoting tumor invasion, migration, metastasis, angiogenesis, epithelial-to-mesenchymal transition (EMT), glycolytic regulation and lipid metabolism. HIF-1α promotes tumor cell invasion and migration through the RIT1 axis, and IL-8/Akt/NF-κB axis upregulates LOXL2 to promote angiogenesis, promotes cancer cell glycolysis through the PPAR-γ/PKM2 axis, induces EMT to promote HCC metastasis process, and FABP5 mediates lipid metabolism through HIF-1 to drive HCC progression [60].

1.3.3 The role of HIF in immune escape

Hypoxia promotes tumor immune escape. In hypoxic environments, HIF induces tumor cells to release large amounts of immunosuppressive factors to reduce immune cytotoxicity, such as VEGF and encodes cancer-related proteins to cause

radio resistance and resistance to multiple chemotherapeutic agents, affecting the antitumor immune response. In addition, HIF-1α induces PD-L1 expression in tumor cells and MDSCs, promotes immune tolerance in the tumor microenvironment, and increases the resistance of tumor cells to cytotoxic T lymphocytes (CTL) [61]. HIF-1α mediates the expression of cancer cell surface protein CD47 and protects cancer cells from destruction by macrophages [62]. HIF-1α also increases the expression of metalloproteinase ADAM10, decreases the expression level of MHC-related molecules, and cannot activate the initial signaling pathway of immune cells [63].

1.3.4 Hypoxia signature genes as Potential Molecular Target in Cancers

Research data suggest that HIF inhibitors may contribute to antitumor and anti-angiogenic effects. Some approved drugs that indirectly alter HIF-1α expression may also be helpful as adjuvant therapies in cancer treatment. For example, the chemotherapeutic drug rapamycin can reduce the expression of HIF-1α and also act synergistically with mTOR inhibitors (decrease HIF-1α expression) to inhibit tumor growth in preclinical models of HCC [54, 64]. DNA alkylating agent temozolomide exhibits enhanced antitumor activity with HIF inhibitors in glioma [65]. MK6482 is the first FDA-approved HIF inhibitor for treating advanced renal cell carcinoma patients [66]. Therefore, combining HIF inhibitors and ICI therapy will be a potent combination. While ICI plays a vital role in antitumor, HIF inhibitors can mediate PD-L1 expression and eliminate the ability of tumor cells

to adapt to a hypoxic environment and develop therapeutic resistance.

1.4 Drug resistance

Immunotherapy has opened a new chapter in cancer treatment. However, in these studies, most patients did not benefit due to drug resistance, and some patients had recurrences after treatment. Researchers have divided drug resistance into three classifications: primary, adaptive, and acquired. Primary resistance is a clinical condition in which cancer patients resist immunotherapy and have no immune response. Adaptive resistance is when the immune system recognizes the tumor, but resistance clones exist before treatment and protect themselves by adjusting to the immune response. Acquired resistance occurs when cancer patients initially respond to immunotherapy, only to relapse later and develop drug resistance [67].

1.4.1 Tumor-Cell-Intrinsic Factors

Intrinsic factors of immunotherapy leading to drug resistance in tumor cells include modulation of the expression of specific genes or pathways that may be associated with immunosuppression in the tumor microenvironment. These mechanisms may initially exist or undergo evolution, culminating in tumor drug resistance mechanisms. Recent studies have identified various intrinsic tumor mechanisms that may be associated with drug resistance mechanisms: (1) Tumor

cells lead to the production of proteins such as VEGF and IL-8 through the MAPK pathway, which has a suppressive effect on T cell recruitment [68]. (2) PTEN expression deficiency enhances PI3K signaling and decreased IFN-γ, granzyme B gene expression and CD8+ T cell infiltration [69]. (3) The cancer cell surface ligand PD-L1 also suppresses T cell responses. The expression mechanisms include PTEN loss, PI3K/AKT mutation, EGFR mutation and MYC overexpression [70-74].

1.4.2 Acquired Resistance to Immunotherapy

With the widespread use of immunotherapy, the chance of patients with acquired drug resistance after a period has increased. The underlying mechanisms may escape mutations in genes within the tumor, downregulation of tumor antigen presentation and lack of T cell recognition, B2M mutations leading to loss of HLA expression, altered interferon signaling, and loss of T cell function [75]. Since antitumor T cells specifically identify their cognate cancer cells, gene deletions, mutations or even genetic changes in signaling pathways that alter the expression of tumor antigens may lead to acquired resistance to ICI therapies [76].

Even though immune combination therapy has the potential to restore immune response as described above, excessive trimming of the tumor vasculature might intensify hypoxia in the tumor microenvironment, thereby boosting

immunosuppression. Hypoxia induces immunosuppression by decreasing cytotoxic cell activity, promoting the expression of immunosuppressive cytokines, and increasing infiltration of immunosuppressive cell populations [77]. Thus, hypoxia-altering PD-L1 expression via HIF may be a potential mechanism for acquired resistance within the tumor, and understanding these mechanisms will offer valuable clues about the actions needed to address immunotherapy resistance in HCC.

Chapter 2 Identify the pathways governing the response mechanism of PD-L1 inhibition

2.1 Materials and Methods

2.1.1 Microarray Data Collection and Processing

Two public datasets, GSE14520 and GSE41666, were obtained from the Gene Expression Omnibus (GEO) database. In the GSE14520 dataset, a single-channel array platform was utilized to analyze the gene expression levels of tumor samples from 214 HCC patients and their corresponding 214 non-tumor samples. In the GSE41666 dataset, HepG2 HCC cell line samples were exposed to hypoxic conditions at 0% oxygen concentration and normoxic conditions at 21% oxygen concentration for 24 hours. Each condition was performed in triplicate, and the gene expression levels of a total of 6 samples were analyzed using an expression bead chip platform.

For each gene detected by multiple probes on the microarray chip, the average expression level was calculated to generate an expression matrix corresponding to unique gene symbols. The expression matrix of the GSE14520 dataset underwent log2 transformation, whereas the GSE41666 dataset did not, as it had already undergone variance stabilizing normalization (VSN). Both matrices were standardized to achieve normally distributed expression levels, N (0,1). The detailed data processing and analysis workflow is illustrated in Figure 1 and 2.

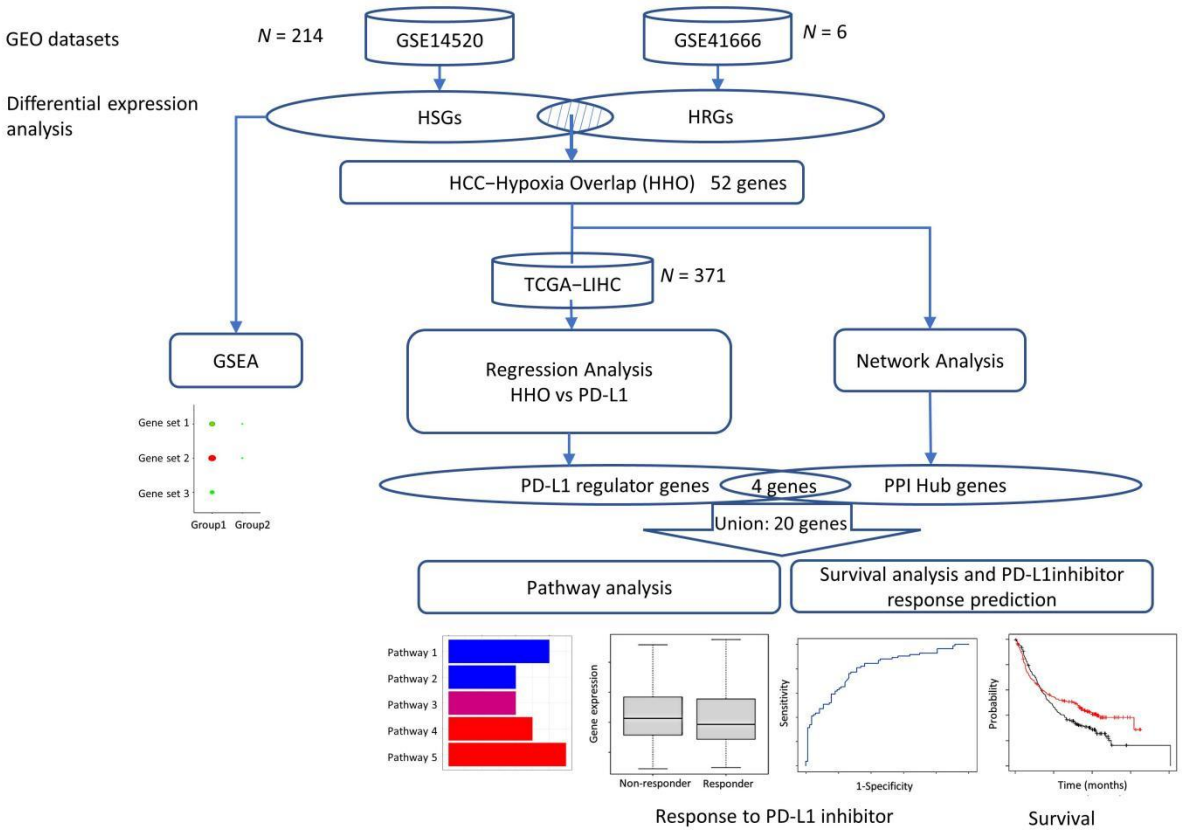

Figure 1. Data processing and analysis workflow of Chapter 2.

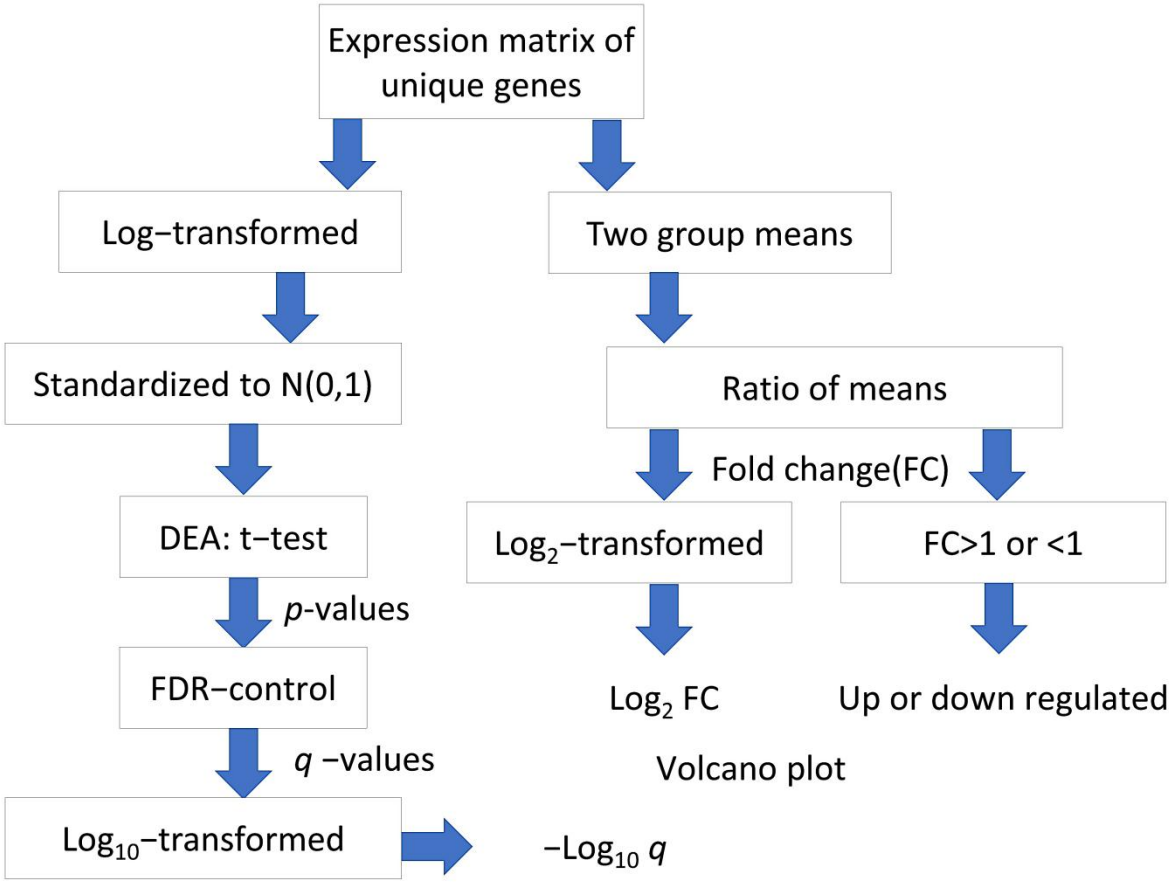

Figure 2. Flowchart of processing and analysis of microarray datasets.

2.1.2 Identification of HCC-signature genes (HSGs) and hypoxia-related genes (HRGs)

Differential expression analysis was conducted based on t-tests and fold change (FC). The p-value generated by the t-test for each gene was used to indicate the statistical significance of its differential expression. To address the issue of multiple hypothesis testing across a large number of genes, q-values, representing the estimated false discovery rates (FDR), were derived from p-values using the Storey-Tibshirani q-value method [78]. For the GSE14520 dataset, paired-sample t-tests were employed to analyze differences between tumor and paired non-tumor samples. HCC-signature genes (HSGs) were defined as differentially expressed genes in HCC tumor samples relative to paired non-tumor samples, with criteria set at q-value < 0.05 and FC > 1.4 (upregulated) or <1/1.34 (downregulated). For the GSE41666 dataset, hypoxia-related genes (HRGs) were identified based on the criteria of q-value < 0.05 and FC > 1.301 (upregulated) or <1/1.199 (downregulated). The cut-off values for FC were determined based on the number of selected upregulated and downregulated genes. Venn diagrams were created using the Venny 2.1 platform (https://bioinfogp.cnb.csic.es/tools/venny/, accessed November 25, 2022), and the HCC-Hypoxia Overlap (HHO) gene set was defined as the intersection of HSGs and HRGs.

2.1.3 GO function and KEGG pathway enrichment analysis of HSGs and HRGs

In this study, Gene Ontology (GO; http://geneontology.org, accessed on November 29, 2022) analysis was first performed on HSGs and HRGs, using Python to obtain enrichment results in Biological Process (BP), Cellular Component (CC), and Molecular Function (MF). Subsequently, Kyoto Encyclopedia of Genes and Genomes (KEGG; https://www.kegg.jp/, accessed on November 29, 2022) pathway enrichment analysis was conducted, yielding the corresponding pathway enrichment results. Adjusted p-values < 0.05 and FDR-adjusted p-values < 0.05 were considered statistically significant and served as thresholds for selecting the major enrichment functions and pathways of HSGs and HRGs.

2.1.4 Gene set enrichment analysis (GSEA) of HSGs and HRGs

GSEA is a computational method used for analyzing and interpreting changes in gene pathway levels and performing association analysis in transcriptomics experiments, including genome-wide association studies and RNA-seq gene expression experiments. The random permutation procedure (permutation = 1000) in the gseapy-v1.0.0 Python library was employed to obtain the null distribution. Subsequently, the Enrich method in the gseapy-v1.0 library was utilized to identify HCC signaling pathways regulated by hypoxia-related features (adjusted

p-value < 0.05). The gseapy-v1.0.0 package currently supports analysis across 202 databases.

2.1.5 PPI Network Construction and Identification of Hub Genes

STRING (Search Tool for the Retrieval of Interacting Genes, http://string-db.org/, accessed December 12, 2022) is an online database for searching protein-protein interactions. To further explore the interactions among HHOs (i.e., the overlapping genes between HSGs and HRGs), the HHO genes were imported into the STRING database to construct a PPI network with a confidence score greater than 0.7 [79]. Based on this network, PPI hub genes were identified using the degree algorithm of CytoHubba, which ranks genes by their connectivity degree (i.e., the number of connected neighbors) [80]. The top 10 PPI hub genes with the highest degree values were then selected for further analysis.

2.1.6 Multiple Regression Analysis of the Effect of HHOs on PD-L1

To investigate the effect of HHOs on PD-L1 expression, this study used multiple regression analysis. RNA sequencing (RNAseq) expression data from the TCGA-LIHC cohort, comprising 371 HCC tissue samples, were obtained from the UCSC Xena website (https://xenabrowser.net/datapages/, accessed December 6, 2022). The RNAseq expression levels of HHOs and PD-L1 were extracted and standardized for analysis. Compared to machine learning models, multiple

regression can produce more stable and reproducible results without the need to fix a specific random seed. Various feature selection methods were considered. mRMR effectively reduces feature redundancy. LASSO combines selection and regularization. Random Forest capture nonlinear relationships. Stepwise forward regression was chosen due to its suitability for continuous outcomes and superior interpretability. It enables clear identification of each gene's contribution. We applied a stepwise forward algorithm (p-value < 0.05) to identify genes within the HHOs that significantly and substantially impact PD-L1 expression, denoted as Y in the following formula.

$$Y = b_0 + b_1X_1 + b_2X_2 + \ldots + b_nX_n$$

In this formula, X_n represents the expression level of the nth selected gene, and bn represents the corresponding coefficient that quantifies its effect on PD-L1 expression. These selected genes are referred to as PD-L1 regulator genes.

2.1.7 Survival Analysis and PD-L1 Inhibitor Response Prediction

Kaplan Meier plotter (KM plotter; http://kmplot.com/analysis/ as of December 21, 2022) is a survival analysis platform that integrates clinical data, gene expression data, and survival information from the GEO, EGA, and TCGA databases. Using this platform, we plotted survival curves and calculated hazard ratios with 95% confidence intervals, as well as log-rank p-values for PPI hub genes and PD-L1

regulator genes in cancer patients. Patients were stratified into high-expression and low-expression groups based on the median expression level of each gene prior to PD-L1 inhibitor treatment.

The ROC plotter (https://www.rocplot.org/ as of December 23, 2022) is an analytical tool designed to identify predictive biomarkers based on gene expression levels using transcriptomic data from many cancer patients. In this study, this tool was utilized to evaluate the ability of the expression levels of PPI hub genes and PD-L1 regulator genes to predict the response to PD-L1 inhibitors in 454 pan-cancer patients within the database.

Additionally, we conducted KEGG pathway enrichment analysis on the union of PD-L1 regulator genes and PPI hub genes using the ShinyGo 0.76.3 platform (http://bioinformatics.sdstate.edu/go/, accessed January 1, 2023), with an FDR threshold of < 0.05 set as the criterion for selection.

2.1.8 Establishment of a Hypoxia Scoring Model

Based on RNA-seq data from HCC patients (N=367) in the TCGA Liver Cancer (LIHC) database, univariate Cox regression models were initially constructed. Subsequently, hypoxia-characteristic genes were selected for the multivariate survival model using the Least Absolute Shrinkage and Selection Operator

(LASSO) algorithm. A hypoxia-related risk score was calculated using the model established from these characteristic genes, stratifying patients into high-risk and low-risk groups. Finally, this model was validated using liver cancer cases (N=232) from the International Cancer Genome Consortium (ICGC) database (ICGC-LIRI-JP).

2.2 Results

2.2.1 Identification of HSGs and HRGs in HCC

By setting the cutoff values for q and FC at 1.139 and 1.128, respectively, 800 HSGs (400 upregulated and 400 downregulated) were identified from the GSE14520 dataset, showing significant differential expression between tumor and adjacent non-tumor tissues (Figure 3a). The corresponding heatmap is shown in Supplementary Figure S1. In the GSE41666 dataset, the cutoff values for q and FC were set at 1.277 and 1.370, respectively, leading to the identification of 800 HRGs (400 upregulated and 400 downregulated), which exhibited significant differential expression between hypoxic and normoxic conditions (Figure 3b), with the corresponding heatmap presented in Supplementary Figure S2. Further analysis revealed that 52 overlapping genes were common to both HCC-signature genes (HSGs) and hypoxia-related genes (HRGs), termed HCC-Hypoxia Overlaps (HHOs) (Fisher exact test, $p < 1.047 \times 10^{-11}$). Among these, 37 genes were upregulated and 15 were downregulated in the hypoxic group compared to the normoxic group in the GSE41666 dataset (Figure 3c, d).

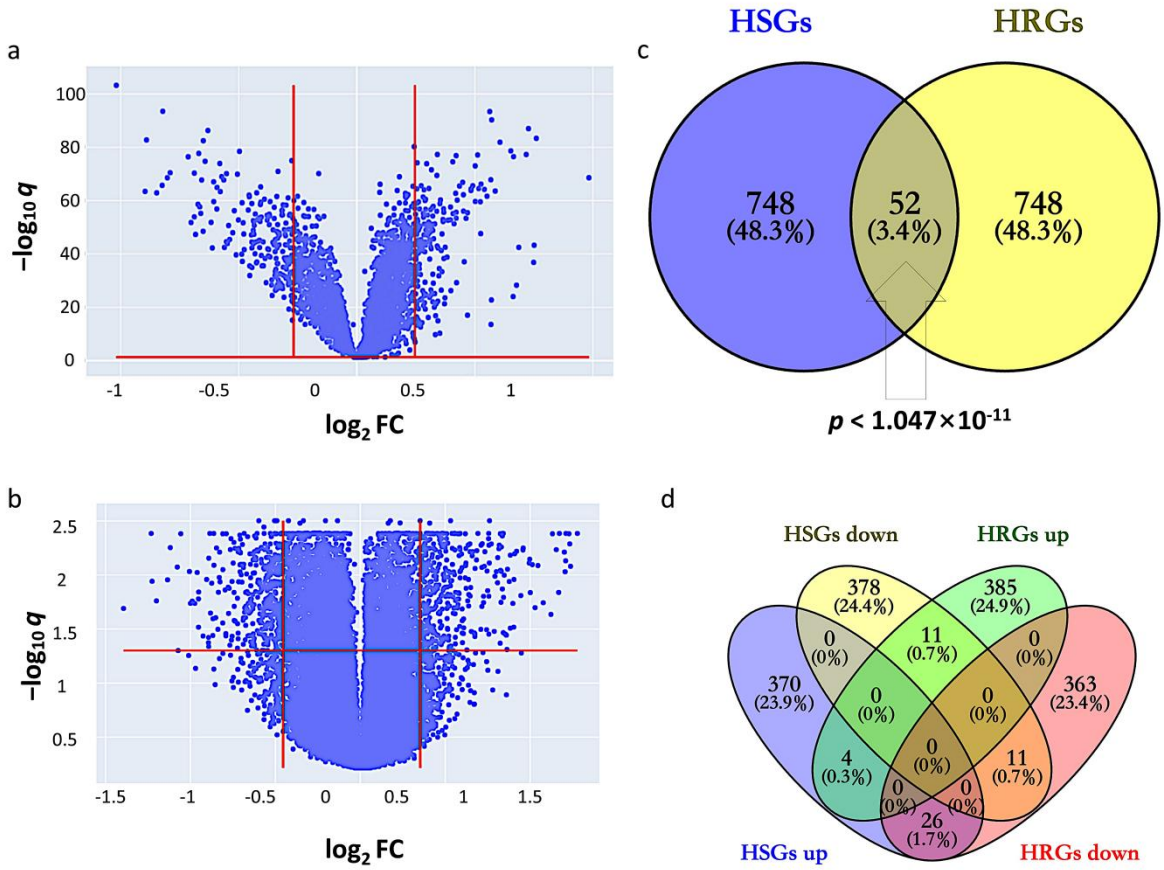

Figure 3. Identification of HCC-signature genes (HSGs) and hypoxia-related genes (HRGs). (a) Volcano plot for GSE14520; (b) Volcano plot for GSE41666; (c) Overlapping genes between HSGs and HRGs; (d) Overlapping genes among upregulated and downregulated genes in HSGs and HRGs.

2.2.2 Gene Set Enrichment Analyses of HSGs and HRGs

Using the gseapy package in Python, enrichment analysis of HSGs and HRGs was conducted across 202 databases (as of November 29, 2022). Significant enrichment results were identified in 190 and 161 databases, respectively. Notably, we focused on three groups of databases that showed significant enrichment results closely related to hypoxia, HCC, and PD-L1.

In the GO database, the upregulated HSG genes were significantly enriched in the gene sets related to "nucleus," "mitosis," and "organelles," while the upregulated HRG genes were predominantly enriched in the gene sets associated with "spindle," "mitosis," and "nuclear chromosome" (Figure 4a, b). The downregulated HSG genes were primarily enriched in the "monooxygenase activity" gene set, whereas the downregulated HRG genes were mainly enriched in the "cellular response to decreased oxygen levels" gene set (Figure 4a, b). The bar chart depicting the expression profiles of these enriched genes is presented in Supplementary Figure S3. In the KEGG Human database, the upregulated HSG genes were significantly enriched in pathways such as "cellular senescence signaling," "RNA transport," "drug metabolism," "apoptosis signaling" and "chemical carcinogenesis" (Figure 4d). Moreover, in the "RNAseq Automatic GEO Signatures Human" database, it was found that the downregulated HSG and HRG genes were significantly enriched in the "Rb-immunity downregulating Pd-

L1" gene set, with CENPA, TPX2, LMNB1, DLGAP5, and KIF20A, being the common genes among them. Additionally, the upregulated HRG genes were significantly enriched in both the "tissue-resident pancreas Pd-1/Pd-L1" gene sets and "Rb-immunity downregulating Pd-L1" (Figure 4c).

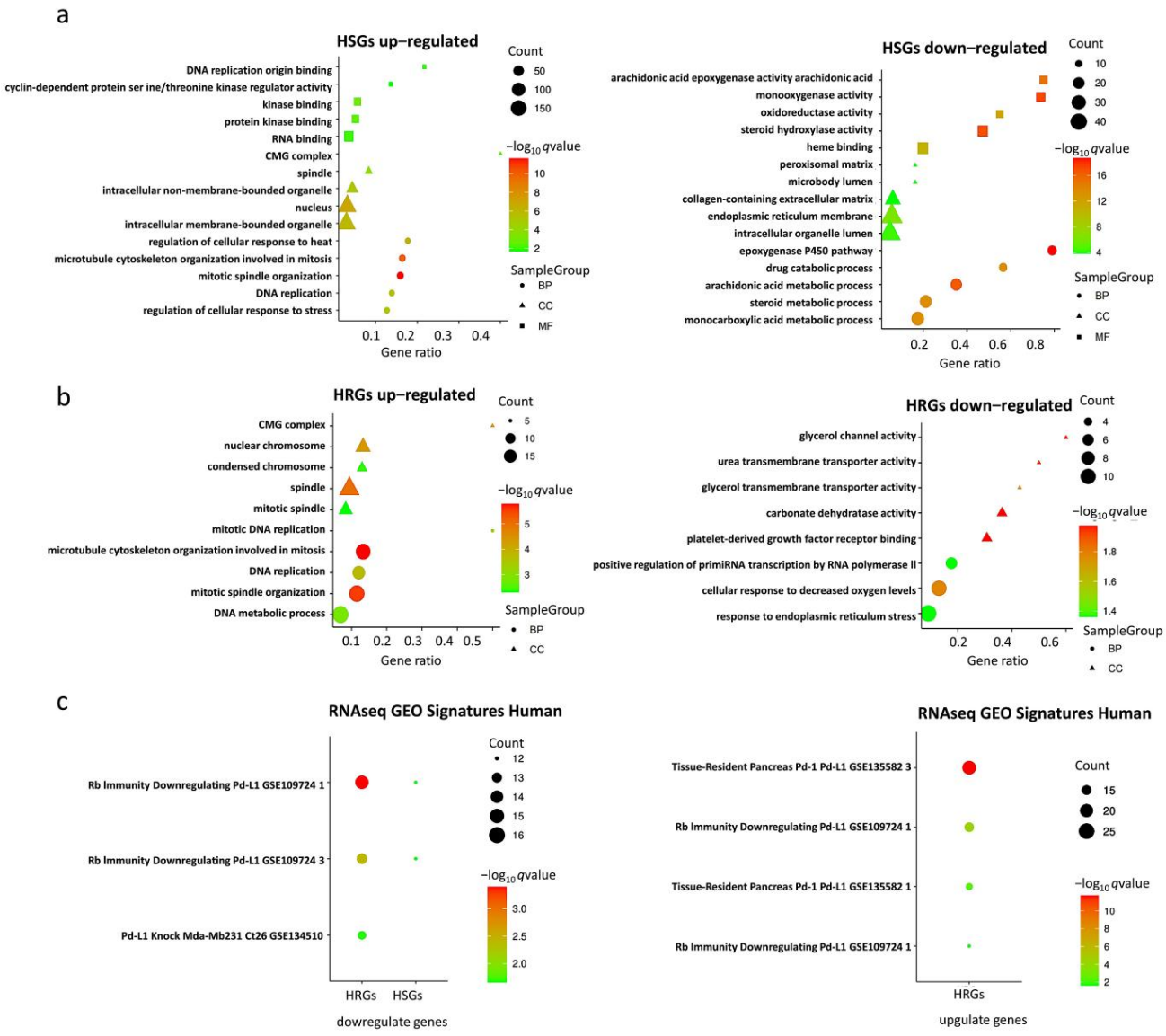

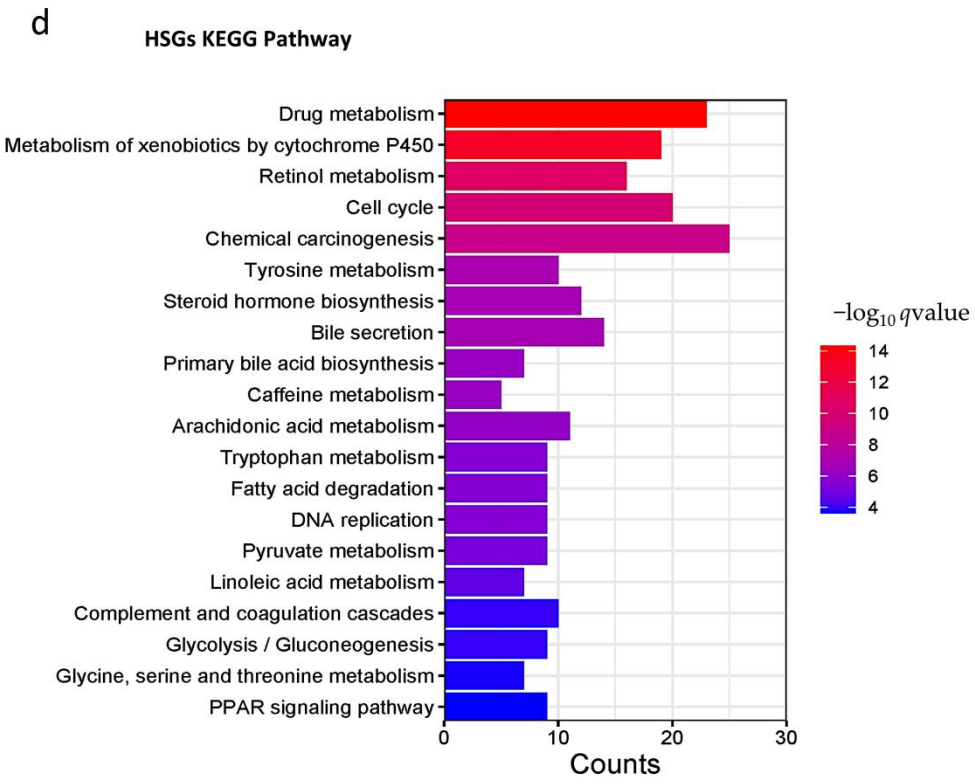

Figure 4. Gene set enrichment analysis. (a) GO enrichment analysis of HSGs; (b) GO enrichment analysis of HRGs; (c) RNAseq GEO Signatures Human enrichment analysis of HRGs and HSGs; (d) KEGG enrichment analyses of HSGs.

2.2.3 Evaluation of the Effect of HHOs on PD-L1 Expression in the TCGA-LIHC Dataset

The impact of HHOs on PD-L1 expression was evaluated through multiple regression analysis, ultimately identifying 14 risk genes significantly associated with PD-L1 expression. A drug resistance gene regulatory model was then constructed based on these genes. This model is represented as a linear combination of regression coefficients and the relative expression levels of PD-L1 regulatory genes, illustrating the relative contribution of each gene to drug resistance.

$$\begin{aligned} PD\text{-}L1 = {} & 0.076 + 0.240 \times FOS + 0.261 \times FAM13A \\ & + 0.443 \times DLGAP5 - 0.264 \times ALDH5A1 \\ & + 0.223 \times GABARAPL1 - 0.123 \times CABYR \\ & + 0.145 \times PIK3R1 - 0.150 \times HGFAC \\ & + 0.317 \times LMNB1 - 0.418 \times KIF20A \\ & - 0.434 \times TPX2 + 0.410 \times NDC80 \\ & + 0.121 \times EPHA2 - 0.096 \times NEDD4L \end{aligned}$$

Each of the PD-L1 regulator genes included in the model shows a significant association with drug resistance ($p < 0.05$). Notably, the genes DLGAP5, NDC80, LMNB1, KIF20A, and TPX2 have the largest absolute regression coefficients, indicating their critical role in drug resistance.

2.2.4 Construction of Protein–Protein Interaction Network and Identification of Hub Genes

The 52 HHO genes were analyzed for PPI networks using the STRING database platform, and the results were imported into Cytoscape software to construct the PPI network. Among the 52 HHO genes, 26 genes demonstrated connections in the PPI network with a confidence score greater than 0.7, while the remaining genes were excluded from the network representation (Figure 5a). Additionally, the node connectivity was calculated using the CytoHubba plugin, and 10 genes with a connectivity degree greater than 33 were identified as hub genes. These hub genes are CCNB1, BUB1B, KIF4A, KIF20A, KIF11, NDC80, TPX2, CENPA, POLE2, and DLGAP5 (Figure 5b).

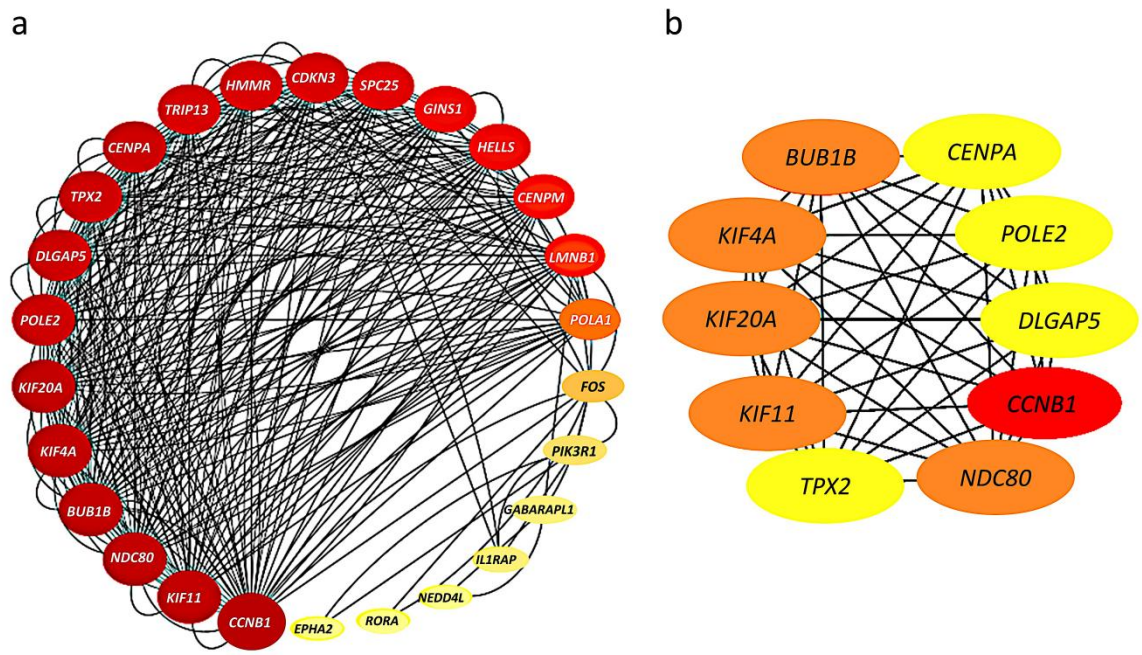

Figure 5. Protein–protein interaction (PPI) networks: (a) Connections among 26 genes with a confidence score > 0.7; larger nodes indicate higher connectivity, and darker colors represent higher combined score values; (b) 10 hub genes with a connectivity degree > 33; genes with a confidence score ≤ 0.7 are not shown; darker colors indicate greater criticality.

2.2.5 Survival Analysis and PD-L1 Inhibitor Response Prediction KEGG Pathway Enrichment

We used the Kaplan Meier Plotter software to generate survival curves for the combined set of PPI hub genes and PD-L1 regulator genes. The results of the survival analysis indicated that the expression levels of 15 genes were significantly associated with poor patient prognosis (Table S3). Notably, patients with high expression levels of NDC80 (HR = 0.76, p = 0.024) and TPX2 (HR = 0.77, p = 0.03) demonstrated significantly better survival rates following PD-L1 treatment (Figure 6a, b). Additionally, we validated the response of PPI hub genes and PD-L1 regulator genes to PD-L1 treatment. Among the sample, the three top-performing genes were GABARAPL1 (AUC = 0.56, p = 0.016), PIK3R1 (AUC = 0.549, p = 0.04), and POLE2 (AUC = 0.553, p = 0.027) (Figure 6c).

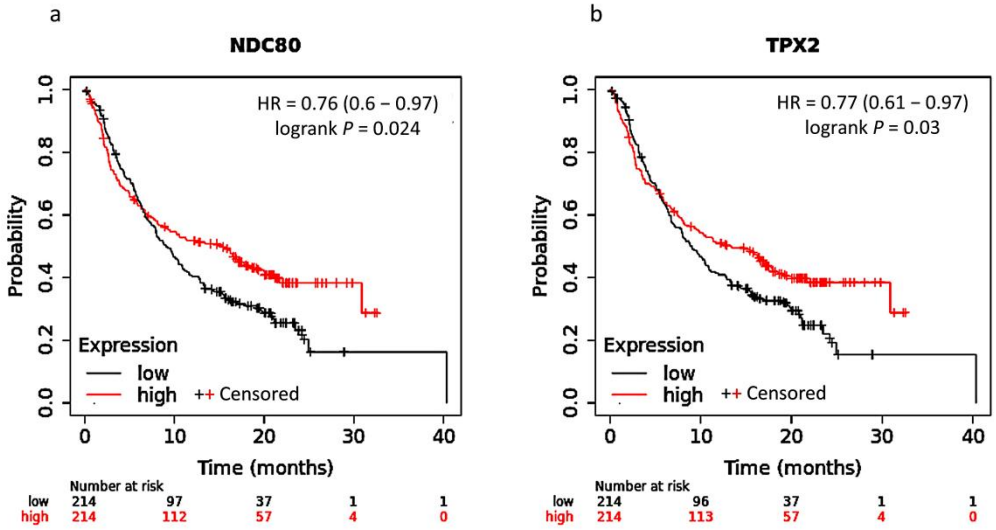

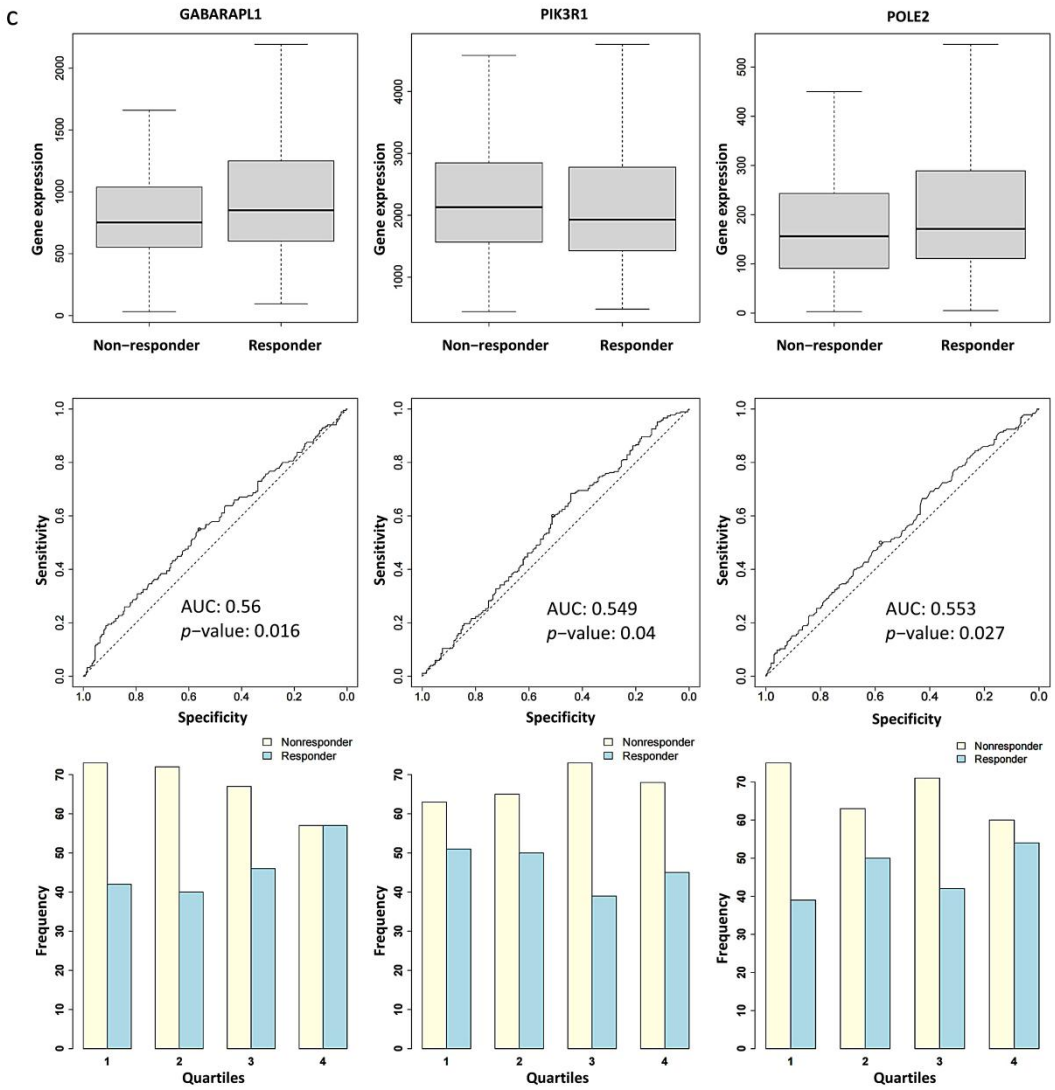

Figure 6. Kaplan–Meier survival curves comparing high and low expression levels: (a) NDC80 (HR = 0.76, p = 0.024); (b) TPX2 (HR = 0.77, p = 0.03). (c) Boxplots, receiver operating characteristic (ROC) curves, and responder frequencies for the top three genes in predicting PD-L1 inhibitor response: GABARAPL1 (AUC = 0.560, p = 0.016), PIK3R1 (AUC = 0.549, p = 0.04), and POLE2 (AUC = 0.553, p = 0.027). The “o” indicates the optimal cutoff point, representing the minimal distance from the ideal discriminator.

2.2.6 KEGG Pathway Enrichment

The KEGG pathway enrichment analysis of PPI hub genes and PD-L1 regulator genes was performed using the ShinyGo platform. The results revealed significant enrichment in 19 pathways (false discovery rates (FDRs) < 0.032), with most pathways closely related to immune cells, inflammatory factors, and apoptosis (Figure 7). Notably, the genes FOS (AP-1) and PIK3R1 were identified within the "PD-L1 expression and PD-1 checkpoint pathway in cancer," while the "endocrine resistance pathway" was activated by hypoxia induction.

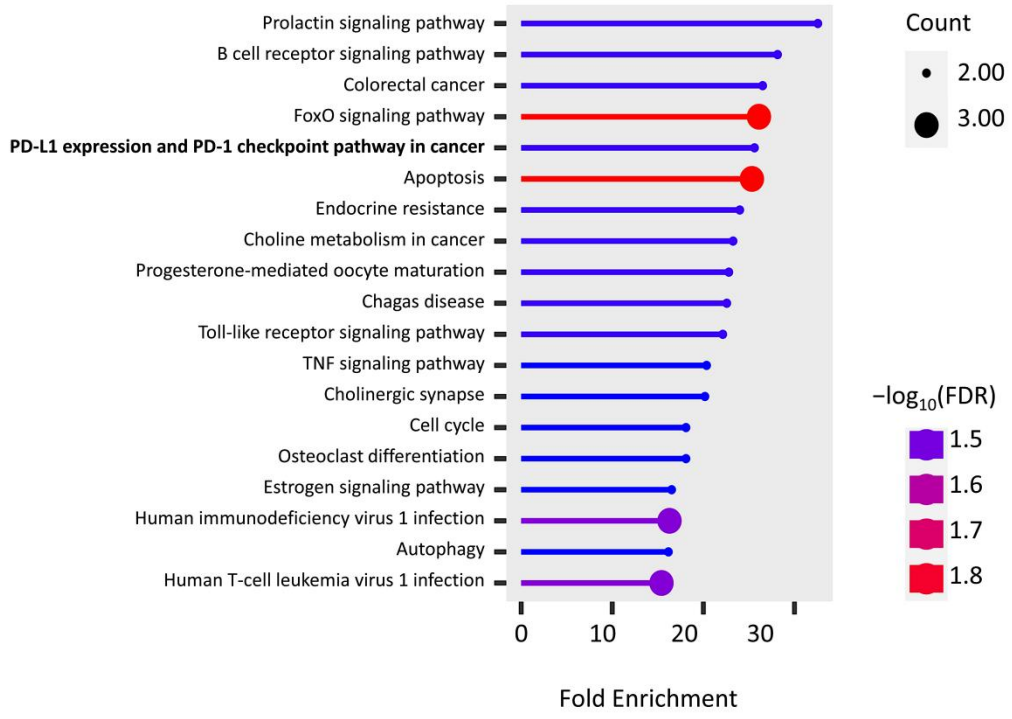

Figure 7. KEGG pathway enrichment of the union of PPI hub genes and PD-L1 regulator genes.

2.2.7 Hypoxia Risk-scoring Model

Univariate Cox analysis revealed that 21 of these HHO genes were significantly associated with overall survival in HCC patients (Figure 8a). Through LASSO regression analysis, 9 hypoxia risk score genes, including CENPA, KIF20A, DLGAP5, HMMR, UPB1, AFM, CABYR, PHLDA2, and N4BP2L1, were ultimately retained in the survival model (Figure 8b). Based on these 9 genes, the TCGA-LIHC samples were classified into high-risk (n = 183) and low-risk (n = 184) groups (Figure 9a). Kaplan-Meier (KM) analysis indicated a significant difference in survival outcomes between the two groups ($p < 0.032$) (Figure 9b). In the ICGC-LIRI-JP validation set, risk scoring similarly stratified samples into high-risk (n = 116) and low-risk (n = 116) groups (Figure 10a). KM analysis further confirmed that patients in the high-risk group had significantly shorter survival times compared to those in the low-risk group ($p < 0.0001$) (Figure 10b). Receiver Operating Characteristic (ROC) curve analysis demonstrated that the model achieved area under the curve (AUC) values of 0.815, 0.774, and 0.771 at 1, 2, and 3 years, respectively, indicating strong predictive performance in risk stratification (Figure 10c).

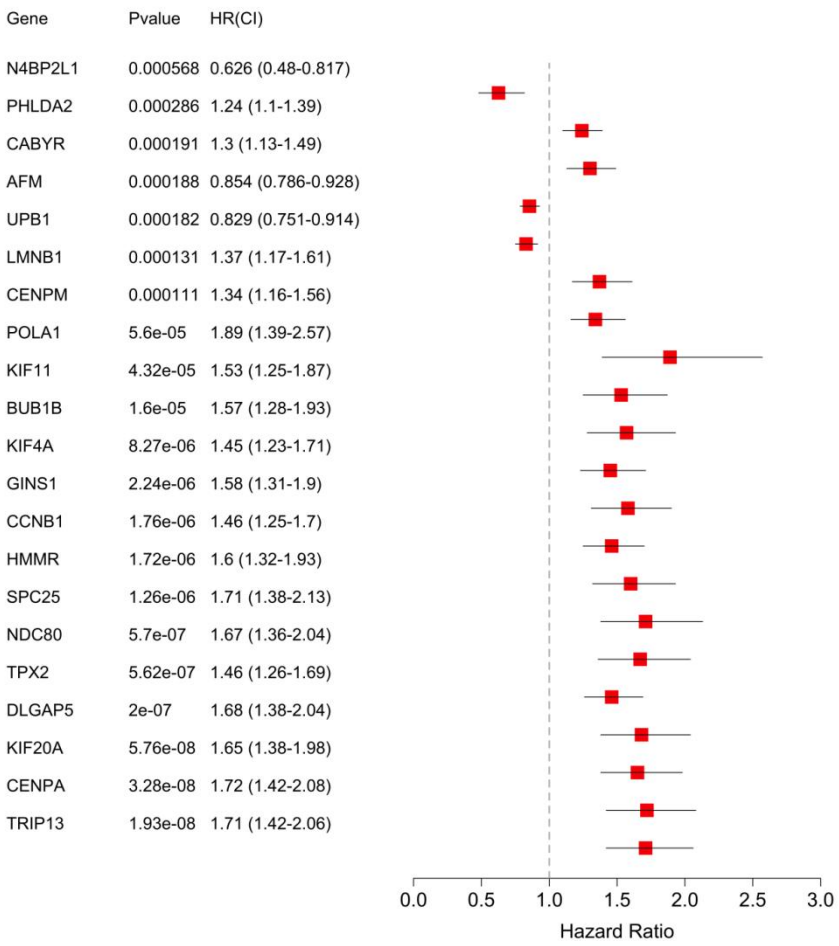

Figure 8. Univariate Cox and LASSO regression analysis: (a) Forest plot showing the hazard ratios (HRs) and 95% confidence intervals (CIs) for the selected feature genes based on univariate Cox proportional hazards regression analysis. Each gene's HR, CI, and p-value indicate its significance in predicting survival outcomes in HCC patients. The red squares represent the HRs, with horizontal lines denoting the 95% CIs, emphasizing the importance of these genes in survival prediction.

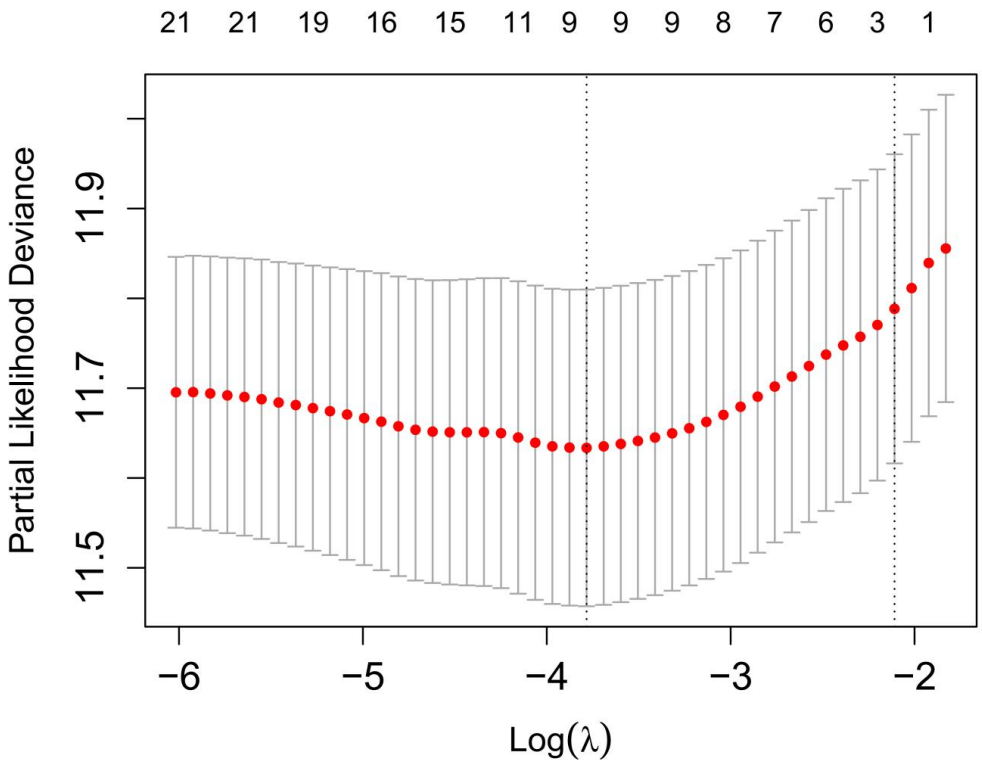

Figure 8. (b) The LASSO regression results illustrate the relationship between log(λ) and partial likelihood deviance. The x-axis shows log(λ) values, while the y-axis represents partial likelihood deviance. Red dots correspond to different λ values, with vertical bars indicating standard errors. The vertical dashed lines mark the λ values selected by cross-validation, identifying the optimal number of genes for the survival model. The numbers at the top represent the count of genes retained at each λ value.

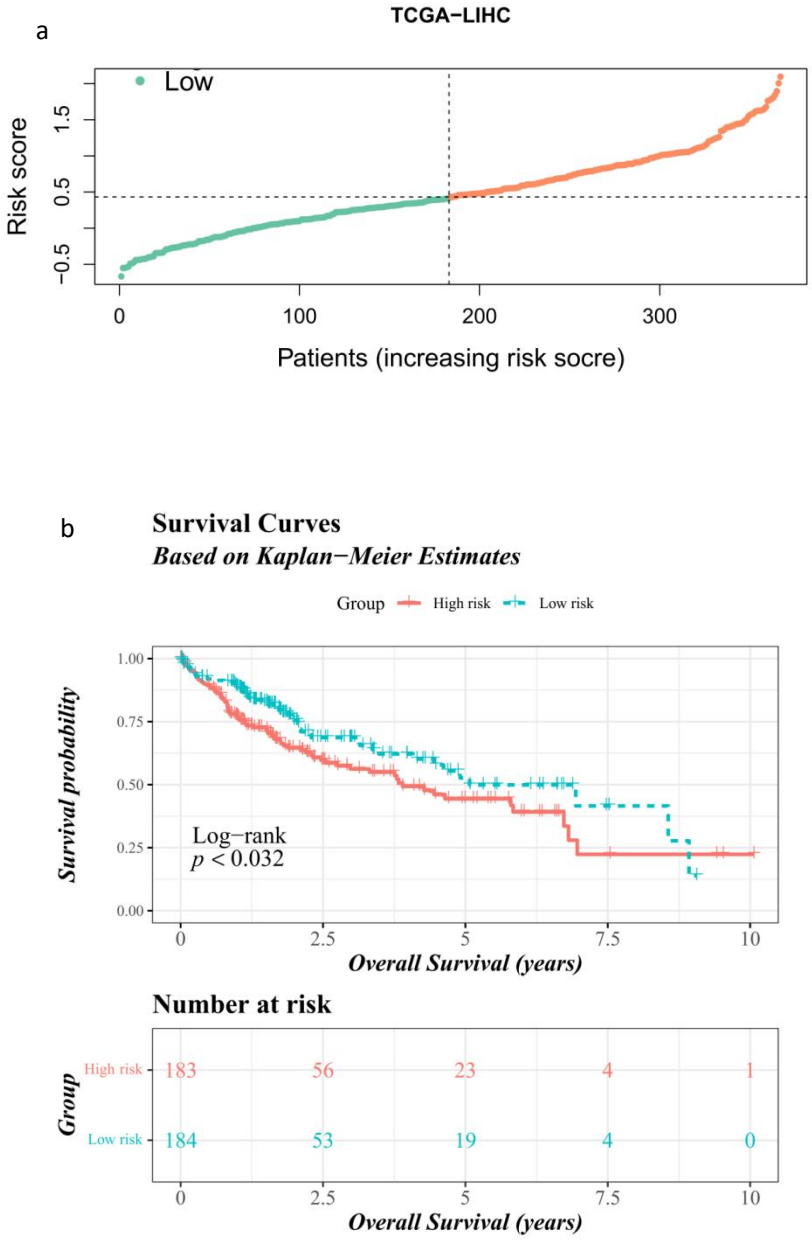

Figure 9. Initial Hypoxia Risk Score Model Survival Analysis: (a) The risk score distribution of patients from the TCGA-LIHC dataset. The horizontal dashed line separates the low-risk group (green) from the high-risk group (orange) based on the median risk score. (b) KM survival curves for OS in the TCGA-LIHC cohort, divided into high-risk (red, n = 183) and low-risk (blue, n = 184) groups ($p < 0.032$).

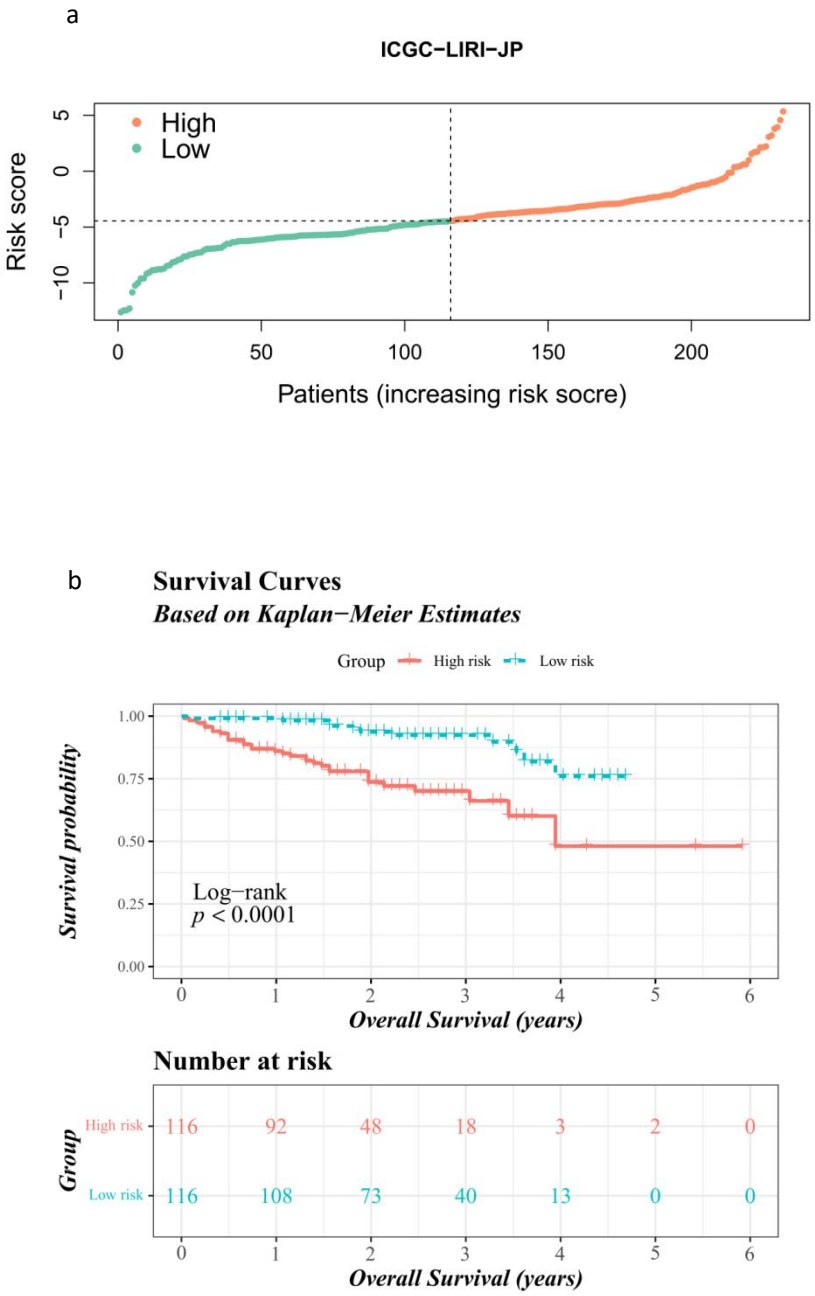

Figure 10. Validation of Initial Hypoxia Risk Score Model Survival Analysis: (a) The risk score distribution of patients from the ICGC-LIRI-JP dataset. The horizontal dashed line separates the low-risk group (green) from the high-risk group (orange) based on the median risk score. (b) KM survival curves for OS in the ICGC-LIRI-JP cohort, divided into high-risk (red, n = 116) and low-risk (blue, n = 116) groups ($p < 0.0001$).

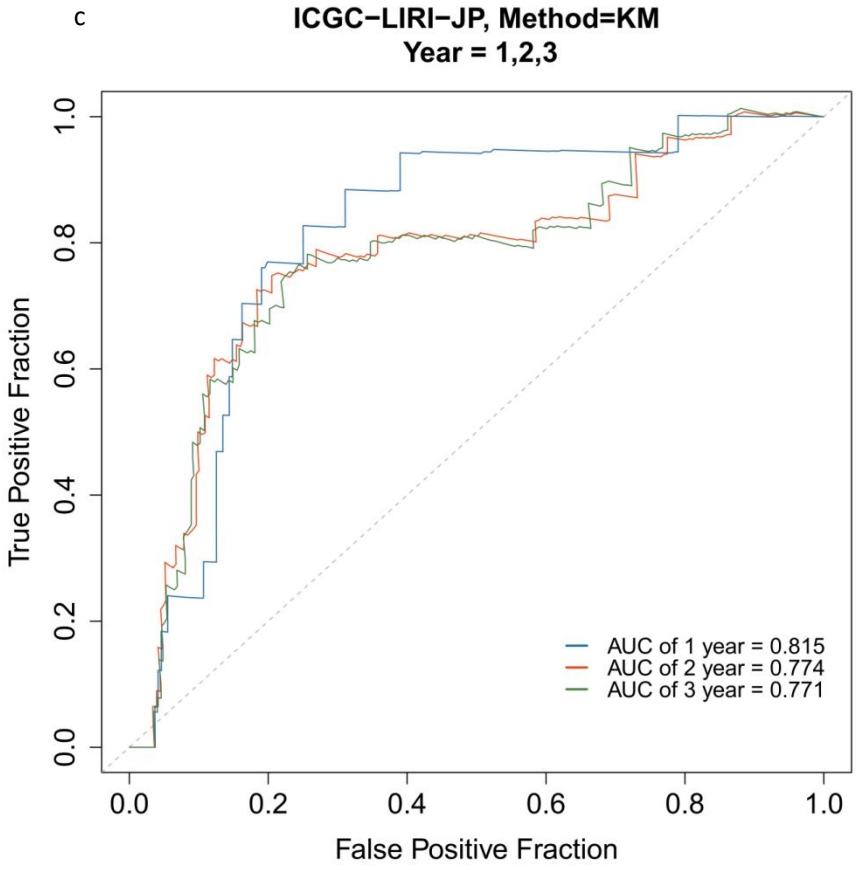

Figure 10. (c) ROC curves for the risk model predicting 1-year, 2-year, and 3-year OS in the ICGC-LIRI-JP cohort. The AUC values are 0.815, 0.774, and 0.771 for 1, 2, and 3 years, respectively.

2.3 Discussion and Conclusion

In this chapter, we identified a total of 52 HHOs, which are overlapping genes between HSGs and HRGs derived from GEO datasets. Gene set enrichment analysis (GSEA) revealed that some HSGs and HRGs were closely associated with the PD-L1 expression pathway. Notably, TPX2, KIF20A, CENPA, DLGAP5, and LMNB1 within the HHOs were significantly enriched in the retinoblastoma (RB) immunity downregulation of the PD-L1 expression pathway. Previous research has demonstrated that hyperphosphorylated RB protein within this pathway plays a tumor-suppressive role by inhibiting NF-κB activity and PD-L1 expression[81]. Additionally, regression analysis of the TCGA dataset allowed us to identify 14 PD-L1 regulator genes from the HHOs, and 10 hub genes were extracted from the PPI network, with TPX2, KIF20A, NDC80, and DLGAP5 being the overlapping genes. Based on clinical data, we analyzed the survival and treatment response of PPI hub genes and PD-L1 regulator genes following PD-L1 inhibitor treatment to further validate our computational results. TPX2, NDC80, POLE2, GABARAPL1, and PIK3R1 were found to be significantly associated with treatment outcomes. These findings suggest that TPX2 and NDC80 play crucial roles in regulating PD-L1 expression, thereby influencing the efficacy of PD-L1 inhibitors.

The phosphoinositide-3-kinase regulatory subunit 1 (PIK3R1) gene, encoding the p85α regulatory subunit of PI3K enzymes, plays a key role in cancer by

regulating PIP3 expression, AKT activation, and PTEN phosphorylation via the PI3K pathway [82, 83]. In HCC, PIK3R1 expression is higher than in normal tissues, and its knockdown reduces tumor growth by decreasing p-PI3K, p-AKT, and p-mTOR levels [84, 85]. Targeting protein for Xenopus kinesin-like protein 2 (TPX2), a microtubule nucleation factor, promotes tumor growth in HCC by regulating the PI3K/AKT/p53/p21 pathway [86, 87]. Nuclear division cycle 80 (NDC80/Hec1), involved in mitosis, is overexpressed in HCC, potentially promoting cancer progression [88, 89]. DNA polymerase epsilon subunit 2 (POLE2), a DNA polymerase subunit, activates AKT and reduces HIF-1 α , driving cancer cell proliferation [90]. Gamma-aminobutyric acid (GABA), a receptor-associated protein-like 1 (GABARAPL1), linked to autophagy, suppresses cancer progression by inhibiting AKT/mTOR signaling [91, 92].

Research has shown that 20 genes, combining PD-L1 regulator genes and PPI hub genes, are not only differentially expressed in hypoxic HCC tissues but also regulate cancer cells through the PI3K/AKT pathway. These genes play a critical role in PD-L1 regulation in hypoxic HCC tissues and may serve as potential therapeutic and prognostic biomarkers to enhance sensitivity to PD-L1 inhibitors and overcome drug resistance. However, the specific regulatory mechanisms remain unclear. In the future, Gene Regulatory Network (GRN) analysis may be used to further explore the underlying mechanisms, followed by validation through biological experiments such as gene knockdown, overexpression studies,

and pathway-specific assays.

The PI3K/AKT/HIF axis is significant in hypoxia-induced drug resistance in HCC, particularly in regulating PD-L1 expression. TPX2, a key gene, is involved in various cancers, including HCC, through its interaction with the PI3K/AKT pathway [93]. KRAS, another critical gene, influences this pathway, further linking hypoxia to PD-L1 regulation and drug resistance [94, 95]. Additionally, ROS-mediated activation of the PI3K/AKT/HIF-1α pathway contributes to tumor progression under hypoxia [96].

Combining PD-L1 inhibitors with HIF inhibitors, such as MK6482, has shown promise in treating hypoxic tumors. This combination could enhance anti-tumor immunity and reduce drug resistance [97]. However, the efficacy and safety of these combinations require further exploration, particularly regarding their impact on PD-L1 expression in both tumor and normal tissues. In this study, key molecules like KRAS, NDC80, TPX2, and PIK3R1 were identified as potential targets for overcoming drug resistance in hypoxic HCC when combined with PD-L1 inhibitors. These findings suggest a multi-targeted approach to developing effective therapies for hypoxic tumors.

This chapter also highlights the significant impact of hypoxia-related genes on the survival of HCC patients. Our analysis identified 21 HHO genes associated with

survival, and through LASSO regression, we refined this to 9 key genes—CENPA, KIF20A, DLGAP5, HMMR, UPB1, AFM, CABYR, PHLDA2, and N4BP2L1—forming the basis of a survival model. These genes appear to be central to how the hypoxic microenvironment influences HCC progression and prognosis. The identification of these hypoxia-related genes enhances our understanding of HCC's molecular mechanisms under hypoxia and suggests potential targets for therapies aimed at improving patient outcomes.

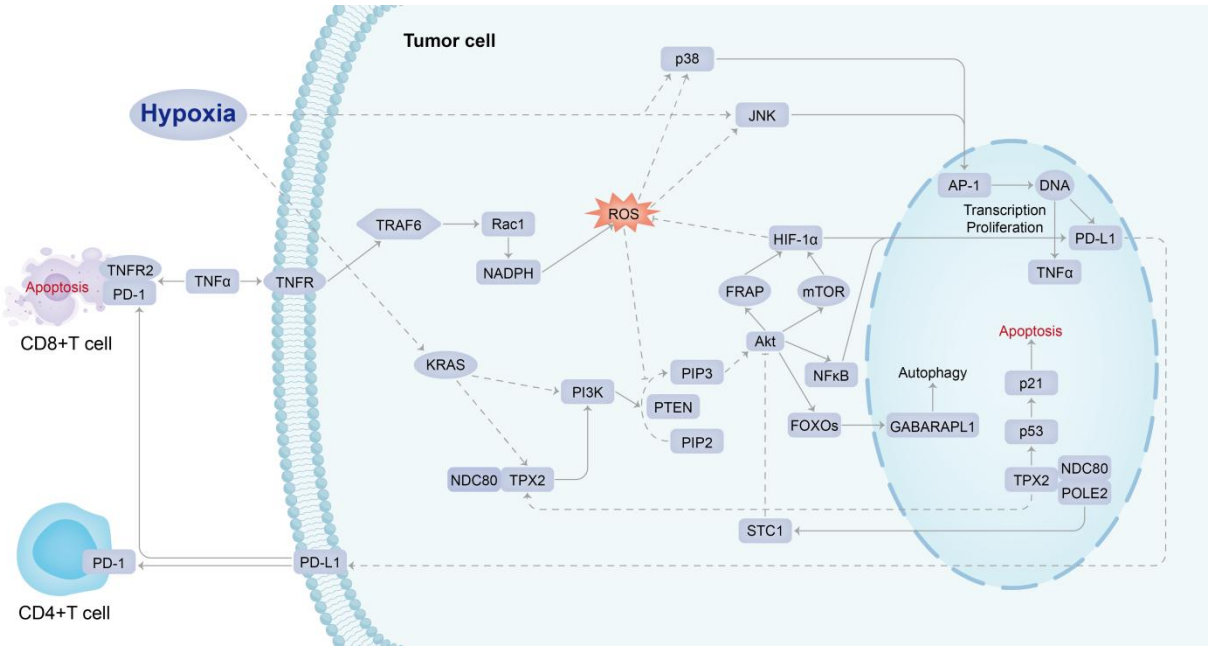

Figure 11. Conceptual signaling mechanism of hypoxia-induced PD-L1 inhibitor resistance.

Chapter 3 Molecular expression profile associated with clinical immunotherapy drug response and resistance in advanced HCC

3.1 Materials and Methods

3.1.1 Collection and processing of public data of gene expression

The EGAD00001008128 dataset was downloaded from the European Genome-Phenome Archive (EGA) (https://ega-archive.org/datasets/, on October 10, 2023). The dataset comprises comprehensive RNA sequencing data analyzed via high-throughput sequencing technologies from pathological biopsies of 290 patients. These biopsies of patients were obtained prior to immunotherapy (Atezolizumab and Atezolizumab + Bevacizumab). In this dataset, 90 patients who exhibited positive therapeutic response, in contrast to 200 patients who had non-response to the treatment. The dataset was split into training and test sets for establishing the immunotherapy response prediction models. As the non-response class represents most of the patients when compared with the response class, the split of training and test sets, 9:1, was applied to the non-response cases so that 20 out of 200 non-response cases and 20 out of 90 response cases were randomly selected to form the test set. The training set consists of the remaining 180 non-response cases and 70 response cases.

The datasets GSE41666, SRP356151, and GSE233802 were acquired from the

NCBI database (https://www.ncbi.nlm.nih.gov/) in January 2022, March 2024 and June 2024, respectively. The GSE41666 dataset includes gene expression profiles of HepG2 cell lines under hypoxic (0% O_2) and normoxic (21% O_2) conditions for 24 hours, obtained using a microarray platform. Each condition was replicated three times to ensure biological reproducibility. The SRP356151 dataset contains total RNA sequencing data analyzed via a high throughput sequencing platform, featuring samples from hypoxic HepG2 cells subject to HIF1α-knockout and LacZ-control. Hypoxia was induced using 100 μmol/L $CoCl_2$, with each condition replicated three times to ensure robust biological results. The GSE233802 dataset comprises total RNA sequencing data from HepG2 cells under hypoxic condition (1% O_2) for 24 and 48 hours, with normoxic condition as control, also replicated three times to ensure the robustness of biological results. These datasets facilitate a comprehensive analysis of gene expression under various oxygen conditions, providing insights into hypoxia-related biological processes in HepG2 cells.

For RNA sequencing data, the datasets EGAD00001008128, SRP356151 and GSE233802 were processed using a standard processing pipeline that includes initial quality assessment with (i) FastQC, trimming of low-quality bases and removal of adapters using (ii) Fastp, alignment of cleaned reads to the human reference genome (GRCh38.104 from NCBI) with (iii) HISAT2, and gene quantification with (iv) FeatureCounts, all to ensure the integrity, quality, and

reliability of the data for comprehensive analysis. All three datasets are equipped with comprehensive clinical information and an adequate number of samples for thorough analysis.

Due to the variability in sequencing instruments used for the samples, we employed different methods, which were used in the relevant literature, to filter out low-quality gene expression data. For the EGAD00001008128 dataset, we calculated the median normalized counts-per-million (CPM) value and the coefficient of variation (CV) for each gene expression profile. A gene was considered for further analysis if its CPM and CV values across samples exceed the respective 25th percentiles the CPM and CV values across all the genes and its expression levels are detectable in at least 75% of the samples. For the SRP356151 dataset obtained from 6 samples, a gene was considered if it expressed in at least 4 samples. For the GSE233802 dataset obtained from 9 samples, a gene was considered if it expressed in at least 6 samples.

The pre-processing, analysis, model identification and performance evaluation of public data are illustrated in Figure 12.

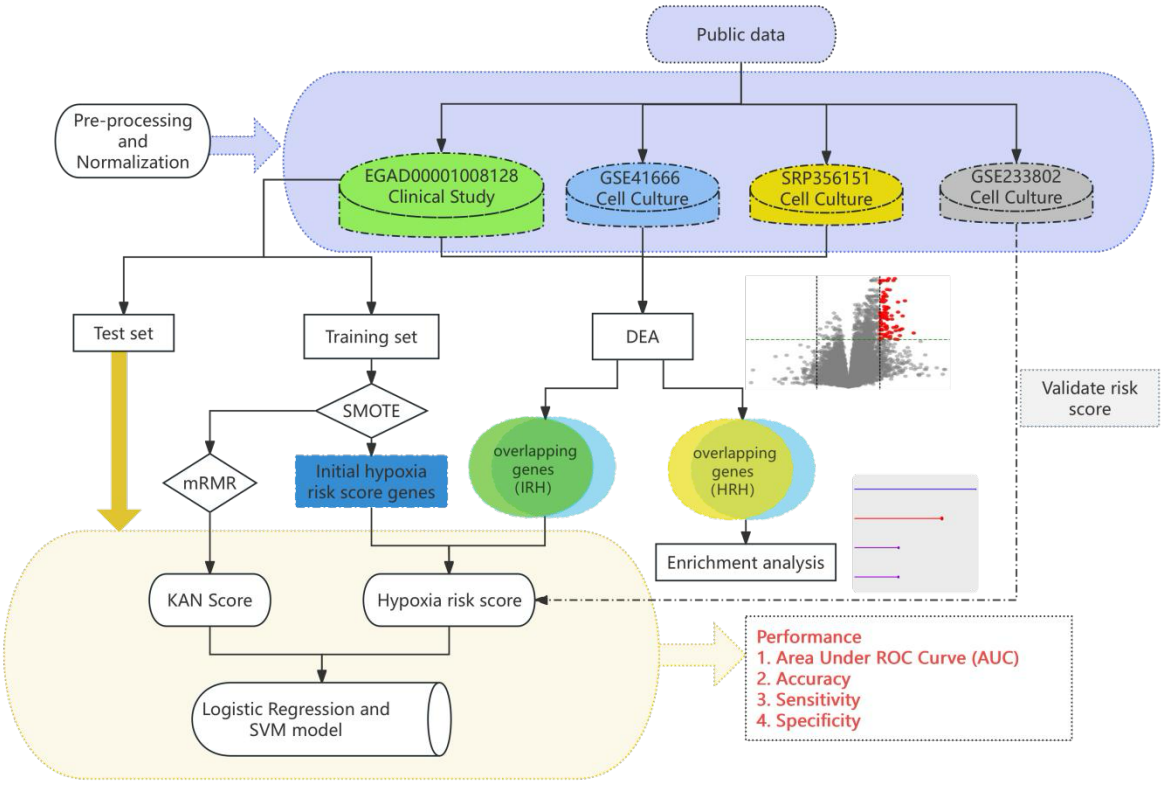

Figure 12. Flowchart of the pre-processing, analysis, model identification and performance evaluation in chapter 3.

3.1.2 Normalization of gene expression data

To effectively eliminate sequencing depth and technical variation between samples of RNA sequencing data, the preprocessed EGAD00001008128, SRP356151 and GSE233802 datasets were first normalized using DESeq2 normalization (deseq2_norm) Python/R function where sample-specific scaling factors were applied to expression matrices.

To make the EGAD00001008128 data suitable for the machine learning, deep learning and statistical models, the StandardScaler function from the Sklearn Python package was used to obtain a scaler with the training data. The obtained scaler was then used to standardize training and test sets to the standard normal distribution, N (0,1).

The log2-transformation was not applied to the preprocessed GSE41666 dataset, which has undergone Variance Stabilizing Normalization (VSN). Standardization was performed to obtain normally distributed expression levels, N (0,1).

For validating the Cox regression model, the log transformation and standardization were applied to the preprocessed GSE233802 data to form an expression matrix following the standard normal distribution, N (0,1).

As SRP356151 dataset has 6 samples and underwent differential expression

analysis only, no standardization was performed.

3.1.3 Differential expression analysis

The normalized data underwent differential expression analysis (DEA) through t-tests and Fold-Change (FC) assessments. Through the Statsmodels Python package, the q-values were calculated from p-values using the Storey-Tibshirani method [78] for GSE41666 microarray data and Benjamini-Hochberg method [98] for EGAD00001008128, and GSE233802 RNA sequencing data. A differentially expressed gene (DEG) is defined as q-value < 0.05. To further control the number of selected upregulated and downregulated genes, the cutoffs of FCs were set.

Given the limited sample size of RNA sequencing in the SRP356151 dataset, the combined use of the Wald test and t-test can enhance the efficiency and accuracy of the analysis. Initially, the Wald test is applied to calculate p-values for each gene, allowing for the preliminary identification of genes that may exhibit significant differential expression (p-value < 0.05). These initially identified genes are then subjected to a t-test, and the false discovery rate is controlled by calculating q-values using the Benjamini-Hochberg method. DEGs are defined as those with a q-value < 0.05. To further control the number of selected upregulated and downregulated genes, the cutoffs of FCs were set.

Considering the diversity in measurement techniques and sample sizes inherent to the raw data, appropriate methodologies were employed for DEA to ensure methodological compatibility and analytical precision.

3.1.4 Inter-relationship between immunological profile and hypoxia

Venn diagrams were constructed using the Venny 2.1 platform (https://bioinfogp.cnb.csic.es/tools/venny/, accessed on May 25, 2024). The DEGs from the GSE41666 dataset were intersected with DEGs from the EGAD00001008128 and SRP356151 datasets to identify overlapping genes. These overlapping genes were subsequently classified into two categories: IRH (immunotherapy response to Hypoxia) genes and HRH (Hypoxia-Regulated HIF-1α Pathway) genes.

3.1.5 Incorporating the treatment option of Bevacizumab into prediction models

The EGAD00001008128 dataset includes two immunotherapy strategies: monotherapy using Atezolizumab and combination therapy using Atezolizumab and Bevacizumab. Bevacizumab, a VEGF inhibitor, is significantly associated with tumor hypoxia characteristics, and its use has important implications for immunotherapy response [99]. Therefore, the treatment option of Bevacizumab was extracted from the clinical information of the dataset and categorized as a

binary feature into 1 indicating “used”, or 0 indicating “not used” for each case. This binary feature was then standardized together with the expression profiles in the training and test sets, as mentioned in 3.1.2.

3.1.6 Class Balancing of Training Set

Numerous studies have demonstrated that data with balanced classes can enhance the predictive performance of models. In the training set of the EGAD00001008128 dataset, the imbalance between the response class of 70 patients, and the non-response class of 180 patients was found. The Synthetic Minority Over-Sampling Technique (SMOTE) was used as a preliminary preprocessing step to balance the class distribution in the training set. The SMOTE technique considers the line segment between a data sample and one of its nearest neighbors in the minority class, i.e. response class in EGAD00001008128, and randomly selects a point on the line to create a new synthetic data sample. A data sample is regarded as the standardized gene expression profiles and treatment option of Bevacizumab. This technique increases the number of minority class data samples, ensuring that the synthesized samples can retain the characteristics of the original minority class samples and thus resemble them closely. The oversampled training set consists of 180 response samples and 180 non-response samples.

3.1.7 Development and Validation of Hypoxia Scoring Model Associated with Drug Response

Hypoxia-based risk score is defined as log hazard ratio of patient survival generated from Cox regression model on hypoxia-related and HCC signature genes. The score was validated using another RNA-seq dataset of cell line experiment unseen to the model.

To develop a novel hypoxia score model related to drug response, we utilized sample data (N=367) from the TCGA-LIHC FPKM dataset. Initially, we extracted the expression levels of IRH (immunotherapy response to Hypoxia) related genes and 9 genes from the initial hypoxia score model within this dataset. These gene expression data were then combined with the corresponding survival data. We employed the phreg function from the Statsmodels library to fit the proportional hazards regression model (Cox regression model). Using the Cox regression model, we calculated the regression coefficients for each gene, assessing the association between gene expression levels and patient survival time.

To validate the effectiveness of the hypoxia scoring model in assessing tumor hypoxia, we utilized the standardized GSE233802 dataset, which includes short-term and long-term hypoxic cell lines. To evaluate the tumor risk index under prolonged hypoxic conditions, we compared the hypoxia scores between datasets exposed to 0 hour, 24 hours and 48 hours of hypoxia. Given the challenge of

assessing the degree of internal hypoxia in solid tumors using existing clinical techniques, this model was employed to evaluate the hypoxia risk in different HCC patients within the standardized EGAD00001008128 dataset. The hypoxia risk scores were subsequently added to the feature columns for further analysis.

3.1.8 Establishing and Validation the KAN predictive model for immunotherapy response

The Minimum Redundancy Maximum Relevance (mRMR) feature selection algorithm was employed to prioritize genes based on their correlation with immunotherapy response, identifying the top 50 most relevant feature genes. To simplify the model and reduce overfitting, Stepwise Forward Selection was used to incrementally build the model by adding the most important feature genes, continuing until the genes with the strongest predictive power for immunotherapy response were selected.

The Kolmogorov-Arnold Network (KAN) is a neural network architecture based on the Kolmogorov-Arnold representation theorem. To ensure data quality, the distribution of the target data was analyzed using the Counter method. The feature genes from the training dataset, extracted using the mRMR algorithm, were converted into PyTorch Tensors using torch. Tensor to meet the requirements of deep learning. The KAN model was initialized by defining the model structure

parameters and loading pretrained model checkpoints. Predictions on the training data were made using the trained KAN model, with a classification threshold set at 0.5. The predicted results were converted from PyTorch Tensor format to NumPy arrays. By applying the threshold, the predicted probabilities were binarized to generate classification labels (0 for non-response and 1 for response). The accuracy score was used as the evaluation metric to calculate the prediction accuracy. The prediction scores were then added to a dataframe containing the original features and target classification labels for subsequent analysis and validation.

For the test dataset, the Bevacizumab usage was added as a binary feature, 0 or 1, and standardized using scaler. The processed data were then converted to PyTorch Tensors and input into the trained KAN model for prediction, and the prediction accuracy was calculated. Finally, the prediction scores were generated by the trained KAN model.

$$f(x) = f(x_1, \dots, x_n) = \sum_{j}^{m} \phi_{1,j} \left(\sum_{i}^{n} \phi_{0,j,i} \left(x_i \right) \right)$$

The model utilizes a double summation approach combined with various gene expression levels to predict the response to immunotherapy. The outer summation $\sum_j$ represents multiple predictors in the model, each transformed by the parameterized function $\phi_{1,j}$. The inner summation $\sum_j$ processes multiple gene

expression levels and Bevacizumab usage, x_1, x_2, …, x_n for each predictor, transforming and integrating these features through the function$\phi_{0,j,i}$. Ultimately, the model generates an overall prediction *f(x)* based on these transformed features, which is used to assess the likelihood of a patient's response to immunotherapy. This model enhances the accuracy and reliability of the prediction through a layered summation approach.

3.1.9 Training the Logistic Regression and SVM model for immunotherapy response prediction

Using the Logit function from the Statsmodels library, logistic regression models were fitted separately for the features extracted by the Kolmogorov-Arnold Network (KAN) and the hypoxia scores. After fitting the models, the predicted results were classified as integers (0 for non-response and 1 for response) and compared with the actual immunotherapy response classification labels to calculate the training set accuracy. The same features were used to predict the test set, and the test set accuracy was calculated to evaluate the model's effectiveness.

$$Z = \beta_0 + \beta_1 X_1 + \beta_2 X_2 + \ldots + \beta_p X_p$$

This formula represents the linear component of a logistic regression model, whereX_1, X_2, ..., X_p denote the extracted genomic features (KAN score and hypoxia scores), and Z represents the predicted outcome of immunotherapy

response. By applying weighted combinations of these genomic features, the model estimates the value of *Z*, which in turn predicts the probability of an immunotherapy response.

Combining features extracted from the KAN and hypoxia scores, a composite model training feature set was constructed. A Support Vector Machine (SVM) model with a radial basis function (RBF) kernel was employed for training, with model parameters set to 'gamma=0.2' and 'C=0.1'. Upon completion of the immunotherapy response prediction model training, the accuracy of the model on the training dataset was calculated. The same feature set was then used to predict the test dataset, and the accuracy on the test set was evaluated to assess the effectiveness of the composite model.

$$\varphi(x, x_c) = exp(-\frac{||x - x_c||^2}{2\sigma^2})$$

The variables x and x_c represent extracted genomic features, with the Euclidean distance $||x - x_c||$ measuring the similarity between a sample and a central feature x_c. The parameter σ controls the smoothness and spread of the RBF. This function maps genomic features into a higher-dimensional space, generating a value that

indicates the sample's position relative to the feature center, which may correspond to the characteristics of patients who respond to immunotherapy.

3.2 Results

3.2.1 Identification of IRH and HRH genes from public dataset

By setting the thresholds, q-value <0.05, FC > 1.999 (upregulation) and FC < 1/1.999 (downregulation) for the EGAD00001008128 dataset, 84 upregulated differentially expressed genes (DEGs) were identified, indicating differences in expression between HCC patients who respond to immunotherapy and those who do not. Given the substantial difference in the number of DEGs among the three groups, the overlap was adjusted to achieve greater significance. Based on previous studies, the GSE41666 dataset was adjusted to FC > 1.3202 (upregulation) and FC < 1/1.411 (downregulation), identifying 600 hypoxia-related genes (HRGs), including 300 upregulated genes and 300 downregulated genes, which demonstrated differential expression under hypoxic and normoxic conditions. By setting the threshold, q-value < 0.05 for the SRP356151 dataset, 171 DEGs were identified, including 127 upregulated and 44 downregulated, potentially related to HIF-1α and hypoxia pathways.

a

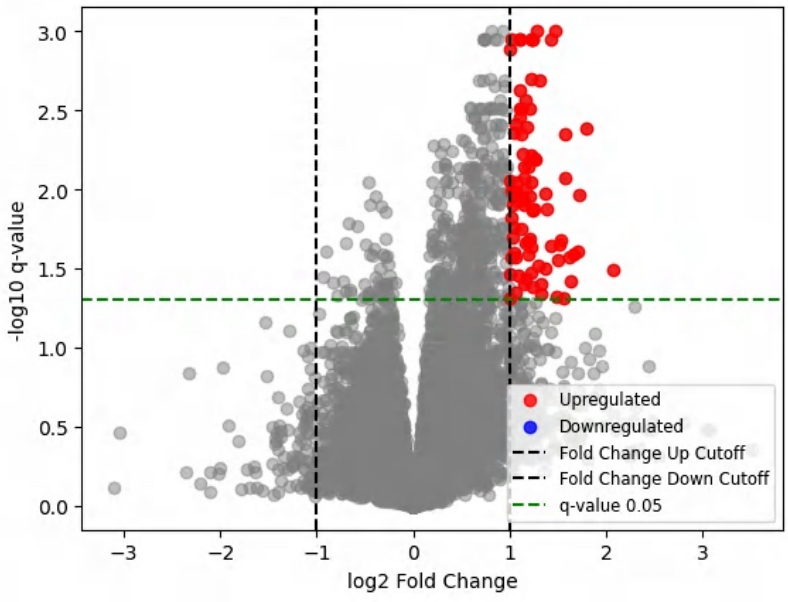
-log10 q-value
log2 Fold Change
Upregulated
Downregulated
Fold Change Up Cutoff
Fold Change Down Cutoff
q-value 0.05

b

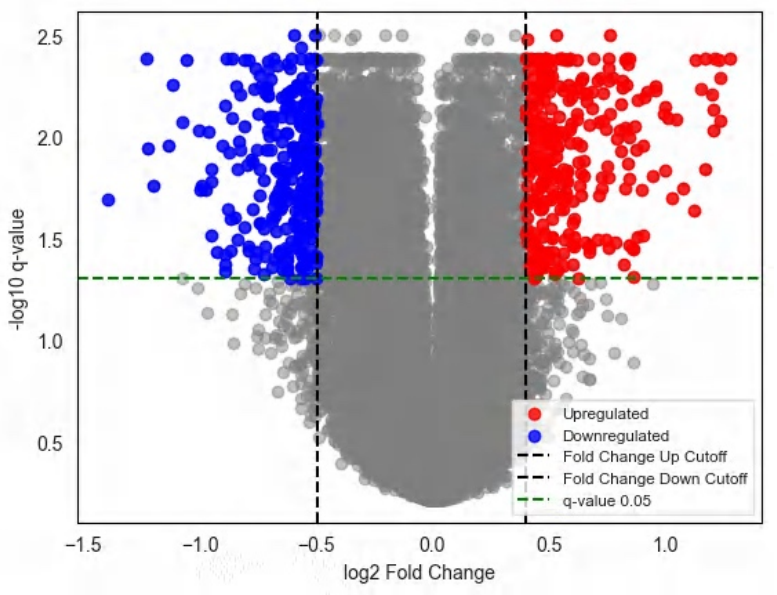
-log10 q-value
log2 Fold Change
Upregulated
Downregulated
Fold Change Up Cutoff
Fold Change Down Cutoff
q-value 0.05

c

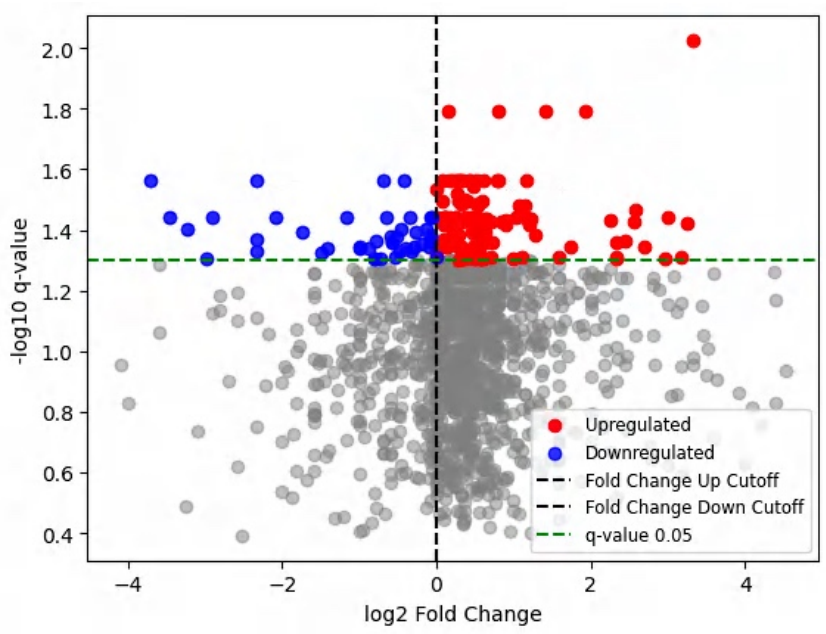

Figure 13. Identification of differential expression genes. (a) Volcano plot for EGAD00001008128; (b) Volcano plot for GSE41666; (c) Volcano plot for SRP356151.

In the EGAD00001008128 and GSE41666 datasets, 3 overlapping genes (p value=0.026), PMAIP1 (NOXA)，CD3D and CD2, were identified and classified as an immunotherapy response to Hypoxia (IRH) genes. Among them, the aberrant expression of PMAIP1 (NOXA) has been well-documented in various research to be associated with hypoxia. Additionally, analysis of the GSE41666 and SRP356151 datasets revealed 8 significantly overlapping genes (p value=0.0032), including SLC2A5, EGLN3, MXD1, STC1, TOR3A, TJP3, NEDD4L, and BNIP3L, which were classified as Hypoxia-Regulated HIF-1α Pathway (HRH) genes.

a

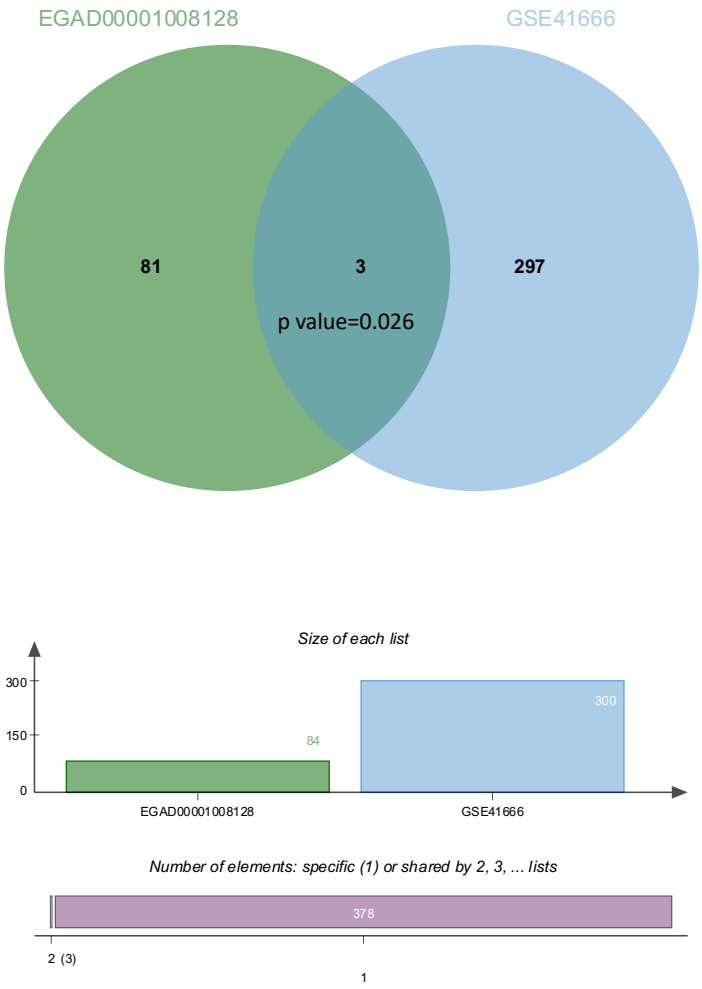
EGAD00001008128
GSE41666
81
3
297
p value=0.026
Size of each list
300
150
0
84
300
EGAD00001008128
GSE41666
Number of elements: specific (1) or shared by 2, 3, ... lists
378
2 (3)
1

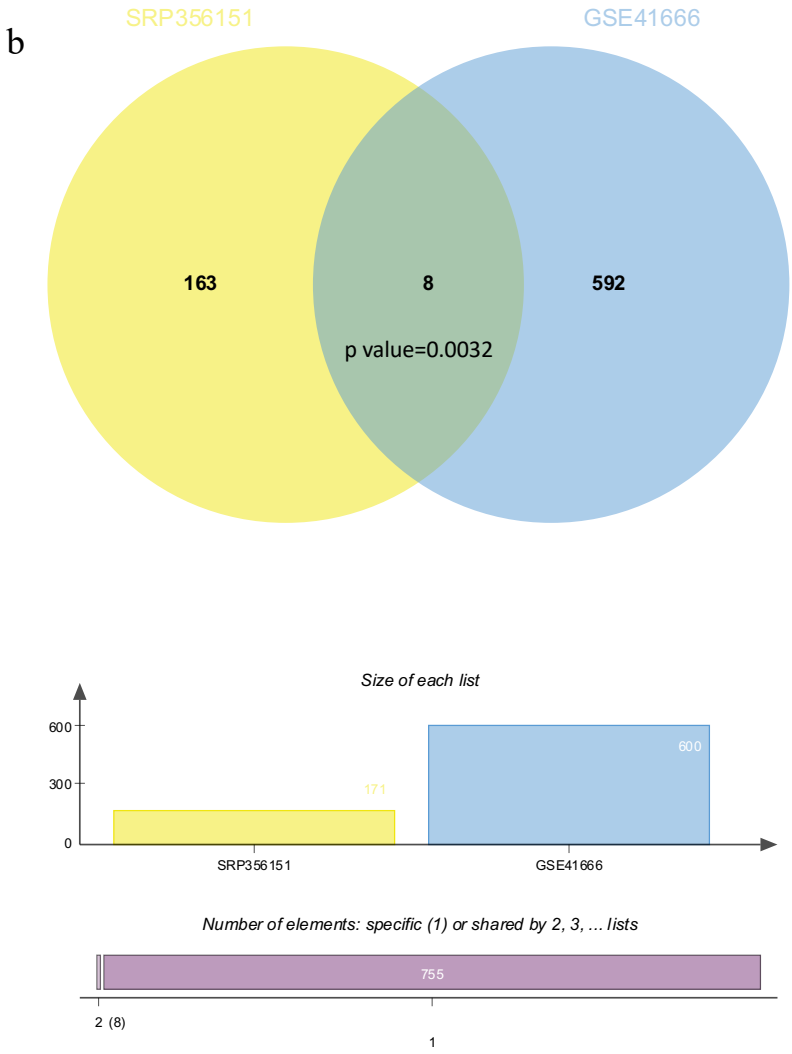

Figure 14. Identification of immunotherapy response to Hypoxia (IRH) genes and Hypoxia-Regulated HIF-1α Pathway (HRH) genes. (a) IRH genes: Overlapping DEGs between EGAD00001008128 and GSE41666 datasets; (b) HRH genes: Overlapping DEGs between GSE41666 and SRP356151 datasets.

Based on the enrichment method used in Chapter 2 by Shinygo platform, pathways were identified among the HRH genes. GO database enrichment analysis indicated that these genes were mainly involved in biological processes such as response to hypoxia, response to decreased oxygen levels, and adaptation to hypoxia. KEGG pathway enrichment analysis revealed that these genes were primarily enriched in pathways such as carbohydrate digestion and absorption, renal cell carcinoma, autophagy in animals, and tight junctions. Furthermore, in the hallmark Msigdb database, these genes were also enriched in pathways including angiogenesis, hypoxia, MTORC1 signaling, and glycolysis. EGLN3 expression level is associated with overall survival in liver cancer ($p = 6.5\times10^{-5}$) and eight genes except NEDD4L are significant associated with overall survival after pan-cancer immunotherapy.

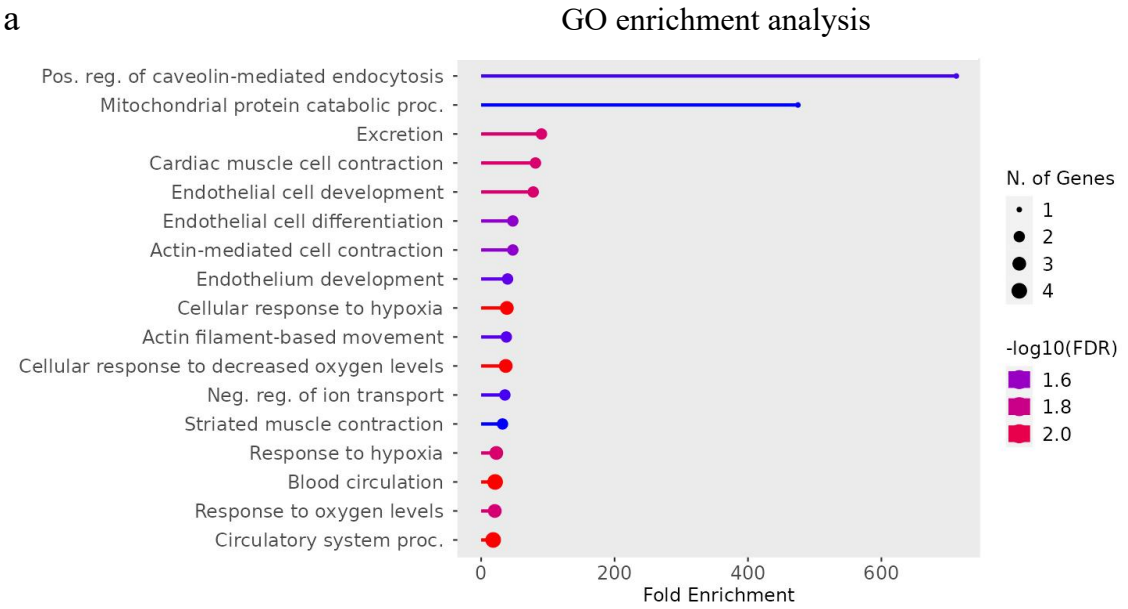

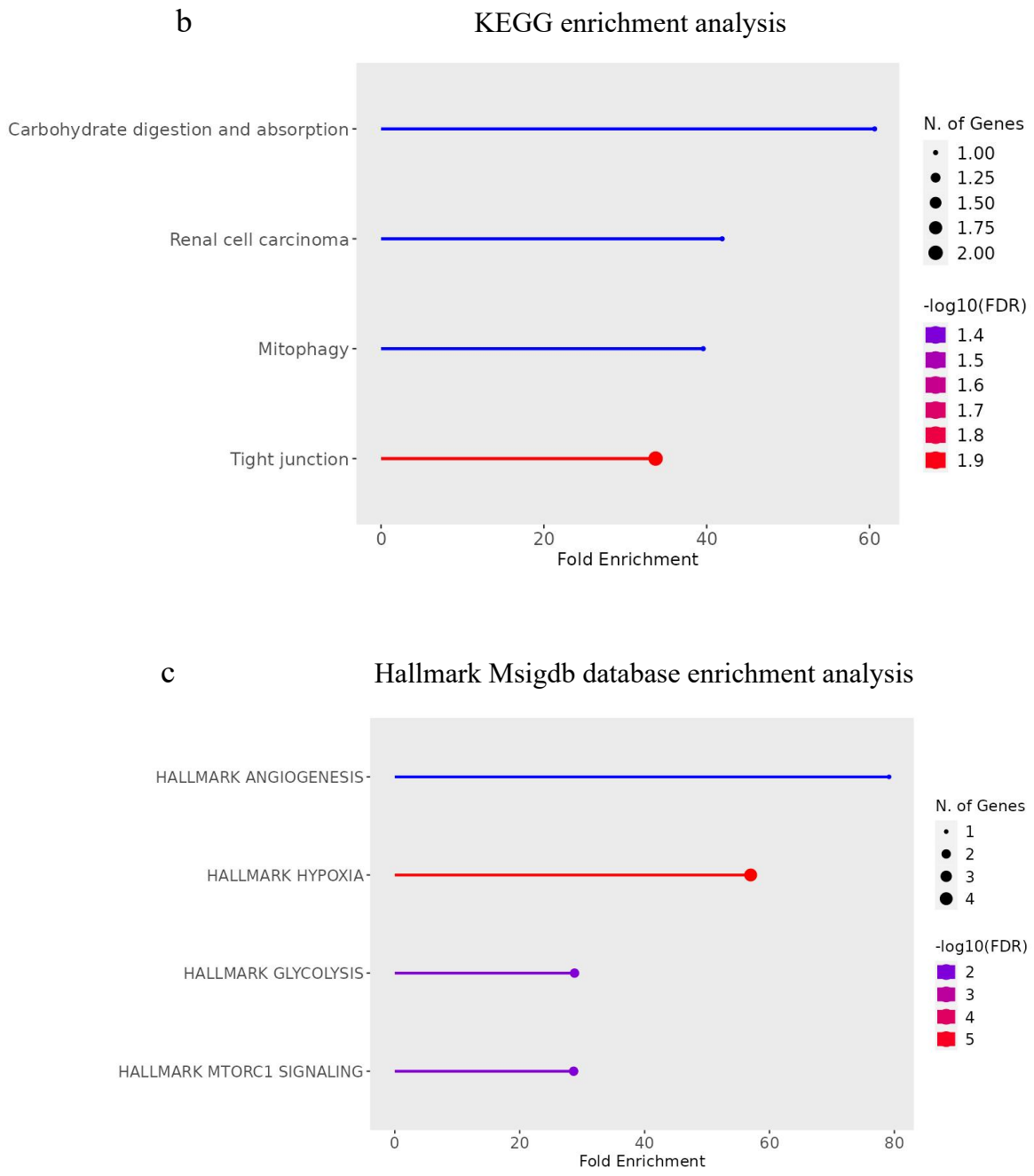

Figure 15. Enrichment analysis of HRHs. (a) GO enrichment analysis; (b) KEGG enrichment analysis; (c) Hallmark Msigdb database enrichment analysis.

3.2.2 Identification of Hypoxia Scoring Model Associated with Drug Response

Based on an initial hypoxia risk scoring model that included 9 characteristic genes and IRH genes, a hypoxia risk scoring model associated with predicting drug response was constructed through a COX analysis of the TCGA-LIHC dataset. This model was developed by creating a weighted combination of the variables, where each gene variable in the formula is preceded by a coefficient representing its impact on survival time. A positive coefficient indicates that the variable increases risk, while a negative coefficient suggests that the variable decreases risk. The model was subsequently applied to the GSE233802 dataset, which includes HepG2 cell lines subjected to 0h, 24h, and 48h of hypoxia. Hypoxia risk scores were calculated for the cell lines at different hypoxia durations, and a T-test yielded p-values of less than 0.02. In this dataset, the risk scores for HepG2 cell lines exposed to 48h of hypoxia were higher than those exposed to 24h, while the risk scores at 0h were higher than those at 24h. These results indicate that during the early stages of hypoxia, tumor cells experience a relative reduction in risk due to a slowdown in proliferation caused by transient oxygen deprivation. However, after prolonged hypoxia, the risk index significantly increases. This model demonstrates superior capability in assessing the hypoxia risk characteristics within tumors.

$$h(t|X) = h0(t)exp(0.1497 \times PHLDA2 + 0.0757 \times DLGAP5 - 0.2318 \times N4BP2L1 + 0.0990 \times CENPA - 0.0584 \times UPB1 + 0.1509 \times CABYR - 0.0022 \times AFM + 0.3139 \times HMMR + 0.0587 \times KIF20A - 0.1203 \times PMAIP1)$$

The formula represents a linear combination of gene expression levels and their corresponding regression coefficients, where each gene's expression is weighted to predict its contribution to hypoxia risk. The genes included in this model are PHLDA2, DLGAP5, N4BP2L1, CENPA, UPB1, CABYR, AFM, HMMR, KIF20A, and PMAIP1. The expression value of each gene is weighted by its respective regression coefficient, determining the sample's hypoxia risk score.

Table 1. Cox Regression Analysis for the Hypoxia Risk Scoring Model related to Drug Response Prediction

Gene	log HR	log HR SE	HR	t	p	95% CI Lower	95%CI Upper
PHLDA2	0.1497	0.0753	1.1615	1.9887	0.0467	1.0022	1.3462
DLGAP5	0.0757	0.2695	1.0787	0.281	0.7787	0.636	1.8293
N4BP2L1	-0.2318	0.1636	0.7931	-1.4163	0.1567	0.5755	1.093
CENPA	0.099	0.227	1.104	0.4361	0.6628	0.7076	1.7226
UPB1	-0.0584	0.0725	0.9433	-0.8061	0.4202	0.8184	1.0872
CABYR	0.1509	0.0752	1.1629	2.0063	0.0448	1.0035	1.3476
AFM	-0.0022	0.0609	0.9978	-0.0368	0.9707	0.8856	1.1242
HMMR	0.3139	0.1889	1.3687	1.6618	0.0965	0.9452	1.982
KIF20A	0.0587	0.2379	1.0604	0.2465	0.8053	0.6652	1.6904
PMAIP1	-0.1203	0.1857	0.8866	-0.648	0.517	0.6162	1.2758

Table 2. Hypoxia Risk Scores in the GSE233802 Dataset.

Sample name	Hypoxia risk score	Hypoxia duration
SRR24775098	0.048819	0h
SRR24775099	0.042419	0h
SRR24775100	0.601232	0h
SRR24775095	-0.618357	24h
SRR24775096	-0.99101	24h
SRR24775097	-0.600739	24h
SRR24775092	0.786606	48h
SRR24775093	0.411489	48h
SRR24775094	0.319541	48h

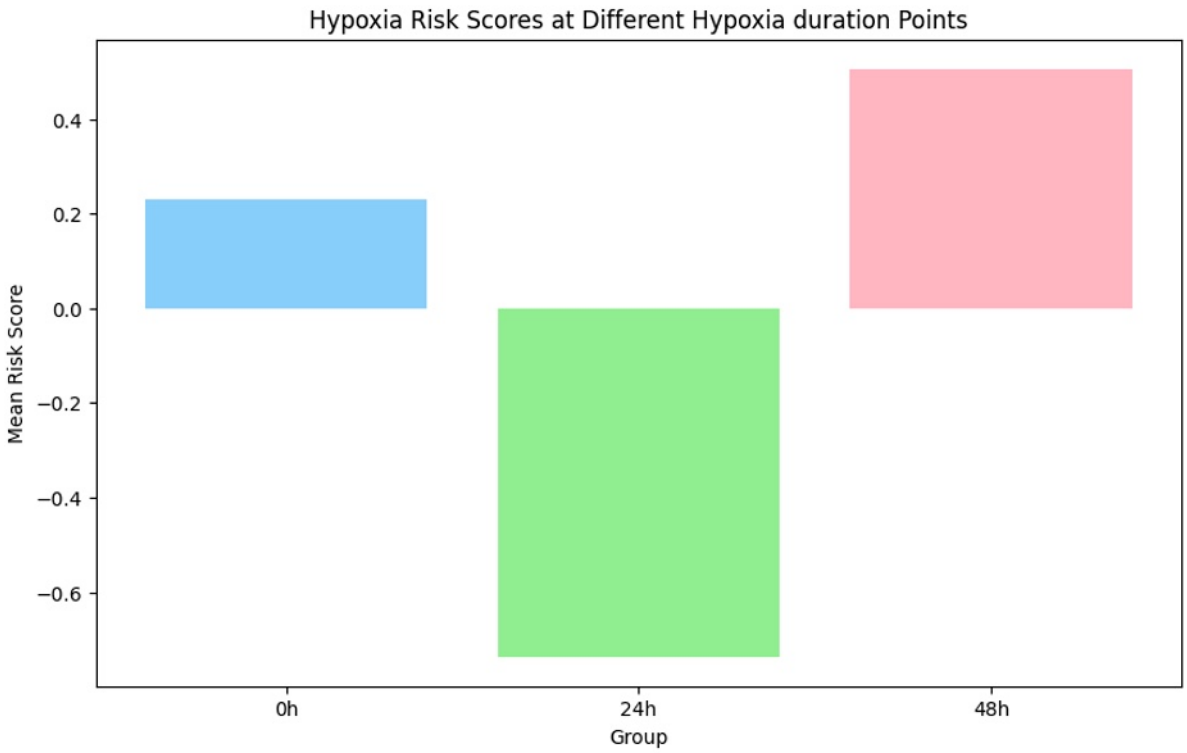

Figure 16. Mean hypoxia risk scores of HepG2 cell lines at different hypoxia durations (0h, 24h, 48h) from the GSE233802 dataset.

3.2.3 KAN predictive model

The algorithmize derivation and computational implementation of mRMR feature selection and KAN model training were adopted from the work of Chief Supervisor. Using the mRMR algorithm, genes were prioritized in descending order of inter-redundancy and ascending order of relevancy to immunotherapy response, 11 genes mostly relevant to predicting immunotherapy response (TLR8, SCHIP1, ZNF729, ATG9B, BAMBI, OXSR1, ZNF564, CCR8, ADAM23, RRN3P3_1, and RDH14) were selected from the EGAD00001008128 dataset. A training dataset was constructed by combining these 11 selected genes with the Bevacizumab usage as features. The features and labels of both the training and validation sets were converted into PyTorch 2.6 tensors, and the missing and undefined values were checked to ensure data integrity. The KAN model was used for training, with the model structure comprising input, hidden, and output layers with dimensions corresponding to the number of input features. The classification threshold of the output score for predicting immunotherapy response in the training set was set at 0.5, and the predicted results were binarized. The training set's prediction accuracy was 0.9361, indicating that the KAN model performed well on the training data and could effectively conduct binary classification predictions.

The trained KAN model was used to predict the test dataset, with the classification threshold similarly set at 0.5. The prediction accuracy for the test set was 0.7,

further validating the model's effectiveness. The prediction results (KAN score) for both the training and test datasets were added to the feature columns for subsequent analysis and validation of the model's predictive capability.

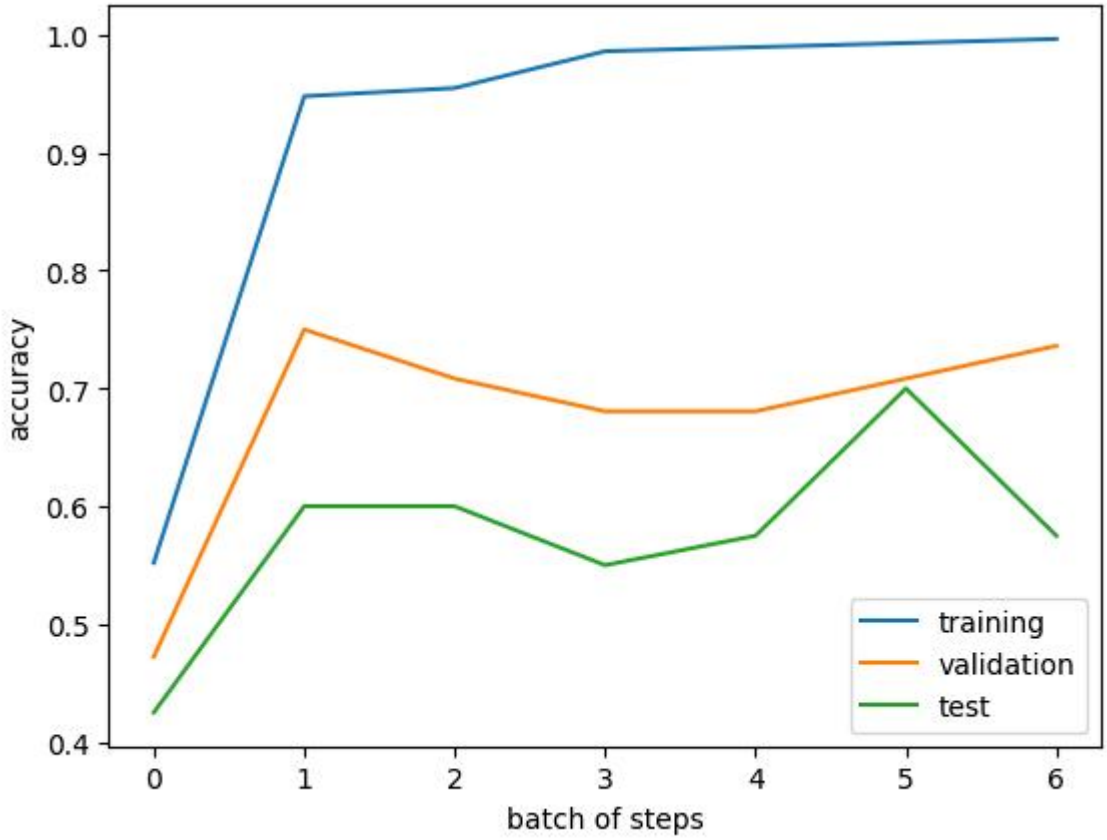

Figure 17. Accuracy comparison of the KAN model across training, validation, and test datasets after applying the mRMR algorithm to select 11 feature genes.

3.2.4 Logistic regression Model

To enhance model performance and interpretability, the output scores from the trained KAN model were used as input features for traditional machine learning models. The KAN scores represent immune-related gene expression patterns, while the hypoxia risk score reflects the tumor microenvironment. Combining these two factors helps capture both immune and hypoxia-related mechanisms, improving the predictive accuracy of the final model.

A logistic regression model was trained using the KAN score to classify immunotherapy response in the EGAD00001008128 dataset. The training set comprised the KAN score and immunotherapy response classification labels. The fitted logistic regression model achieved a training accuracy of 0.9361. Evaluation on the test set yielded an accuracy of 0.7. The logistic regression summary indicated that the KAN score had a significant positive coefficient of 4.5581 ($p < 0.001$), demonstrating a strong association with immunotherapy response classification. The model successfully converged after 7 iterations, with a final function value of 0.322704 and a pseudo-R-squared value of 0.5344, indicating a good fit to the data.

Table 3. Logistic Regression Summary for KAN Score

Feature	coefficient	std err	z	p	95%CI Lower	95%CI Upper
KAN score	4.5581	0.382	11.942	0	3.81	5.306

A logistic regression model was trained using the Hypoxia score to classify immunotherapy response in the EGAD00001008128 dataset. The training set comprised the Hypoxia score and immunotherapy response classification labels. The fitted logistic regression model achieved a training accuracy of 0.5417. Evaluation on the test set yielded an accuracy of 0.525. The logistic regression summary indicated that the Hypoxia score had a significant positive coefficient of 0.3903 ($p = 0.026$), demonstrating a strong association with immunotherapy response classification. The model successfully converged after 4 iterations, with a final function value of 0.6861 and a pseudo-R-squared value of 0.0102. These results suggest that, although the Hypoxia score has limited predictive power in distinguishing between different immunotherapy response categories, it still holds statistical significance.

Table 4. Logistic Regression Summary for Hypoxia score

Feature	coefficent	std err	z	p	95%CI Lower	95%CI Upper
Hypoxia score	0.3903	0.176	2.22	0.026	0.046	0.735

A logistic regression model was trained using the immunotherapy response to Hypoxia (IRH) PMAIP1 (NOXA) gene expression feature to classify immunotherapy response in the EGAD00001008128 dataset. The training set comprised the PMAIP1 (NOXA) expression feature and immunotherapy response classification labels. The fitted logistic regression model achieved a training accuracy of 0.5972. Evaluation on the test set yielded an accuracy of 0.525. The logistic regression summary indicated that the PMAIP1 (NOXA) expression feature had a coefficient of 0.5972 ($p < 0.001$), demonstrating significant association with immunotherapy response classification. The model successfully converged after 6 iterations, with a final function value of 0.6666 and a pseudo-R-squared value of 0.0383. These results suggest that the PMAIP1 (NOXA) expression feature has strong predictive power in distinguishing between different immunotherapy response categories, holding statistical significance.

Table 5. Logistic Regression Summary for PMAIP1 (NOXA)

Feature	coefficient	std err	z	p	95%CI Lower	95%CI Upper
PMAIP1	0.5972	0.159	3.757	<0.001	0.286	0.909

A logistic regression model was trained using the KAN score, PMAIP1 (NOXA), and Hypoxia scores to classify immunotherapy response. The training set

comprised these features and immunotherapy response classification labels. The fitted logistic regression model achieved a training accuracy of 0.9389. Subsequently, the same model was evaluated on the test set, yielding a test accuracy of 0.7. The logistic regression summary indicated that the KAN score had a coefficient of 4.5237 ($p < 0.001$), the PMAIP1 (NOXA) had a coefficient of 0.1573 ($p = 0.467$), and the Hypoxia score had a coefficient of 0.5031 ($p = 0.081$). These results (Figure 18) suggest that the KAN score has significant predictive power in distinguishing between different immunotherapy response categories, whereas the predictive power of the PMAIP1 (NOXA) and Hypoxia scores is relatively weaker. The model successfully converged after 7 iterations, with a final function value of 0.3174 and a pseudo-R-squared value of 0.5421, indicating a good fit to the data. These findings demonstrate the effectiveness of the combined features in classifying immunotherapy responses.

Table 6. Logistic Regression Summary for KAN score, PMAIP1 (NOXA), and Hypoxia score

Feature	coefficient	std err	z	p	95%CI Lower	95%CI Upper
KAN score	4.5237	0.393	11.5	0	3.753	5.295
PMAIP1	0.1573	0.216	0.727	0.467	-0.267	0.581
Hypoxia score	0.5031	0.288	1.747	0.081	-0.061	1.068

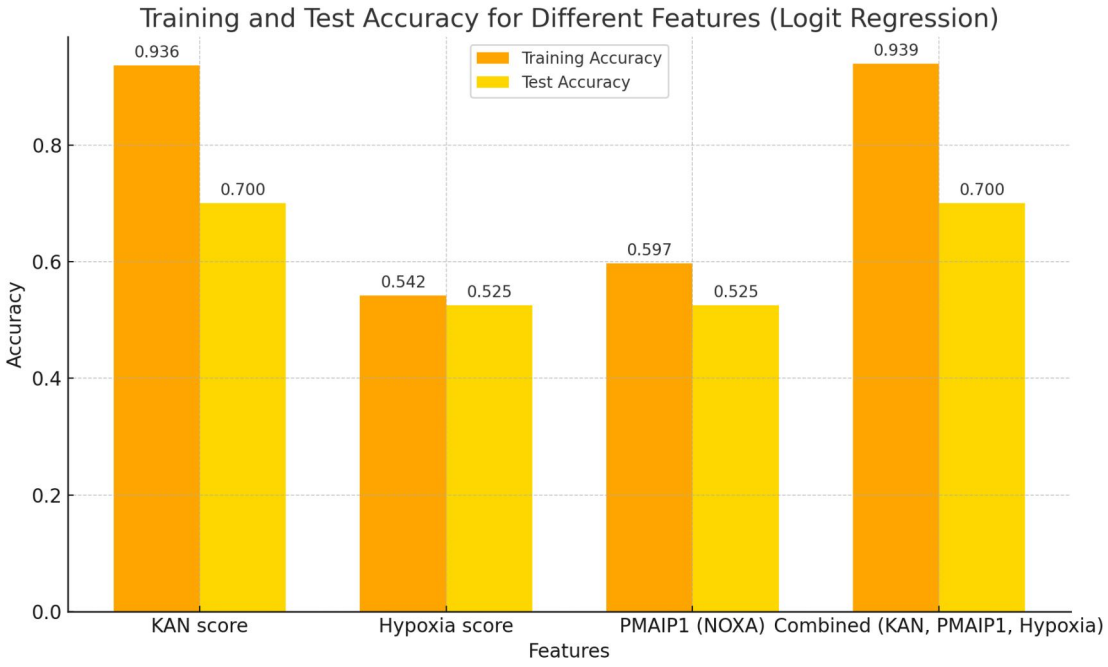

Figure 18. Training and Test Accuracy for Different Features in Logit Regression Model

3.2.5 SVM Model

A support vector machine (SVM) model was trained using the KAN score and Hypoxia scores to classify immunotherapy response in the EGAD00001008128 dataset. The training set comprised these two features and immunotherapy response classification labels. The fitted model achieved a training accuracy of 0.9361. The same model was evaluated on the test set, yielding a test accuracy of 0.725. The SVM model employed a radial basis function (RBF) kernel with parameters gamma=0.2 and C=0.1. The model successfully converged, indicating that the KAN score and Hypoxia scores have strong predictive power in distinguishing between different immunotherapy response categories, with statistical significance. Furthermore, an SVM model was trained using the KAN score, PMAIP1 (NOXA), and Hypoxia scores to classify immunotherapy response. The training set comprised these three features and immunotherapy response classification labels. The fitted model, when evaluated on the test set, achieved an accuracy of 0.7. The SVM model again employed an RBF kernel with parameters gamma=0.2 and C=0.1. When using only the KAN score and PMAIP1 (NOXA), the SVM model also yielded a test accuracy of 0.7. The results were shown in Figure 19.

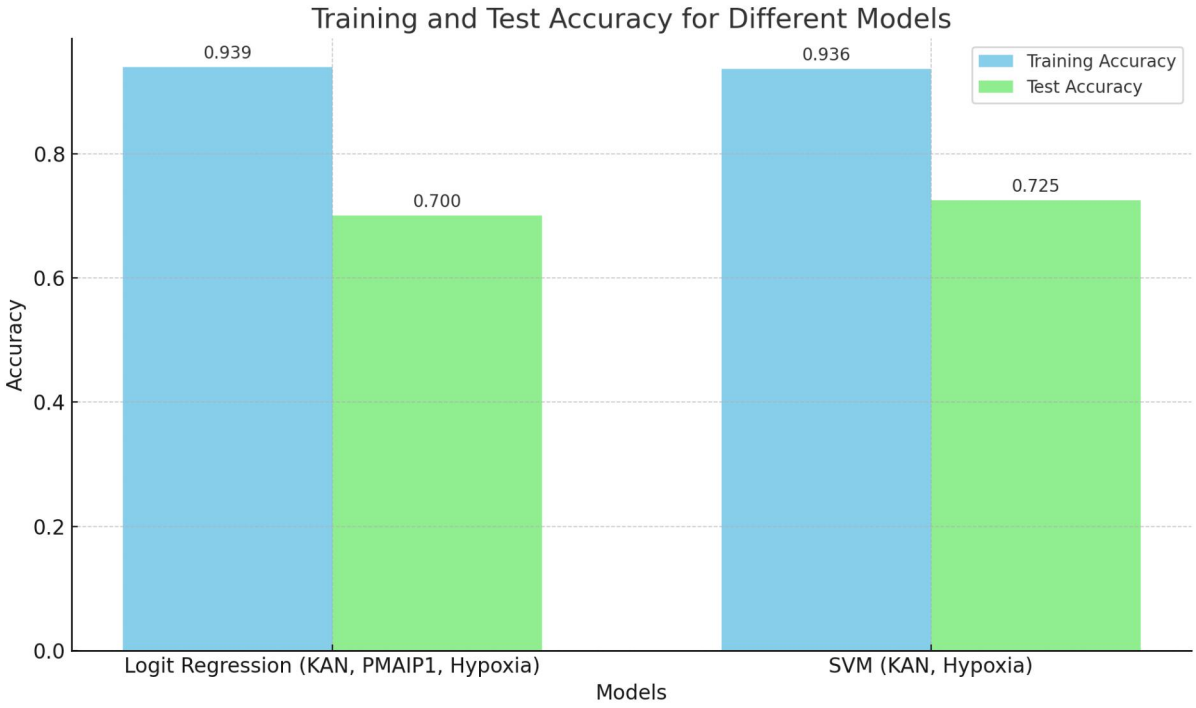

Figure 19. Training and Test Accuracy for Different Features in Logit Regression and SVM Model

3.3 Discussion and Conclusion

In recent years, the application of machine learning and deep learning in the medical field, particularly in oncology research, has seen significant advancements. These technologies enable the extraction of a vast array of genomic features and the uncovering of deeper layers of data, facilitating the quantitative translation of microscopic changes in genes or proteins within tumors. This capability allows for the visualization of tumor heterogeneity and the early prediction of treatment outcomes. Consequently, assessing the likelihood of an immunotherapy response to therapy in HCC patients prior to treatment could enable effective risk stratification. Such an approach would allow for the identification of patients likely to benefit from immunotherapy, while also identifying those unlikely to respond, thereby preventing ineffective treatments, conserving resources and financial costs, and avoiding the adverse effects of immunotherapy that could potentially exacerbate disease progression.

In this chapter, we established an HCC immunotherapy response prediction model using the EGAD00001008128 dataset, which is based on patient responses to immunotherapy, and datasets of hypoxia HepG2 cell lines (GSE41666, GSE233802, and SRP356151). In the initial hypoxia risk scoring model developed in the chapter 2, we identified 9 feature genes. To enhance the accuracy of predicting immune therapy responses, we applied bioinformatics and machine learning techniques to process the EGAD00001008128 dataset. We identified

three differentially expressed overlapping genes associated with immunotherapy response and hypoxia characteristics, among which the abnormal expression of PMAIP1 (NOXA) under hypoxic tumor microenvironment has been well-documented in the literature. Under hypoxic tumor microenvironment, tumor cells typically activate HIF-1α, which binds to the promoter region of the PMAIP1 (NOXA) gene, thereby promoting its transcription and expression. This mechanism leads to the upregulation of PMAIP1 (NOXA) in the hypoxic tumor microenvironment, contributing to signaling pathways that slow cancer cell proliferation, allowing them to adapt to hypoxia and develop resistance to treatment. Consequently, we incorporated PMAIP1 (NOXA) into the hypoxia risk scoring model associated with predicting immunotherapy response. Cox regression analysis was performed on the TCGA-LIHC database to derive the risk coefficient for each feature gene. The new hypoxia scoring model was thoroughly validated in the GSE233802 dataset across different hypoxia duration in HepG2 cell lines. It was found in the cultured HCC cells that the score was positively associated with the hypoxia duration of the incubated culture environment. Regarding 0h as the reference condition, the prolonged hypoxic condition of 48h induced more malignant HCC cells than that of 24h. This finding supports that the hypoxic condition of the tumor microenvironment affects the tumor malignancy and the patient survival.

To optimize the immune therapy response prediction model, we used machine

learning in combination with deep learning to extract high-level features from the EGAD00001008128 dataset. Using the mRMR algorithm, we selected 11 genes most strongly associated with immunotherapy response and employed SMOTE to address the imbalance in the training data, thereby enhancing the model's predictive performance. Compared to traditional deep learning algorithms, the KAN model performs better on small sample datasets, making it well-suited for handling high-dimensional gene expression data while mitigating the risk of overfitting. We trained the KAN model using the 11 selected feature genes along with the Bevacizumab feature and validated it on the test set. The constructed prediction model achieved an accuracy of 0.9361 in the training set and 0.7 in the test set, with each clinical sample receiving a corresponding KAN score.

Based on the KAN score, the hypoxia risk score, and the PMAIP1 (NOXA), we constructed logistic regression and SVM models. Ultimately, the SVM model incorporating both the KAN score and the hypoxia risk scores achieved an accuracy of 0.725 in the test set, demonstrating better predictive performance than the logistic regression model and the standalone KAN model. This indicates that the new hypoxia risk score based on PMAIP1 (NOXA) significantly enhances the predictive accuracy of the immunotherapy response model. These findings suggest that hypoxia plays a crucial role in the tumor microenvironment and immunotherapy response. Prolonged hypoxia in the tumor microenvironment alters proliferative signaling pathways in cancer cells, suppresses immune system

function, and significantly increases the risk level for tumor patients. As a result, this condition is more likely to lead to non-responsiveness to immune therapy or failure to achieve partial response criteria, and it may also exacerbate tumor progression.

This work employed bioinformatics, machine learning, and deep learning methodologies to extract and analyze multiple genomic features for predicting immune therapy response in HCC patients. The results met the expected outcomes, enabling risk stratification based on hypoxia characteristics, which can further guide the selection of immunotherapeutic agents and improve clinical treatment strategies.

Chapter 4 The Role of NOXA in the resistance of PD-L1 inhibitors in HCC via Hypoxia-related pathways

Background

Through the bioinformatics and deep learning analysis, PMAIP1 (NOXA) was identified in Chapter 3 as one of the differentially expressed genes associated with both immunotherapy response and hypoxia characteristics. Such abnormal expression of NOXA under the hypoxic tumor microenvironment has been well-documented in the literature. This chapter aims to verify the role of NOXA in the PD-L1 inhibitor resistance in HCC under hypoxic conditions.

4.1 Materials and Methods

4.1.1 Cell Lines

In this study, the HCC cell line (HepG2) and the human T lymphocyte cell line (Jurkat T) were used. Both cell lines were obtained from the Chinese Academy of Sciences Cell Bank. The HepG2 cell line was maintained in Dulbecco's Modified Eagle Medium (DMEM) supplemented with 10% fetal bovine serum (FBS) and 1% penicillin-streptomycin, while the Jurkat T cell line was cultured in RPMI-1640 medium with 10% FBS and 1% penicillin-streptomycin. All cell cultures were maintained in an incubator at 37°C with 5% CO_2.

4.1.2 Establishment of Hypoxia-Induced Potentially Resistant Cell Lines

On the first day, 1.2 x 10^7 Jurkat cells were cultured in RPMI-1640 medium containing 10% heat-inactivated FBS, P/S, and 2 mM L-glutamine, and activated with 2 μg/mL PHA for 48 hours. Concurrently, HepG2 cells were trypsinized and labeled with CellTrace reagent at a ratio of 1:1000, with a cell concentration of 1 x 10^6 cells/mL, incubated at 37°C for 30 minutes. A minimum of 3 x 10^6 HepG2 cells were required. Subsequently, an additional 2x volume of medium (DMEM + 10% FBS + P/S) was added, and the cells were incubated for 5 minutes, then centrifuged, and the supernatant was discarded. The CellTrace-stained HepG2 cells were then resuspended and seeded into 6-well plates at a density of 2 x 10^5 cells/well. Due to the potential toxicity of CellTrace reagent, which may kill some HepG2 cells during staining, it is crucial to recount the live cells before seeding into the plates. On the second day, the medium of the HepG2 cells was refreshed (DMEM + 10% FBS + P/S) and treated with 10 ng/mL IFN-γ and 200 μM $CoCl_2$ for 24 hours. On the third day, Jurkat cells were collected and washed twice with PBS to remove PHA, then resuspended in RPMI-1640 medium containing 10% heat-inactivated FBS, P/S, and 2 mM glutamine. Simultaneously, the medium of HepG2 cells was refreshed with DMEM + 10% FBS + P/S + 200 μM $CoCl_2$ + PD-L1 inhibitor (PD-L1i, atezolizumab biosimilar: Cat. SIM0009). For each well, 2 x 10^6 Jurkat cells were added to the HepG2 culture (or medium without cells as a control for HepG2 only) for 48 hours, ensuring a ratio of 10:1. Finally, the medium containing Jurkat T cells was removed and washed with PBS. HepG2

cells were cultured in cycles following the above steps. The workflow of cell co-culture and the layout of the 6-well plate are shown in Figure 20.

a

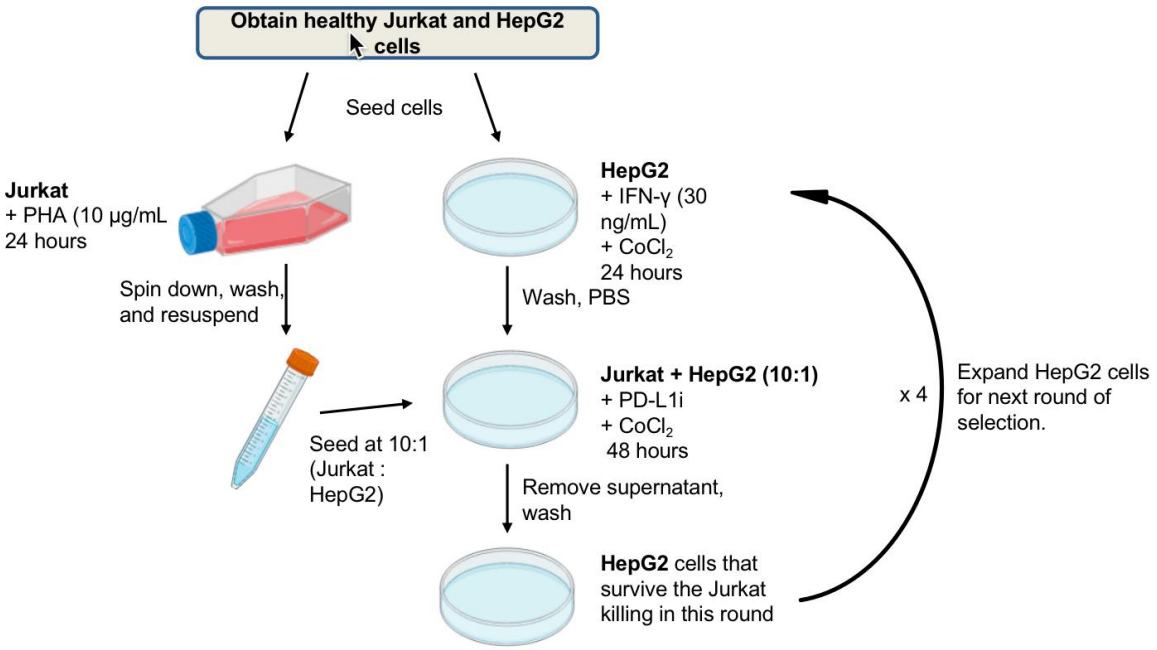

b

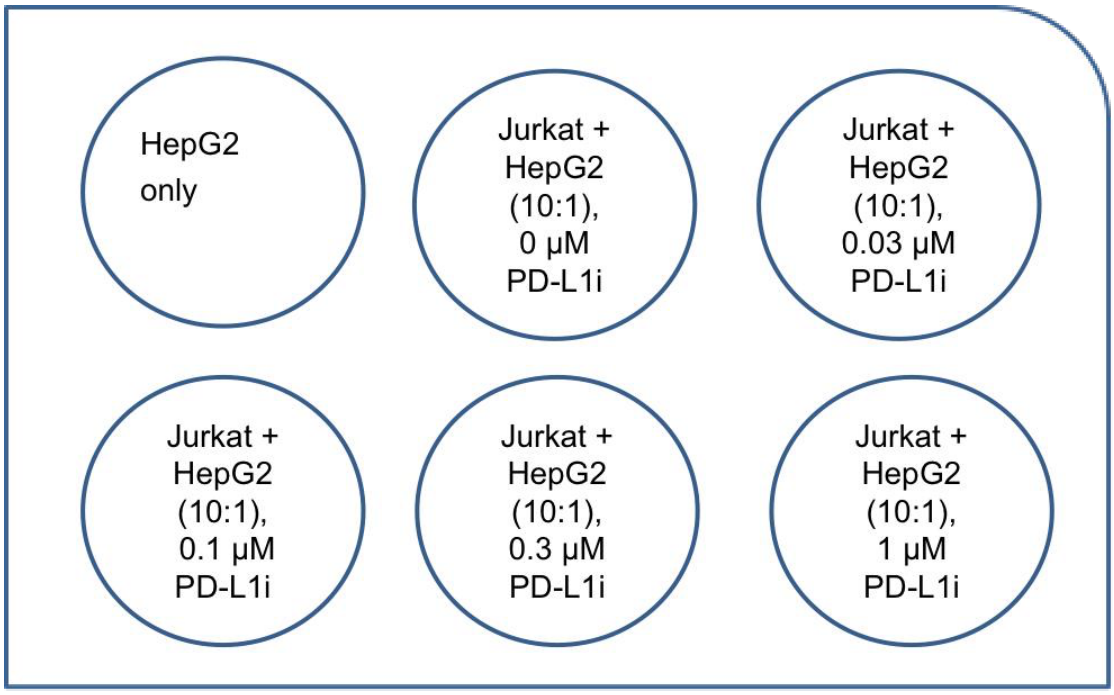

Figure 20. HepG2 Co-culture experiments (a) Flowchart of HepG2 Co-culture workflow; (b) 6-well Plate layout for the co-culture experiment (performed in duplicate, 12 samples in total).

4.1.3 NOXA Gene Knockdown in Hypoxia-Induced Resistant Cells and Co-Culture

To establish NOXA-knockdown HepG2-4-Rounds cell lines, cells were seeded at a density of 2×10^5 cells per well in a 6-well plate. After 24 hours of incubation at 37°C with 5% CO_2, cells were transfected with small interfering RNAs (siRNAs) targeting NOXA (siNOXA1, siNOXA2, siNOXA3, and siNOXA4, purchased from Jima Company) using Lipofectamine 3000 (Thermo Fisher Scientific). The siRNA stock solutions were prepared by dissolving the lyophilized siRNAs in RNase-free water to a working concentration of 100 nM. For transfection, 20 nM siRNA was mixed with Opti-MEM medium (Thermo Fisher Scientific) and incubated with Lipofectamine 3000 at room temperature for 20 minutes.

Following complex formation, the existing medium in each well was carefully removed, and the siRNA-Lipofectamine complexes were added to the wells containing complete medium. Cells were incubated for 6 hours, after which the medium was replaced with conditioned medium. As a negative control, cells were transfected with scrambled siRNA, while untreated cells served as a blank control. Transfection efficiency was assessed using Western blotting and reverse transcription quantitative PCR (RT-qPCR) to ensure suitability for subsequent co-culture experiments. The experimental method was the same as in 4.1.2. The experimental workflow diagram is shown in Figure 21.

a

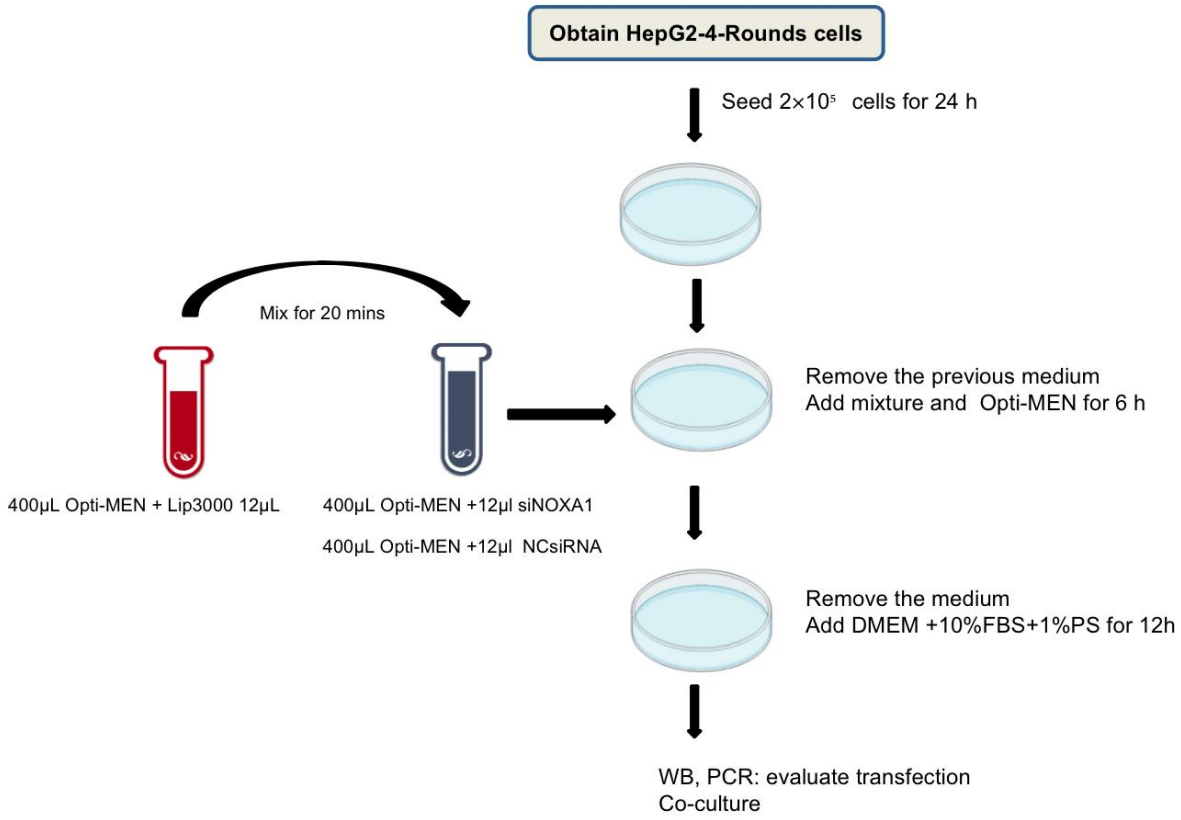
Obtain HepG2-4-Rounds cells
Seed 2×10⁵ cells for 24 h
Mix for 20 mins
400μL Opti-MEN + Lip3000 12μL
400μL Opti-MEN +12μl siNOXA1
400μL Opti-MEN +12μl NCsiRNA
Remove the previous medium
Add mixture and Opti-MEN for 6 h
Remove the medium
Add DMEM +10%FBS+1%PS for 12h
WB, PCR: evaluate transfection
Co-culture

b

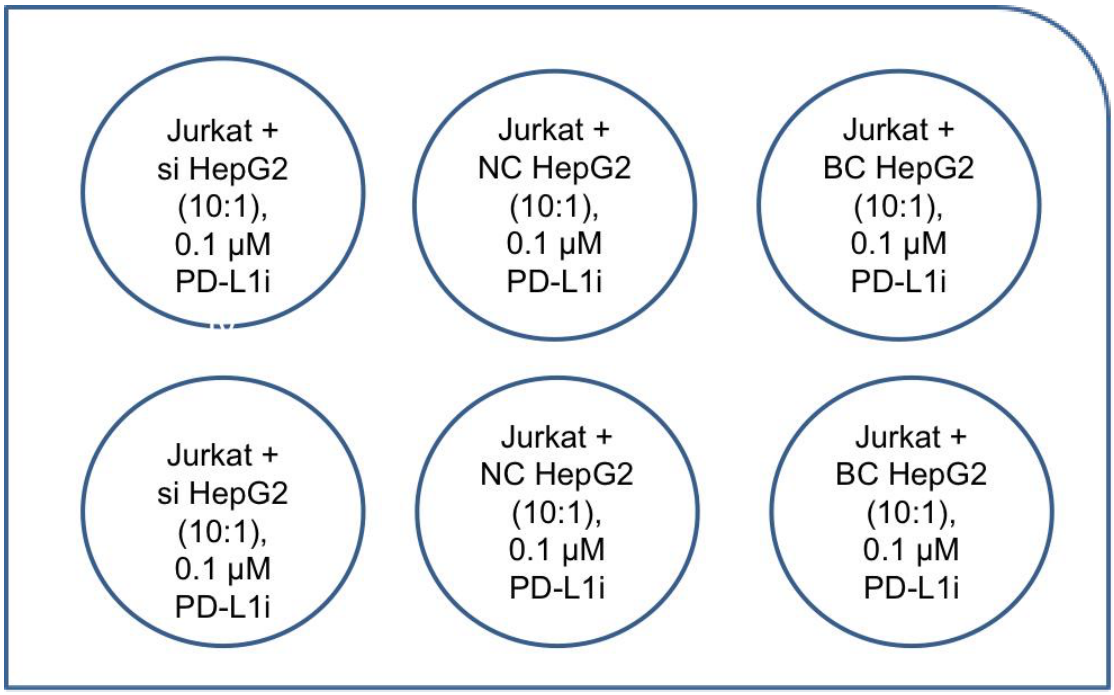

Figure 21. NOXA knockdown by transfection and co-culture experiments in HepG2-4-Rounds cells (a) Workflow of NOXA knockdown by transfection; (b) 6-well Plate layout for the co-culture experiment (performed in triplicate, 9 samples in total)

4.1.4 Western Blotting

Cells were lysed using RIPA buffer containing a protease inhibitor cocktail (Thermofisher Scientific). A total of 100 μL RIPA buffer was added to each well, and the lysate was collected into 1.5 mL EP tubes after scraping. Protein concentration was determined using a Quick BCA Protein Assay Kit (Thermofisher Scientific). After adjusting protein concentrations, lysates were mixed with loading buffer and heated at 98°C for 10 minutes for denaturation. The denatured proteins were stored at -80°C until further use.

Protein samples were loaded onto SDS-PAGE gels and separated by electrophoresis at 120 V. The separated proteins were transferred onto a polyvinylidene difluoride (PVDF) membrane at 250 mA for 90 minutes. The membrane was blocked with 5% skim milk in TBST (1% Tween 20 in TBS) for 1 hour. Primary antibodies were diluted according to the manufacturer's recommendations and incubated with the membrane overnight at 4°C. After three washes with TBST, the membrane was incubated with HRP-conjugated secondary antibodies (anti-rabbit or anti-goat) at room temperature for 1 hour. Finally, protein bands were visualized using a high-sensitivity ECL detection reagent (Millipore).

4.1.5 RT-qPCR

RNA concentration was measured using a Thermo Fisher Scientific NanoDrop 2000C spectrophotometer. Complementary DNA (cDNA) synthesis was performed using a reverse transcription kit from Takara Bio (Tokyo, Japan) in an Applied Biosystems Veriti 96-well thermal cycler. The reaction conditions were set as follows: reverse transcription at 37°C for 15 minutes, followed by heat inactivation at 85°C for 5 seconds. The final product was stored at 4°C.

Quantitative PCR (qPCR) was conducted using the Applied Biosystems 7500 Real-Time PCR System (Thermo Fisher Scientific) with Roche SYBR Green PCR Master Mix (Baden-Württemberg, Germany). Primer sequences are listed in Table 8. All experiments were performed in triplicate, with no-template negative controls included.

Table 7. The sequences of primers.

Gene	Forward Primer (5-3′)	Reverse primer (5- 3′)
NOXA	CAGAGCTGGAAGTOGAGT GTGC	TGCAGTCAGGTTCCTGAG CAGA
β-actin	AGGATTCCTATGTGGGCGA C	ATAGCACAGCCTGGATAG CAA

4.1.6 Flow cytometry

The co-cultured cells were harvested with trypsin, centrifuged at 500g for 5 minutes, and the supernatant was discarded. The cells were gently washed once with PBS, followed by two gentle washes with precooled PBS. The cells were then resuspended in a binding buffer at a concentration of 1 x 10^6 cells/mL. A 100 µL cell suspension was transferred to a 5 mL flow cytometry tube, and 5 µL of FITC Annexin V and 5 µL of PI (BD Pharmingen, Cat No: 556547) were added. The cells were incubated at room temperature in the dark for 15 minutes. Finally, 200 µL of binding buffer was added, the samples were kept on ice, and flow cytometry analysis was performed within one hour, keeping the samples on ice.

4.2 Results

4.2.1 Establishment of Hypoxia-Induced Moderately Drug-Resistant Cell Lines

To evaluate the successful establishment of hypoxia-induced drug-resistant cells, we analyzed HIF-1α expression as a key marker of hypoxia. Using Western blot analysis, we measured HIF-1α levels under varying $CoCl_2$ concentrations and exposure durations. As shown in Figure 22(a) and (b), the time-dependent pattern of HIF-1α expression reflects the cellular adaptation to hypoxia. HIF-1α expression increases at the early stage (24 h) due to inhibited degradation, but may later be modulated by feedback mechanisms and maintained at a stable level (48 h). This expression trend is consistent with the changes in hypoxia risk scores observed in the GSE233802 dataset, as described in Chapter 3. Therefore, prolonged hypoxia may activate intrinsic mechanisms within cancer cells, enabling adaptation to the hypoxic environment, with a corresponding increase in the hypoxia risk score. In this study, the assessment of HIF-1α levels at both 24 and 48 hours ensured that the hypoxic conditions used in the subsequent co-culture experiments were biologically effective. The densitometric analysis further confirmed a significant dose- and time-dependent upregulation of HIF-1α expression, indicating effective hypoxic induction.

To investigate the impact of hypoxia on PD-L1 inhibitor resistance, HepG2 cells

were co-cultured with Jurkat T cells in a 200 μM $CoCl_2$ environment for four cycles. Subsequently, flow cytometry was employed to accurately determine the percentage of viable cells. As shown in Figure 23 a, b and c, hypoxia cells subjected to four rounds of $CoCl_2$ treatment exhibited higher survival rates compared to normoxic cells and those receiving only one round of treatment. Compared to the normoxic control group, the apoptosis rate in cells treated with 1-round of hypoxia was significantly reduced ($p = 0.0005$, T-statistic = –4.1431, t-test). After 4-round of hypoxia treatment, the apoptosis rate was further significantly decreased ($p < 0.0001$, T-statistic = –10.7825, t-test). A comparison between the 1-round and 4-round hypoxia groups showed that the apoptosis rate in the four-round group was significantly lower than that in the one-round group (T-statistic = –8.3049, $p < 0.00001$, t-test). This finding strongly suggests the successful induction of a hypoxia-adapted resistant phenotype. Conversely, the survival rate of cells that were not exposed to cobalt chloride ($CoCl_2$) was significantly lower. These experimental results confirm the successful establishment of a hypoxia resistant HepG2 cell model. In order to better determine the appropriate concentration of the PD-L1 inhibitor, we used NIS-Element AR software from Nikon to analyze the proliferation rate of the cells before and after co-culture. Based on the CNN algorithm of AI, this software can identify and count the areas of the cells on the 6-well plate before and after co-culture. It enables objective, high-throughput, and morphology-aware quantification of cellular features, making it particularly suitable for analyzing

complex co-culture systems. We used it to quantify fluorescence intensity, and the output was the fluorescence-positive area, which reflects the level of cell proliferation. To ensure accurate segmentation, we manually defined representative positive cells to establish thresholds for cell recognition, enabling consistent identification across multiple image fields. It precisely determined that an appropriate concentration of 0.1 μM of the PD-L1 inhibitor has a better effect of inhibiting cell proliferation. Figure 23 d shows the area of the cells in the culture dish before and after co-culture at different concentrations of the PD-L1 inhibitor. There were no significant differences between the groups treated with different concentrations of PD-L1 inhibitor before and after co-culture, and no strong apoptotic response was observed under any condition. PD-L1 inhibitor require an intact and functional immune microenvironment to achieve optimal efficacy, which is often compromised under tumor hypoxia. The increases in early and late apoptosis may suggest the development of drug resistance or immune evasion.

a

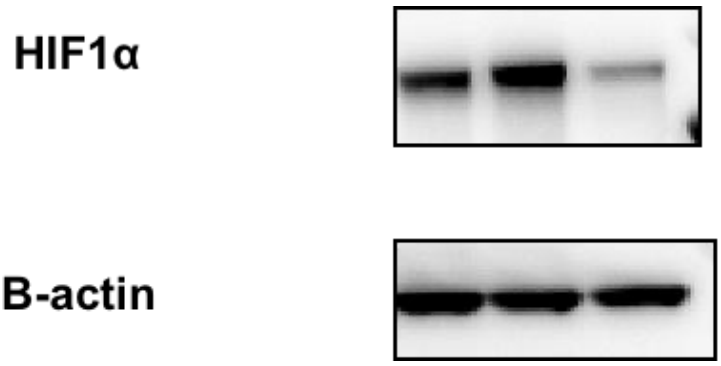

b

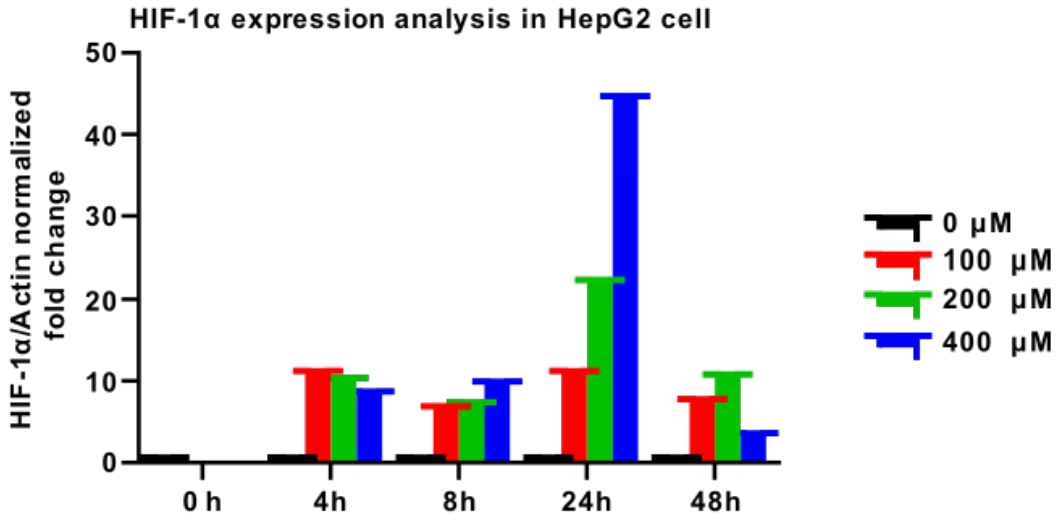

Figure 22. HIF-1α expression of HepG2 cells treated with $CoCl_2$. (a) The Western blotting image of HIF-1α under the culture condition of 200 μM $CoCl_2$; (b) HIF-1α mRNA level in HepG2 cells treated with $CoCl_2$.

a Normoxic HepG2 cells in 48h treatment

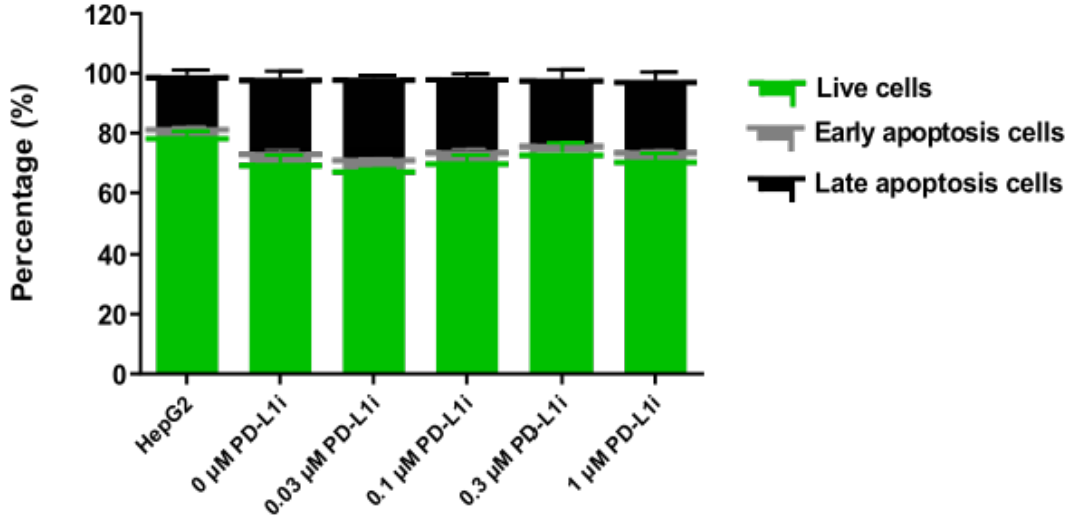

b Hypoxia (1 round) HepG2 cells in 48h treatment

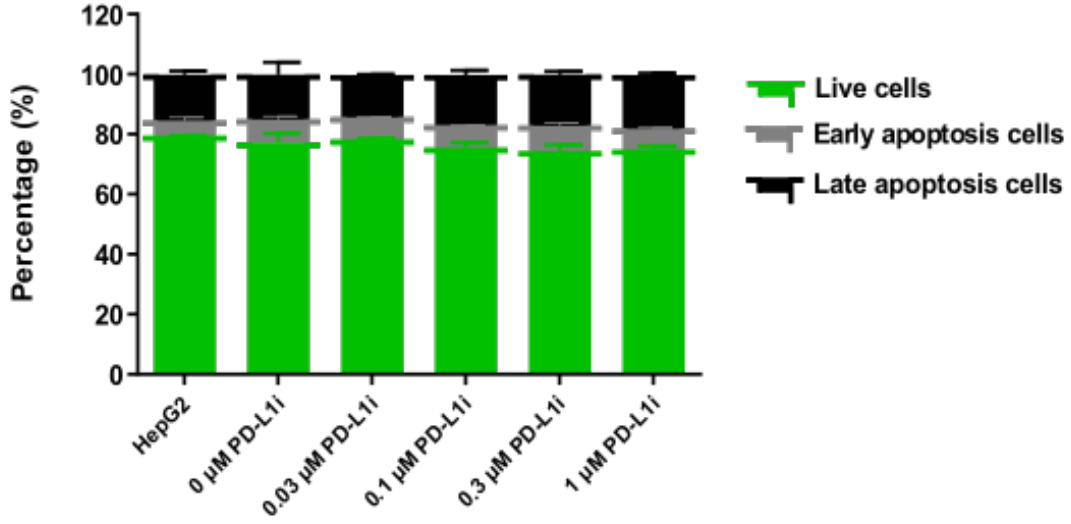

c Hypoxia (4 rounds) HepG2 cells in 48h treatment

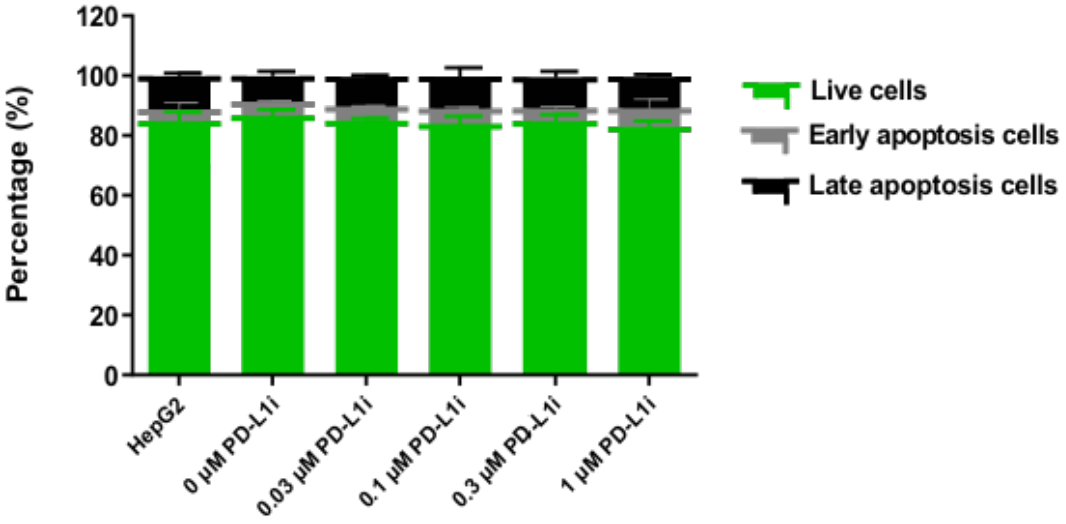

d

Effect of Different PD-L1 Inhibitor Concentrations on the Proliferation Rate of Co-cultured Cells

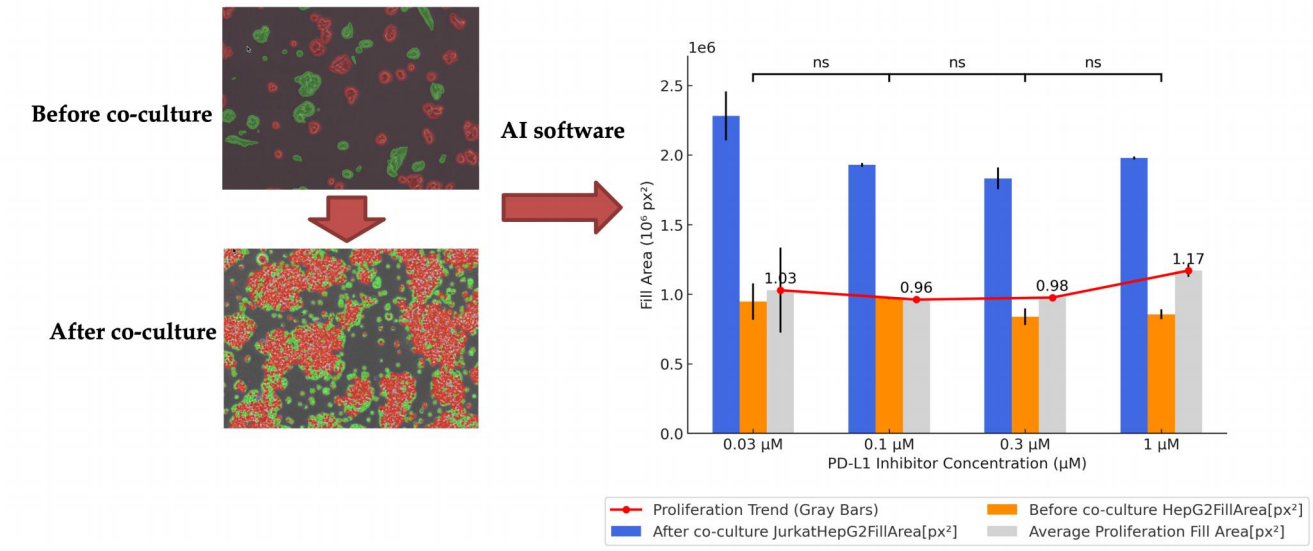

Proliferation Fill area = After Fill area [px^2] — Before Fill area [px^2]

Figure 23. Cell apoptosis in HepG2 Cell line samples. (a) Apoptosis analysis after co-culture of Normoxic HepG2 cells; (b) Apoptosis analysis after co-culture of Hypoxia (1 round) HepG2 Cells; (c) Apoptosis analysis after co-culture of Hypoxia (4 rounds) HepG2 Cells (normoxic : 1 round hypoxia, p-value = 0.0005; normoxic: 4 rounds hypoxia, p-value < 0.0001; 1 round hypoxia: 4 rounds hypoxia , p-value < 0.00001); (d) The proliferative changes in the area proportion of cells in the culture dish before and after co-culture. The data are expressed as mean ± SD, ns p>0.05, **p < 0.01, ***p < 0.001 vs control.

4.2.2 NOXA Knockdown Efficiency

Western blot and qPCR were used to confirm NOXA knockdown efficiency in HepG2 cells. Figure 24 a and b shows the protein expression levels of NOXA after transfection with four different siRNAs. Among them, siNOXA4 demonstrated the most significant knockdown effect (p-value < 0.01), showing a drastic reduction in NOXA protein levels compared to the control (NC siRNA). β-actin was used as the internal control. Additionally, qPCR results confirmed that NOXA mRNA expression was significantly decreased in cells transfected with siNOXA4 (p-value < 0.001), further validating the knockdown efficiency in Figure 24 c.

a

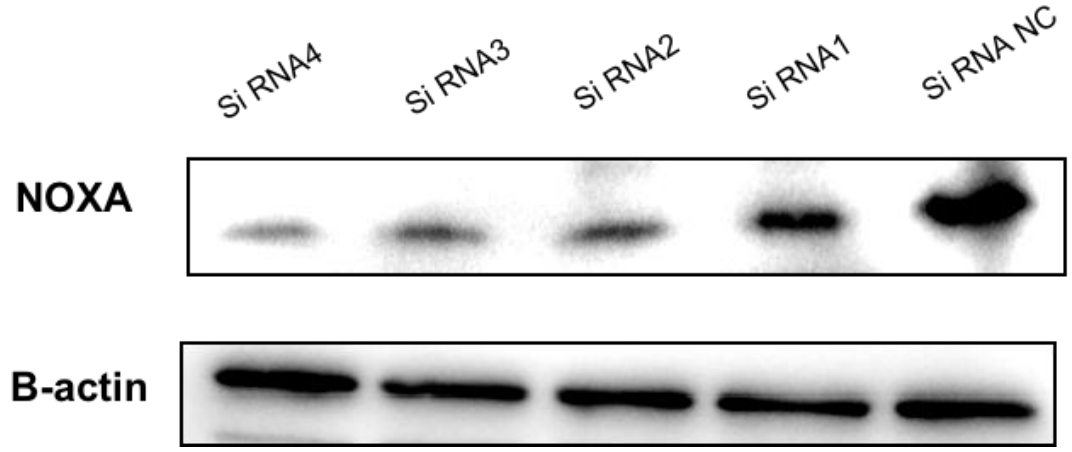
Si RNA4
Si RNA3
Si RNA2
Si RNA1
Si RNA NC
NOXA
B-actin

b

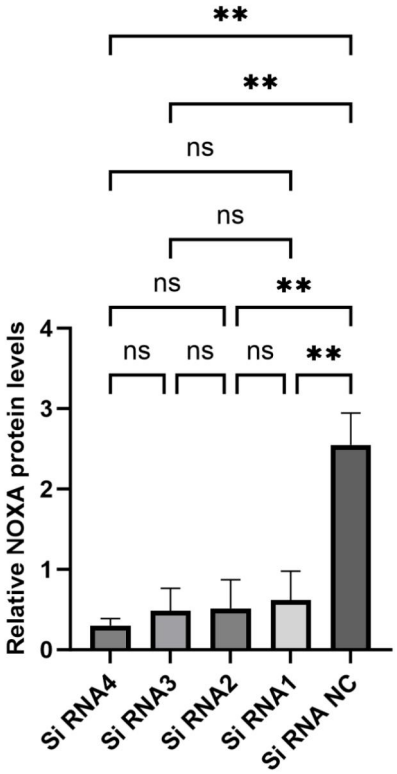
**
**
ns
ns
ns
**
ns
ns
ns
**
Relative NOXA protein levels
0
1
2
3
4
Si RNA4
Si RNA3
Si RNA2
Si RNA1
Si RNA NC

c

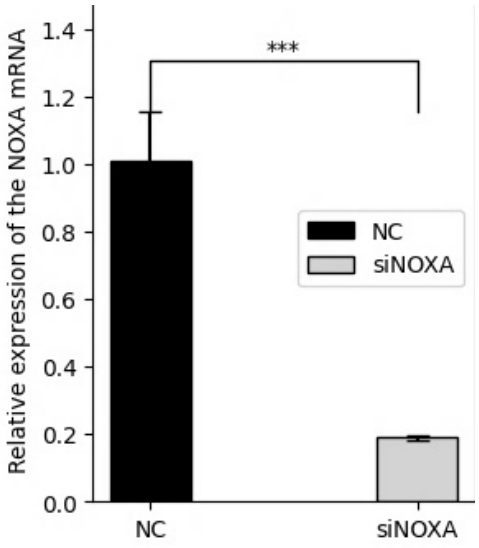

Figure 24. NOXA transfection knockdown validation. (a)Western blotting image of siNOXA; (b) Relative NOXA protein levels; (c) qPCR assay in NC-HepG4-round 4 and siNOXA- HepG4-round 4 cells. The data are expressed as mean ± SD, ns p-value >0.05, **p-value < 0.01, ***p-value < 0.001 vs control.

4.2.3 Apoptosis Analysis of NOXA-Knockdown Potentially Resistant Cells

To assess the role of NOXA in apoptosis regulation, NOXA-knockdown (siNOXA) cells were co-cultured with Jurkat T cells under hypoxic conditions. The control group is HepG2-4-Rounds cells. Apoptosis rates were analyzed using flow cytometry. The Figure 25 shown the effect of siNOXA group on HepG2-4-Rounds cell apoptosis under hypoxic conditions and 0.1 μM PD-L1i treatment. The results indicate that the live cell population increased from 64.10% in the control group to 70.05% in the siNOXA group, suggesting that siNOXA HepG2-4-Rounds cells may enhance cell survival under PD-L1i treatment. Additionally, early apoptosis decreased from 14.77% to 10.50%, while late apoptosis decreased significantly from 16.50% to 10.38% in the siNOXA group. To further quantify the effect of NOXA knockdown on apoptosis, the Cohen's d values for late and early apoptosis rates were 1.2976 and 1.5109, respectively, both exceeding the threshold of 0.8 for a large effect size. These findings suggest that siNOXA HepG2-4-Rounds cells may reduce early apoptosis and late apoptosis, potentially modulating PD-L1i-induced cell death.

a

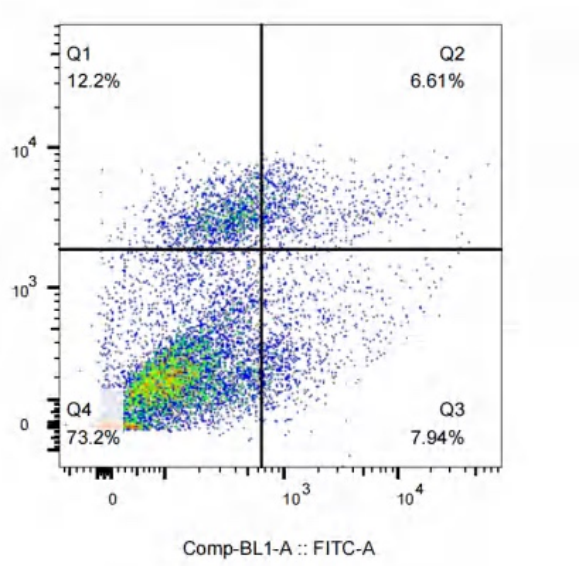

0.1uM PD-L1i siNOXA HepG2-round4 cells

b

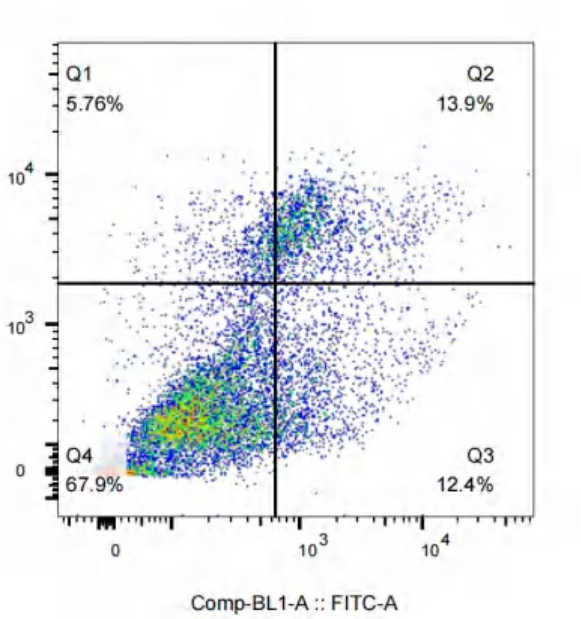

0.1uM PD-L1i HepG2-round4 cells

c

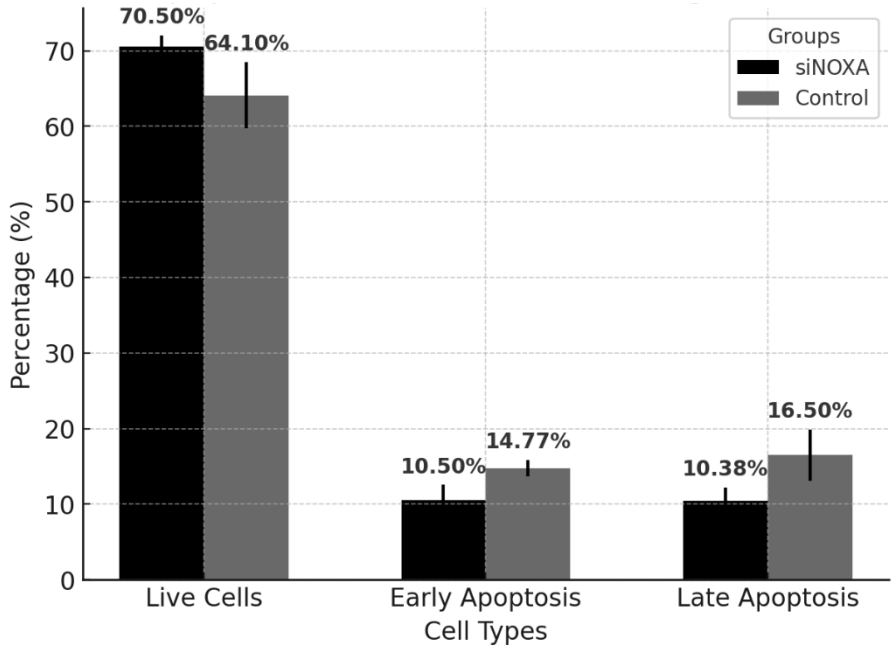

Figure 25. Effect of NOXA-knockdown HepG2-4-Rounds cell apoptosis with Jurkat T cells under hypoxic conditions. (a) The apoptosis experiment of siNOXA HepG2-4-Rounds cells; (b) The apoptosis experiment of hypoxia HepG2-4-Rounds cells; (c) Statistical analysis: Mean of three biological replicate experiments. Cohen's d value for early apoptosis rate is 1.5109. Cohen's d value for late apoptosis rate is 1.2976.

4.3 Discussion and Conclusion

In this study, we successfully established a hypoxia-induced drug-resistant HepG2 cell line by exposing the cells to $CoCl_2$. Our results demonstrated that the expression of HIF-1α increased in response to different $CoCl_2$ concentrations and incubation durations, confirming the effectiveness of hypoxic induction. Furthermore, the survival rate of HepG2 cells subjected to multiple rounds of hypoxic co-culture treatment was significantly higher than that of cells under normoxic conditions, indicating the successful induction of a hypoxia-adapted resistant phenotype. These findings provide a valuable in vitro model for studying the mechanisms of hypoxia-mediated drug resistance in HCC.

To evaluate the effect of PD-L1 inhibition on hypoxia-exposed HepG2 cells, we utilized AI-based image analysis to determine that 0.1 μM PD-L1 inhibitor is the optimal concentration. This finding further supports its potential research significance in targeting hypoxia-induced drug resistance in HepG2 cells.

Furthermore, we investigated the role of NOXA in apoptosis regulation under hypoxic conditions. Flow cytometry analysis demonstrated that NOXA knockdown (siNOXA) significantly altered apoptosis patterns in HepG2-4-Rounds cells. Specifically, siNOXA HepG2-4-Rounds cells exhibited an increase in the number of live cells, while early apoptosis and late apoptosis were significantly reduced. These results suggest that NOXA knockdown may reduce

early apoptosis and late apoptosis, which could be a potential mechanism underlying the development of resistant cells. These findings are consistent with previous studies highlighting NOXA's involvement in apoptosis regulation and drug resistance.

Therefore, our findings suggest that prolonged hypoxia induces resistance to PD-L1 inhibitors in HepG2 cells, and NOXA knockdown modulates the apoptotic progression of resistant cells. These findings lay the foundation for future studies on hypoxia-mediated immune evasion and highlight NOXA as a potential therapeutic target for overcoming PD-L1 inhibitor resistance in HCC.

Chapter 5 Overall Discussion and Conclusion

In recent years, the application of machine learning and deep learning in the medical field, particularly in oncology research, has made significant strides. These technologies enable the extraction of vast genomic features and uncover deeper layers of data, thereby facilitating the quantitative analysis of microscopic changes in genes or proteins within tumors. This capability allows for the visualization of tumor heterogeneity and the early prediction of treatment outcomes. This approach not only aids in identifying patients likely to benefit from immunotherapy but also helps in recognizing those who may not respond, thereby preventing ineffective treatments, conserving resources and financial costs, and avoiding potential adverse effects of immunotherapy that could exacerbate disease progression.

In this study, we integrated bioinformatics, machine learning, and deep learning methodologies to analyze various genomic features, providing an in-depth exploration of hypoxia-related mechanisms in hepatocellular carcinoma (HCC) and their impact on the efficacy of immunotherapy. Our findings emphasize the critical role of hypoxia in modulating the tumor microenvironment, influencing tumor progression, and determining patient responses to PD-L1 inhibitors. Therefore, assessing the likelihood of immunotherapy response in HCC patients before treatment could facilitate effective risk stratification.

In the second chapter of this study, we identified a total of 52 HCC-Hypoxia Overlap genes (HHOs) by intersecting HSGs and HRGs derived from GEO datasets. Gene set enrichment analysis (GSEA) revealed that some of these genes were closely associated with the PD-L1 expression pathway. Notably, TPX2, KIF20A, CENPA, DLGAP5, and LMNB1 were significantly enriched in the retinoblastoma (RB) immunity downregulation of the PD-L1 expression pathway. Previous studies have shown that hyperphosphorylated RB protein within this pathway exerts a tumor-suppressive role by inhibiting NF-κB activity and PD-L1 expression. Additionally, through regression analysis of the TCGA dataset, we identified 14 PD-L1 regulatory genes from the HHOs and extracted 10 hub genes from the PPI network, with TPX2, KIF20A, NDC80, and DLGAP5 being the overlapping genes. Based on clinical data, we analyzed the survival and treatment response of PPI hub genes and PD-L1 regulatory genes following PD-L1 inhibitor treatment to further validate our computational results. The results indicated that TPX2, NDC80, POLE2, GABARAPL1, and PIK3R1 were significantly associated with treatment outcomes, suggesting that TPX2 and NDC80 play crucial roles in regulating PD-L1 expression and, consequently, the effectiveness of PD-L1 inhibitors.

We discovered that the 20 overlapping genes between PD-L1 regulatory genes and PPI hub genes are not only differentially expressed in hypoxic HCC tissues but also regulate cancer cells through the PI3K/AKT pathway. These genes play

a critical role in PD-L1 regulation in hypoxic HCC tissues and may serve as potential therapeutic and prognostic biomarkers to enhance sensitivity to PD-L1 inhibitors and overcome drug resistance. However, the specific regulatory mechanisms remain unclear. In the chapter 2, the PI3K/AKT/HIF axis was found to play a significant role in hypoxia-induced HCC resistance, particularly in regulating PD-L1 expression.

In this study, an HCC immunotherapy response prediction model was established based on the EGAD00001008128 dataset (which includes data on patient responses to immunotherapy) and hypoxia HepG2 cell line datasets (GSE41666, GSE233802, and SRP356151). In the initial hypoxia risk score model developed in the chapter 2, we identified 9 hypoxia risk-associated genes. To improve the accuracy of predicting immunotherapy responses, we applied bioinformatics and machine learning techniques to process the EGAD00001008128 dataset. We identified 3 IRHs, among which PMAIP1 (NOXA) has been well-documented in the literature for its abnormal expression in hypoxic tumor microenvironments.

The role of PMAIP1 (NOXA) under hypoxic conditions has been extensively studied, demonstrating its importance in the adaptation of tumor cells to the hypoxic environment. NOXA is a pro-apoptotic protein belonging to the BCL-2 family, primarily promoting apoptosis through interactions with anti-apoptotic proteins [100]. Under hypoxic conditions, HIF-1α is activated and binds to the

promoter region of the PMAIP1 (NOXA) gene, enhancing its transcription and expression [101]. This mechanism not only helps tumor cells survive in the hypoxic microenvironment but also promotes malignancy by regulating proliferative and apoptotic pathways.

Importantly, the abnormal expression of PMAIP1 (NOXA) under hypoxia is closely related to the drug resistance of tumor cells. Its upregulation may alter proliferative signaling pathways in tumor cells, enabling them to better adapt to adverse growth conditions, which in turn leads to treatment failure [102]. Therefore, PMAIP1 (NOXA) is considered a potential therapeutic target, as targeting its regulatory pathway could effectively reverse hypoxia-induced drug resistance in tumor cells.

In this study, PMAIP1 (NOXA) was incorporated into the hypoxia risk score model to assess its predictive ability for immunotherapy response. The results indicated that the expression of this gene in a hypoxic microenvironment significantly impacts the effectiveness of immunotherapy, particularly under prolonged hypoxia exposure, where risk levels were notably elevated. In the logistic regression model, the prediction of immunotherapy response was significant (coefficient = 0.5972, $p < 0.01$), further validating the critical role of PMAIP1 (NOXA) in tumor drug resistance. Based on these findings, PMAIP1 (NOXA) holds promise as a key target for improving immunotherapy efficacy,

especially in strategies targeting hypoxia-induced drug resistance.

Cox regression analysis was performed on the TCGA-LIHC database to determine the risk coefficient for each feature gene. The hypoxia risk score model was thoroughly validated in the GSE233802 dataset across different hypoxia durations in HepG2 cell lines. It was found in cultured HepG2 cells that the score was positively associated with the hypoxia duration of the incubation environment. Regarding 0h as the reference condition, the prolonged hypoxic condition of 48h induced more malignant HCC cells than that of 24h. This finding supports that the hypoxic condition of the tumor microenvironment affects tumor malignancy and patient survival.

To optimize the immune therapy response prediction model, we used machine learning in combination with deep learning to extract high-level features from the EGAD00001008128 dataset. Using the mRMR and stepwise forward selection methods, we selected 11 genes most strongly associated with immunotherapy response and used SMOTE to address the imbalance in the training data, thereby enhancing the model's predictive performance. Compared to traditional deep learning algorithms, the KAN model performs better on small sample datasets, making it well-suited for handling high-dimensional gene expression data while mitigating the risk of overfitting. We trained the KAN prediction model using the 11 selected feature genes along with the Bevacizumab feature and validated it on

the test set. The constructed prediction model achieved an accuracy of 0.993 in the training set and 0.7 in the test set, with each clinical sample receiving a corresponding KAN immunotherapy response score.

Based on the KAN immunotherapy response score, the hypoxia risk score, and the PMAIP1 (NOXA) gene, we constructed logistic regression and SVM models. Ultimately, the SVM model incorporating both the KAN immunotherapy response score and the hypoxia risk score achieved an accuracy of 0.725 in the test set, demonstrating better predictive performance than the logistic regression model and the standalone KAN model. This indicates that the hypoxia risk score based on PMAIP1 (NOXA) significantly enhances the predictive accuracy of the immunotherapy response model. These findings suggest that hypoxia plays a crucial role in the tumor microenvironment and immunotherapy response. Prolonged hypoxia in the tumor microenvironment alters proliferative signaling pathways in cancer cells, suppresses immune system function, and significantly increases the risk level for tumor patients. As a result, this condition is more likely to lead to non-responsiveness to immune therapy or failure to achieve partial response criteria, and it may also exacerbate tumor progression [103].

In addition to the computational and predictive analyses conducted in this study, we also established an in vitro hypoxia-induced drug-resistant HepG2 cell line to further investigate the molecular mechanisms underlying hypoxia-mediated

resistance to PD-L1 inhibitors. Through $CoCl_2$ treatment, we successfully induced a hypoxia-adapted phenotype in HepG2 cells, as evidenced by an increase in cell survival following multiple rounds of hypoxic exposure. These findings confirm that prolonged hypoxia plays a significant role in the development of drug resistant HepG2 cells, and this cell line can serve as a valuable in vitro model for studying resistance mechanisms.

Additionally, we utilized AI-based image analysis to determine the optimal concentration of PD-L1 inhibitor. We further explored the role of NOXA in apoptosis regulation under hypoxic conditions. Flow cytometry analysis showed that siNOXA-treated round 4 HepG2 cells exhibited reduced early and late apoptosis compared to the control group, suggesting that NOXA depletion may shift apoptotic progression toward a more survival-favorable state. This finding is consistent with previous studies indicating that NOXA plays a crucial role in apoptosis regulation and drug resistance, highlighting its strong association with hypoxia-induced immune evasion.

Recent studies have extensively documented the role of NOXA in hypoxia and immunotherapy. As a pro-apoptotic BH3 domain-specific protein, NOXA knockout has been reported to reduce chimeric antigen receptor T-cell (CAR-T) mediated tumor cell apoptosis, leading to CAR-T therapy resistance [104]. Our study also revealed that NOXA expression was upregulated in hypoxic HepG2

cells and in patients who responded to immunotherapy. Whether in predicting immunotherapy response model or investigating hypoxia-induced resistance in HepG2 cells, these findings underscore NOXA's potential as a therapeutic target.

In conclusion, our study provides new insights into the role of hypoxia in inducing resistance to PD-L1 inhibitors and the function of NOXA in apoptosis regulation. We demonstrated that prolonged hypoxia promotes the development of drug-resistant HCC cells, while NOXA knockdown alters apoptotic progression, potentially affecting treatment outcomes. These findings support the hypothesis that hypoxia-mediated immune evasion contributes to PD-L1 inhibitor resistance in HCC.

By integrating bioinformatics, machine learning, deep learning, and experimental validation, this study offers a comprehensive approach to understanding the hypoxia-immunotherapy relationship in HCC. Identifying PMAIP1 (NOXA) as a possible treatment target further supports the development of new strategies to overcome hypoxia-related resistance, helping to improve the success of immunotherapy.

Appendix

Overview of Publication

The following articles, published in the International Journal of Molecular Sciences (IJMS) and the American Society of Clinical Oncology (ASCO), present the research detailed in Chapter Two of this dissertation. This study explores potential regulatory genes and mechanisms underlying hypoxia-induced PD-L1 inhibitor resistance in hepatocellular carcinoma through bioinformatics. Additionally, an initial hypoxia risk score model was developed using machine learning to identify potential hypoxia-related risk genes in hepatocellular carcinoma. Presented as an appendix, this research supports the conclusions of this dissertation. Each figure in the articles corresponds to the figures in the dissertation and is supplemented with additional materials.

International Journal of
Molecular Sciences

MDPI

Article

Bioinformatics Identification of Regulatory Genes and Mechanism Related to Hypoxia-Induced PD-L1 Inhibitor Resistance in Hepatocellular Carcinoma

Mohan Huang [1], Sijun Yang [2], William Chi Shing Tai [3], Lingfeng Zhang [1], Yinuo Zhou [1], William Chi Shing Cho [4,*], Lawrence Wing Chi Chan [1,*] and Sze Chuen Cesar Wong [3]

[1] Department of Health Technology and Informatics, The Hong Kong Polytechnic University, Hong Kong SAR, China
[2] Department of endocrinology, The First Affiliated Hospital of Wenzhou Medical University, Wenzhou 325000, China
[3] Department of Applied Biology and Chemical Technology, The Hong Kong Polytechnic University, Hong Kong SAR, China
[4] Department of Clinical Oncology, Queen Elizabeth Hospital, Hong Kong SAR, China
* Correspondence: williamcscho@ (W.C.S.C.); wing.chi.chan@ (L.W.C.C.); Tel.: +852-3400-8561 (L.W.C.C.); Fax: +852-2362-4365 (L.W.C.C.)

Abstract: The combination of a PD-L1 inhibitor and an anti-angiogenic agent has become the new reference standard in the first-line treatment of non-excisable hepatocellular carcinoma (HCC) due to the survival advantage, but its objective response rate remains low at 36%. Evidence shows that PD-L1 inhibitor resistance is attributed to hypoxic tumor microenvironment. In this study, we performed bioinformatics analysis to identify genes and the underlying mechanisms that improve the efficacy of PD-L1 inhibition. Two public datasets of gene expression profiles, (1) HCC tumor versus adjacent normal tissue (N = 214) and (2) normoxia versus anoxia of HepG2 cells (N = 6), were collected from Gene Expression Omnibus (GEO) database. We identified HCC-signature and hypoxia-related genes, using differential expression analysis, and their 52 overlapping genes. Of these 52 genes, 14 PD-L1 regulator genes were further identified through the multiple regression analysis of TCGA-LIHC dataset (N = 371), and 10 hub genes were indicated in the protein–protein interaction (PPI) network. It was found that *POLE2*, *GABARAPL1*, *PIK3R1*, *NDC80*, and *TPX2* play critical roles in the response and overall survival in cancer patients under PD-L1 inhibitor treatment. Our study provides new insights and potential biomarkers to enhance the immunotherapeutic role of PD-L1 inhibitors in HCC, which can help in exploring new therapeutic strategies.

Keywords: hepatocellular carcinoma; hypoxia; PD-L1 inhibitor; drug resistance; bioinformatics analysis; molecular target; immune escape; combined treatment

Citation: Huang, M.; Yang, S.; Tai, W.C.S.; Zhang, L.; Zhou, Y.; Cho, W.C.S.; Chan, L.W.C.; Wong, S.C.C. Bioinformatics Identification of Regulatory Genes and Mechanism Related to Hypoxia-Induced PD-L1 Inhibitor Resistance in Hepatocellular Carcinoma. *Int. J. Mol. Sci.* **2023**, *24*, 8720. https://doi.org/10.3390/ijms24108720

Academic Editors: Silvio Naviglio and Luigi Sapio

Received: 5 March 2023
Revised: 28 April 2023
Accepted: 4 May 2023
Published: 13 May 2023

1. Introduction

Hepatocellular carcinoma (HCC) is one of the most common malignancies with the fourth highest cancer mortality rate in the world, seriously damaging human life and health. Chronic hepatitis B and C viruses, chronic alcohol consumption, and metabolic syndrome are all major clinical risk factors for HCC. Current clinical treatment options for liver cancer are classified into surgical therapies, including liver transplantation, cryoablation, resection, and non-surgical therapies, including chemotherapy, targeted therapy, and immunotherapy [1]. However, eligible treatment approaches become very few for patients in advanced HCC where surgical therapy is not appropriate due to large tumor size, location, number of lesions, and comorbidities [2]. Patients with advanced HCC treated with immune-checkpoint inhibitors (ICIs) reached the objective response rate (ORR)

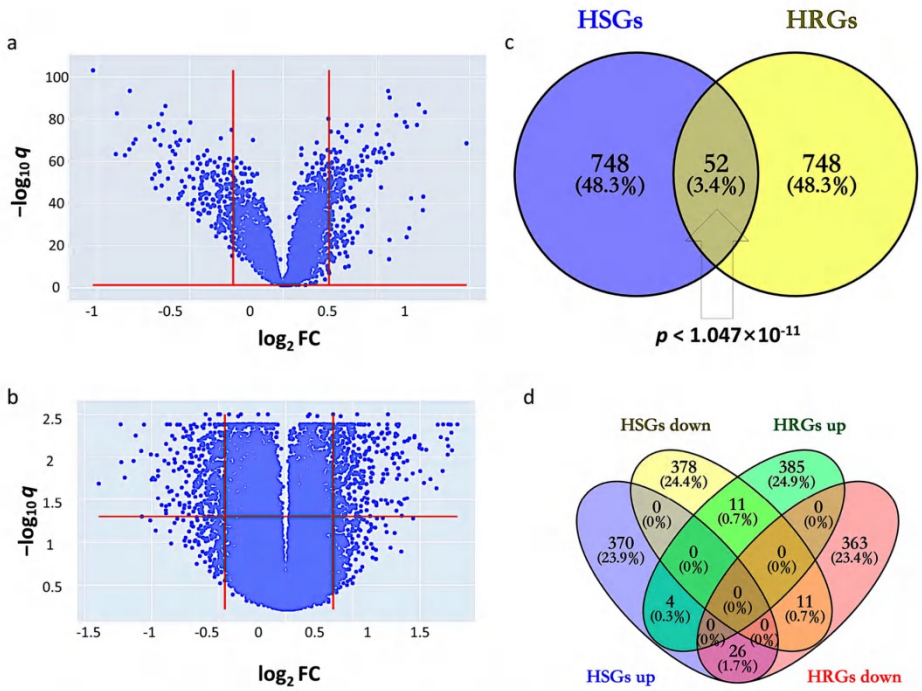

Figure 1. Identification of HCC-signature genes (HSGs) and hypoxia-related genes (HRGs). (**a**) Volcano plot for GSE14520; (**b**) Volcano plot for GSE41666; (**c**) Overlapping genes between HSGs and HRGs; (**d**) Overlapping genes among upregulated and downregulated genes in HSGs and HRGs.

2.2. Gene Set Enrichment Analyses of HSGs and HRGs

Enrichment analysis of HSGs and HRGs on 202 databases (as of 29 November, 2022) was performed using the gseapy package in Python. Significant enrichment results were found in 190 and 161 databases, respectively. Here, we particularly highlight three groups of databases that gave significant enrichment results closely related to hypoxia, HCC, and PD-L1.

In the Gene Ontology (GO) databases, HSGs upregulated genes were significantly enriched in "mitosis", "nucleus", and "organelles" gene sets, HRGs upregulated genes were mainly enriched in "mitosis", "spindle", and "nuclear chromosome" gene sets, HSGs downregulated genes were mainly enriched in "monooxygenase activity", and HRGs downregulated genes were mainly enriched in "cellular response to decreased oxygen levels " gene set (Figure 2a,b). The bar chart of expression profile of enriched genes is shown in Supplementary Figure S3. In the Kyoto Encyclopedia of Genes and Genomes (KEGG) Human databases, upregulated HSGs were enriched in "RNA transport" and "cellular senescence signaling", "drug metabolism", "chemical carcinogenesis", and "apoptosis signaling" pathways (Figure 2d). In the "RNAseq Automatic GEO Signatures Human" database, we found that downregulated HSGs and HRGs together were significantly enriched in the "Rb-immunity downregulating Pd-L1" gene set where *TPX2*, *KIF20A*, *CENPA*, *DLGAP5*, and *LMNB1* were found in the genes in common, whereas upregulated HRGs were significantly enriched in the "Rb-immunity downregulating Pd-L1" and "tissue-resident pancreas Pd-1/Pd-L1" gene sets, respectively (Figure 2c).

of 36% only with drug combination and even lower than 20% with a single drug [3]. Therefore, novel approaches to clarify the underlying mechanism and enhance the response to immunotherapy are important to improve patient survivability and quality of life.

Hypoxia is a common feature of solid tumors, which is closely associated with poor prognosis. Recent experimental analyses have shown that HCC under a hypoxic environment has significant changes in proliferation, apoptosis, migration, invasion, and epithelial-mesenchymal transition [4]. Therefore, it is important to investigate the molecular mechanisms associated with hypoxia in the HCC microenvironment, and the hypoxia-induced factor (HIF) is the main tumor-adapted transcription factor, consisting of HIF-1α, 2α, and 3α [5]. In the hypoxic microenvironment of solid tumors, high expression of HIF-1α is associated with poor prognosis in various cancers, including HCC [6]. It was shown that in the hypoxic environment, HIF-1α is involved in the hypoxic response and activates hundreds of genes associated with the tumor vasculature and tumor cell adaptation to the hypoxic environment. To activate the HIF-downstream pathways that regulate energy metabolism in tumor cells and the expression of immune checkpoint proteins, HIF can bind to the hypoxia response element (HRE) in the promoter region of genes downstream of HIF [7].

PD-L1 is an important immune checkpoint molecule that primarily regulates cellular apoptosis, and therefore, PD-L1 has an essential impact on tumor growth. An increasing number of studies have found that organs exposed to hypoxic conditions and experimental models of hypoxia showed elevated PD-L1 expression at the affected region [8]. In the hypoxic tumor microenvironment, HIF-1α can upregulate PD-L1 expression. Such PD-L1 expression enhancement can be suppressed by the knockdown of HIF-1α [9]. Thus, PD-L1 may be one of the critical mediators expressed by hypoxic tumor cells. PD-L1 inhibitor combination therapy is currently the first-line treatment option for HCC, but no more than 35% of patients manifested a clinical response [10]. In addition, drug resistance acquired due to PD-L1-mediated immune escape after several years of treatment remains a severe problem for patients with cancer recurrence and metastasis. It has been shown that targeting HIF-1α can eliminate PD-L1-mediated immune escape in the tumor microenvironment and increase immune tolerance in normal tissues [11]. Therefore, we hypothesize that the HIF-1α-stimulated increase in PD-L1 expression is a key factor in drug resistance in hypoxic tumors.

This study aimed to gain new insights into the mechanisms regulating PD-L1 expression and the PD-L1 immune checkpoint inhibitor resistance in solid HCC tumors in a hypoxic microenvironment. Based on the genomic mechanisms, the potential theranostic molecular biomarkers could be identified so that new therapeutic strategies can be recognized to overcome hypoxia-induced PD-L1 inhibitor resistance.

2. Results

2.1. Identification of HSGs and HRGs in HCC

By setting the cutoff values of q and fold change (FC) at 1.139 and 1.128, HSGs constitute 800 genes (400 upregulated and 400 downregulated) that indicate differential expression in GSE14520 between tumor and adjacent non-tumor (Figure 1a). The corresponding heatmap is shown in Supplementary Figure S1. By setting the cutoff values of q and FC at 1.277 and 1.370, HRGs constitute 800 genes (400 upregulated and 400 downregulated) that indicate differential expression between hypoxic and normoxic environments in GSE41666 (Figure 1b). The corresponding heatmap is shown in Supplementary Figure S2. The intersection of HCC-signature genes (HSGs) and hypoxia-related genes (HRGs) of the two datasets gave 52 overlapping genes, so-called HCC-Hypoxia Overlaps (HHOs), (Fisher-exact test $p < 1.047 \times 10^{-11}$), 37 of which were upregulated and 15 of which were downregulated in the hypoxic group compared with the normoxic group in GSE41666 (Figure 1c,d).

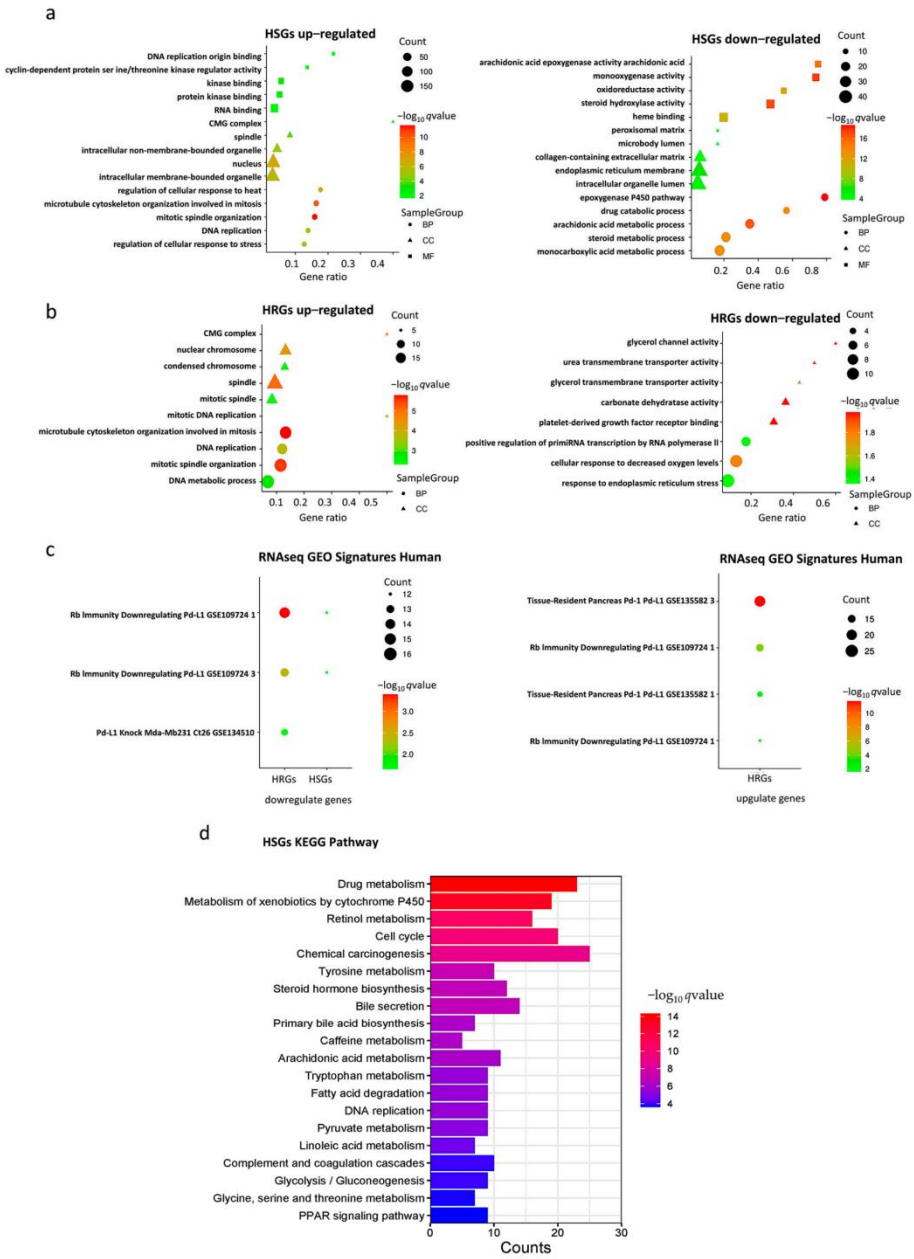

Figure 2. Gene set enrichment analysis. (**a**) Gene Ontology (GO) enrichment analysis of HSGs; (**b**) GO enrichment analysis of HRGs; (**c**) RNAseq GEO Signatures Human enrichment analysis of HSGs and HRGs; (**d**) Kyoto Encyclopedia of Genes and Genomes (KEGG) enrichment analyses of HSGs.

2.3. Evaluation of the Effect of HHOs on PD-L1 Expression in the TCGA-LIHC Dataset

Multiple regression analysis was used to evaluate the effect of HHOs on PD-L1 expression. Ultimately, 14 genes were identified as relevant risk factors affecting PD-L1 expression and were subsequently used to construct a drug-resistance gene regulator model. The model is represented by a linear combination of regression coefficients multiplied by the relative expression levels of PD-L1 regulator genes, indicating the relative effect of each gene on the drug resistance based on multiple regression analysis.

$$\begin{aligned} PD-L1 = \; & 0.076 + 0.240 \times FOS + 0.261 \times FAM13A + 0.443 \times DLGAP5 \\ & -0.264 \times ALDH5A1 + 0.223 \times GABARAPL1 \\ & -0.123 \times CABYR + 0.145 \times PIK3R1 - 0.150 \times HGFAC \\ & +0.317 \times LMNB1 - 0.418 \times KIF20A - 0.434 \times TPX2 \\ & +0.410 \times NDC80 + 0.121 \times EPHA2 - 0.096 \times NEDD4L \end{aligned}$$

Each of the PD-L1 regulator genes included in the model is associated with a significant effect on drug resistance ($p < 0.05$). It is worth noting that the PD-L1 regulator genes with the top five coefficient magnitudes are *DLGAP5*, *NDC80*, *LMNB1*, *KIF20A*, and *TPX2*.

2.4. Construction of Protein–Protein Interaction Network and Identification of Hub Genes

The 52 HHOs were entered into the STRING database platform for protein–protein interaction (PPI) network analysis, and the results were imported into Cytoscape software to construct the PPI network. Among 52 HHOs, 26 genes had connections with confidence score >0.7 in the PPI network, and thus, the rest were removed from the network representation (Figure 3a). In addition, the degree of node connections was calculated using cytoHubba plug-in, and 10 genes with degree >33 were identified as hub genes, namely, *CCNB1*, *BUB1B*, *KIF4A*, *KIF20A*, *KIF11*, *NDC80*, *TPX2*, *CENPA*, *POLE2*, *DLGAP5* (Figure 3b).

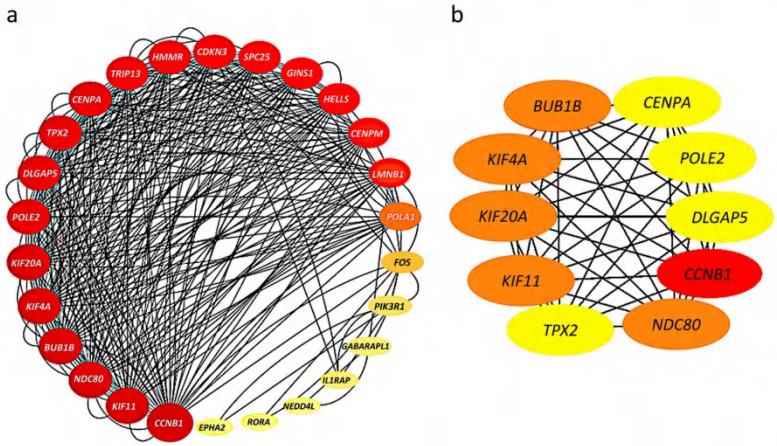

Figure 3. Protein–protein interaction (PPI) networks: (**a**) Connections among 26 genes with confidence score >0.7; The larger the node, the greater the degree of connectivity and the darker the color, the greater the combined score value; (**b**) 10 hub genes with connectivity degree >33; Genes with a confidence score ≤0.7 are not shown here; The darker the color, the stronger the degree of criticality.

2.5. Survival Analysis and PD-L1 Inhibitor Response Prediction

We used Kaplan Meier Plotter software to plot survival curves for genes, which are the union of PPI hub genes and PD-L1 regulator genes. The results of the survival analysis showed that the expression levels of 15 genes significantly correlated with the poor prognosis of the patients (Table S3). Particularly, significantly better survival rates

after PD-L1 treatment were found in patients with a higher expression level of *NDC80* (HR = 0.76, $p = 0.024$) and *TPX2* (HR = 0.77, $p = 0.03$) than those with a lower expression level (Figure 4a,b). We validated the expression of PPI hub genes and PD-L1 regulator genes in response to PD-L1 treatment. Three of the best performing genes in the sample were *GABARAPL1* (AUC = 0.56, $p = 0.016$), *PIK3R1* (AUC = 0.549, $p = 0.04$), and *POLE2* (AUC = 0.553, $p = 0.027$) (Figure 4c).

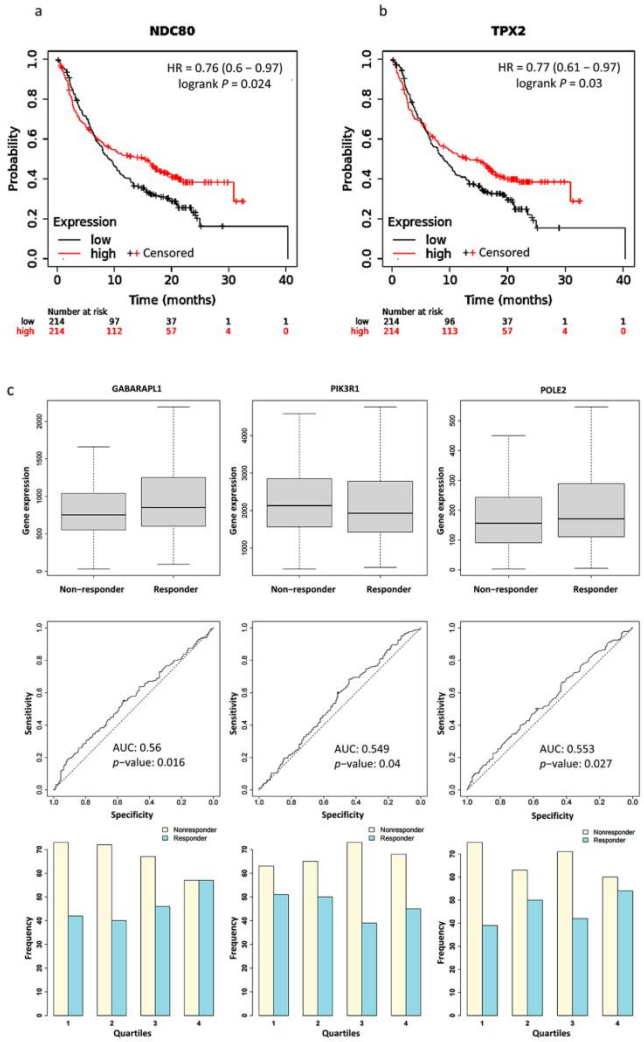

Figure 4. Kaplan–Meier plots for the comparison of survival between high and low expression levels: (**a**) *NDC80* (HR = 0.76, $p = 0.024$); (**b**) *TPX2* (HR = 0.77, $p = 0.03$). (**c**) Boxplots, Receiver operating characteristic (ROC) curves, and responders' frequency of top three genes in predicting PD-L1 inhibitor response: *GABARAPL1* (AUC = 0.560, $p = 0.016$), *PIK3R1* (AUC = 0.549, $p = 0.04$), and *POLE2* (AUC = 0.553, $p = 0.027$); "°" indicates the strongest cutoff, which has the minimal distance from the ideal discriminator.

2.6. KEGG Pathway Enrichment

The KEGG pathway enrichment of PPI hub genes and PD-L1 regulator genes were analyzed using the ShinyGo platform. We found 19 significantly enriched pathways (false discovery rates (FDRs) < 0.032), and most of them are associated with immune cells, inflammatory factors, and apoptosis (Figure 5). It is important to note that two genes, *FOS* (AP-1) and *PIK3R1*, are found in "PD-L1 expression and PD-1 checkpoint pathway in cancer", while the "endocrine resistance pathway" is activated by hypoxia induction.

Figure 5. KEGG pathway enrichment of the union of PPI hub genes and PD-L1 regulator genes.

3. Discussion

Accumulating evidence suggests that hypoxia has a significant impact on HCC, as hypoxia is a prominent feature of malignancy that not only promotes cancer progression but also poses a challenge to the efficacy of immunotherapy. Therefore, there is an urgent need to find HCC biomarkers associated with hypoxia and immunotherapy and elucidate their linkages. In this study, we identified a total of 52 HHOs, which represent overlapping between HSGs and HRGs derived from the GEO datasets. In gene set enrichment analysis (GSEA), we found that some genes in HSGs and HRGs were closely related to the pathways of PD-L1 expression. Particularly, *TPX2*, *KIF20A*, *CENPA*, *DLGAP5*, and *LMNB1* of HHOs were significantly enriched by the retinoblastoma (RB) immunity downregulating PD-L1 expression pathway. The study identifying this pathway illustrated the tumor suppressor function of hyperphosphorylated RB protein in repressing NF-κB activity and PD-L1 expression [12]. Alternatively, 14 PD-L1 regulator genes were selected from HHOs using regression analysis of a TCGA dataset. Further, 10 hub genes were derived from the PPI network of HHOs. Among PD-L1 regulator genes and PPI hub genes, 4 overlapping genes, *TPX2*, *KIF20A*, *NDC80*, and *DLGAP5*, were found. In a future study, we plan to perform

co-immunoprecipitation of these 4 overlapping genes and PD-L1. Therefore, we analyzed the survival and treatment response of PPI hub genes and PD-L1 regulator genes after PD-L1 inhibitor treatment based on clinical data to further validate our in-silico results. *TPX2*, *NDC80*, *POLE2*, *GABARAPL1*, and *PIK3R1* were significantly associated with treatment outcomes. The above-mentioned findings support the crucial roles of *TPX2* and *NDC80* in regulating PD-L1 expression and thus affect the PD-L1 inhibitor treatment outcome.

The phosphoinositide-3-kinase regulatory subunit 1 (*PIK3R1*) gene product is mainly p85α, a regulatory subunit of PI3K enzymes. It is also responsible for splicing the isoforms p55α and p50α, primarily expressed in skeletal muscle and liver [13]. Increasing research has shown that *PIK3R1* plays a vital role in human cancer development. The p85 regulatory subunit of PI3K regulates phosphatidylinositol 3,4,5-triphosphate (PIP3) expression, AKT activation, PTEN phosphorylation, and related mRNA expression, mainly through PI3K pathway, which is involved in tumor growth, apoptosis, and drug resistance [14]. It was found that *PIK3R1* expression was significantly higher in HCC tissues than in adjacent normal tissues [15]. In cell lines of HCC, the knockdown of *PIK3R1* significantly reduced the expression of p-PI3K, p-AKT, and p-mTOR, which were closely associated with the growth and proliferation of tumor cells. Furthermore, in a hypoxic environment, cellular activation of HIF-1α downregulated ROS/PI3K/AKT to adapt to the hypoxic loop, while MAPK also downregulated ROS/PI3K/AKT by reducing ERK1/2 phosphorylation [16].

Targeting protein for Xenopus kinesin-like protein 2 (TPX2) is a microtubule nucleation factor involved in mitotic spindle formation. TPX2 is overexpressed in a variety of malignant tumor tissues, including HCC, colon cancer, breast cancer, esophageal cancer, and cervical cancer. It was found that TPX2 regulates PI3K/AKT/p53/p21 pathway and promotes tumor metastasis and growth in HCC tissues [17]. Downregulation of *TPX2* significantly reduced the expression levels of Bcl-2, c-Myc, and Cyclin D1, inhibited PI3K/AKT signaling, suppressed cell proliferation, and promoted apoptosis, thus possibly preventing the development and progression of HCC [18].

Nuclear division cycle 80 (NDC80/Hec1) is a kinetochore complex protein associated with mitosis and is involved in microtubule binding and spindle assembly [19]. Notably, mutations in NDC80 have been confirmed in the second most prevalent primary liver cancer (cholangiocarcinoma, CCA) [20]. In HCC tissues, NDC80 mRNA expression was significantly higher than that of adjacent tissues and may have a role in reducing apoptosis and promoting HCC development [21]. Interestingly, a few studies have shown that NDC80 is associated with PI3K/AKT, but the core component of its complex, SPC24, is defined to regulate the PI3K/AKT pathway in breast cancer cells and produce oncogenic effects [22].

DNA polymerase epsilon subunit 2 (POLE2) is a DNA polymerase subunit that is involved in the DNA replication process, has DNA repair effects, and reduces the occurrence of mutated genes. POLE2, which potentially acts as a therapeutic target and prognostic factor, is overexpressed in a variety of cancers. One study found that *POLE2* regulates its downstream oncogene STC1, activates AKT phosphorylation, decreases HIF-1α expression levels, and promotes cancer cell proliferation [23].

Gamma-aminobutyric acid (GABA), a receptor-associated protein-like 1 (GABARAPL1), is an autophagosomal protein that is a key PI3K transcriptional target and plays an important role in protein transport, interactions, cell proliferation, and tumorigenesis. GABARAPL1 expression is inversely correlated with cancer metastasis and its high expression is associated with a good prognosis. It has been shown that strong expression of GABARAPL1 attenuates AKT activation, reduces mTOR activation, and increases cancer cell invasion [24–26]. In fact, autophagy is a tumor suppressor mechanism, mainly limiting oncogenic stresses, such as DNA damage or oxidative stress, in the early stages of tumorigenesis, but it can also promote the survival of cancer cells under nutrient starvation or hypoxic conditions in the advanced stages of tumor progression.

In summary, 20 genes in union of PD-L1 regulator genes and PPI hub genes are not only differentially expressed in hypoxic HCC tissues but also potentially regulate cancer cells through the PI3K/AKT signaling pathway, according to the above-mentioned evi-

dence. These genes are essential in regulating PD-L1 in hypoxic HCC tumor tissues. They may be potential therapeutic and prognostic biomarkers to enhance the sensitivity of cancer cells to PD-L1 inhibitors and reverse drug resistance. However, the specific regulatory mechanisms among them have not been clarified. We predicted that the related genes of possible regulatory mechanisms would provide new insights into the drug resistance mechanisms of potential genes functioning in hypoxic HCC tissues. TPX2, a critical target of KRAS, has been reported to be involved in the development of pancreatic ductal adenocarcinoma (PDAC) through the regulation of hypoxia-mediated HIF-1 [27]. KRAS is known to be an oncogenic gene that regulates the PI3K/AKT/mTOR signaling pathway [28]. Notably, hypoxia-mediated HIF-1α increases PD-L1 expression in a variety of solid hypoxic tumors via the PTEN/PI3K/AKT signaling pathway, thereby inducing T-cell unresponsiveness or apoptosis [29], which suggests that the PTEN/PI3K/AKT/HIF axes may be an essential part of the occurrence and development of drug resistance mechanisms in hypoxic HCC. Additionally, we found that the potential genes are also interrelated. However, the mechanism of their interactive regulation and the role of inter-regulation with PD-L1 in hypoxic HCC still needs further experimental exploration and validation.

Currently, researchers believe that immunotherapy resistance is induced in tumor cells due to the lack of antigenic mutations, altered antigen processing mechanisms, major histocompatibility complex (MHC) dysfunction, human leukocyte antigen (HLA) expression deficiency, β2 microglobulin (β2M) mutations leading to HLA loss, constitutive PD-L1 expression, loss of T cell function, and altered signaling pathways (PI3K, MAPK, WNT, IFN), but it remains unclear about the holistic molecular mechanism leading to the PD-L1 overexpression, and thus, drug resistance under hypoxic conditions [30].

In previous studies, it was found that PD-L1 expression in tumor cells could be upregulated by interferons (IFN) or cytokines, such as tumor necrosis factor (TNF) [31]. Furthermore, HIF-1α also upregulates TNF expression and increases the absorption of TNF by innate immune cells [32]. This is consistent with our findings that PD-L1 expression is regulated by the upstream pathway activated by TNF. It has been shown that TNFR2 acts as the predominant TNF receptor on activation of CD8+ effector T cells. TNF directly affects CD8+ effector T cells through TNFR2, leading to activation-induced cell apoptosis [33]. The upregulated PD-L1 expression can further lead to the apoptosis of T cells through the interaction with PD-1.

The signaling mechanism of PD-L1 expression could be initiated from the binding of TNF to TNFR1. TNFR1 mutations result in altered mitochondrial function, enhanced oxidative capacity, and mitochondrial reactive oxygen species (ROS) production [34]. Under a hypoxic environment, ROS can regulate the stability of HIF-1α and induce DNA damage, further accumulating the risk of DNA mutation [35,36]. Research indicates that ROS can mediate hypoxia through activation of PI3K/AKT/HIF-1α pathway [37]. In addition, activator protein 1 (AP-1, *FOS* gene) is activated by ROS oxidative stress and is involved in tumor generation and the regulation of vascular endothelial growth factor (VEGF) involved in tumor vasculogenesis [38].

A study explored the possibility of combining immune checkpoint inhibitor treatment with HIF inhibitor to repress tumor progression, enhance anti-tumor immunity, and reduce drug resistance. MK6482 was the first HIF-2α inhibitor approved by the FDA to treat patients with advanced renal cancer. Several chemotherapeutic agents were also used clinically to target HIF expression, such as rapamycin, but they have poor bioavailability at the tumor site (<15%) and poor solubility in water, thus increasing associated therapeutic toxicity [4,39]. Drugs known to repress HIF-1α expression indirectly, such as mTOR inhibitors, can also be used as adjuvant therapy for cancer because it has been shown in preclinical models of HCC that such treatment can suppress tumor growth. HIF-1α inhibitors can not only downregulate the PD-L1 expression in tumors but also upregulate the PD-L1 expression in normal tissues, increasing the tolerance of normal tissues to immunotherapy and reducing adverse events [39]. Therefore, it is essential to explore the mechanisms of HIF-induced PD-L1 resistance in solid hypoxic tumors and develop

effective and safe new therapies using a potentially multi-targeted approach. In this comprehensive bioinformatics study, the conceptual signaling mechanism of hypoxia-induced PD-L1 inhibitor resistance has been elucidated (Figure 6). KRAS, NDC80, TPX2, and PIK3R1, which act as molecules intimate to hypoxic stress upstream of PD-L1 in the signaling mechanism, were recognized as the potential targets of agents that could be combined with a PD-L1 inhibitor to overcome drug resistance. Such agents include MD6482, PT2385, ABT-869 (mTOR inhibitor); MD6482 has only been used clinically in patients with advanced renal cancer, while the other drugs are currently only being trialed in preclinical models [35,40].

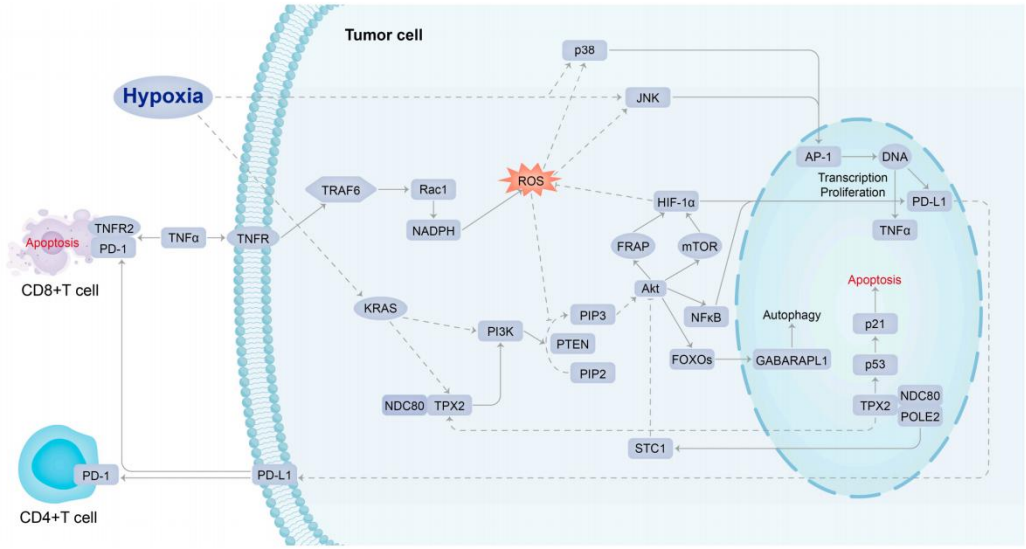

Figure 6. Conceptual signaling mechanism of hypoxia-induced PD-L1 inhibitor resistance.

4. Materials and Methods

Two datasets, GSE14520 and GSE41666, were downloaded from the GEO database and analyzed to determine hypoxia-induced differentially expressed genes in HCC. Functional enrichment analysis and protein–protein interaction (PPI) network construction screened the differentially expressed genes for hub genes. Multiple regression analysis models were constructed using the expression of common differentially expressed genes in the TCGA database to screen for genes highly associated with PD-L1 expression. Finally, we used the Kaplan Meier plotter to analyze PPI hub genes survival and response rates after treatment with PD-L1 immune checkpoint inhibitors and associated pathway analysis to identify potential pathways regulating PD-L1 expression in the hypoxic HCC tumor microenvironment (Figure 7).

4.1. Microarray Data Collection and Processing

Two datasets, GSE14520 and GSE41666, were obtained from the GEO database. In the GSE14520 dataset, a single channel array platform was used to profile the gene expression levels of 214 tumor and 214 paired non-tumor samples of HCC patients. In the GSE41666 dataset, HepG2 HCC cell line samples were exposed to anoxia with 24 h of 0% O_2 and normoxia with a control of 21% O_2, respectively. As 3 biological replicates were performed for each condition, the gene expression levels of 6 samples were profiled by the expression beadchip platform.

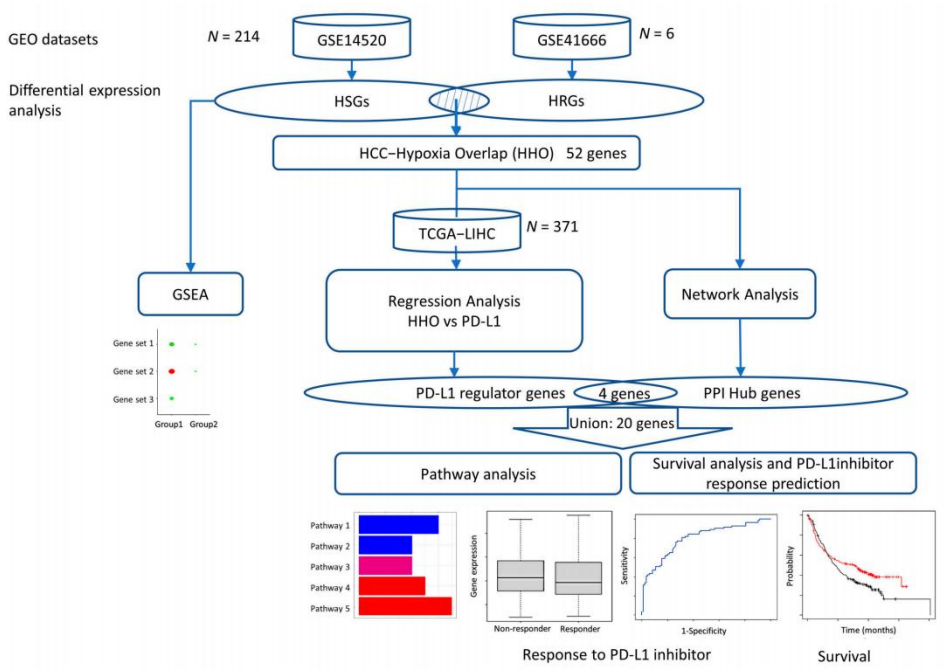

Figure 7. Flowchart of this study.

For each gene interrogated by multiple probes in the microarray chip, the average of expression levels of respective probes was taken to provide an expression matrix of unique gene symbols. The log2-transformation was applied to the expression matrix of the GSE14520 dataset but not to the GSE41666 dataset, which has undergone Variance stabilizing normalization (VSN). Standardization was performed to both matrices to obtain normally distributed expression levels, N (0,1). The flowchart of data processing and analysis is shown in (Figure 8).

4.2. Identification of Differentially Expressed Genes

Differential expression analysis was performed based on t-test and fold change (FC). For each gene, the *p*-value generated by t-test indicates the statistical significance of differential expression. To address the issue of multiple hypothesis tests for a huge number of genes, *q*-values, i.e., the estimated false discovery rates (FDRs), were derived from *p*-values based on the Storey-Tibshirani *q*-value procedure [41]. For GSE14520, the related sample *t*-test was used to examine the difference between the tumor and paired non-tumor samples. HCC-signature genes (HSGs) are defined as differentially expressed genes where *q*-value < 0.05, FC > 1.4 (upregulated) and <1/1.34 (downregulated) in HCC tumor compared to paired non-tumor samples. For GSE41666, hypoxia-related genes (HRGs) are defined as the differentially expressed genes with *q*-value < 0.05 and FC > 1.301 (upregulated) and <1/1.199 (downregulated), respectively. The cut-off values of FC were determined based on the quantities of upregulated and downregulated genes to be selected. The Venn diagrams were drawn using the Venny 2.1 platform (https://bioinfogp.cnb.csic.es/tools/venny/, as of 25 November 2022), and the HCC-Hypoxia Overlap (HHO) is defined as the gene set obtained from the intersection of HSGs and HRGs.

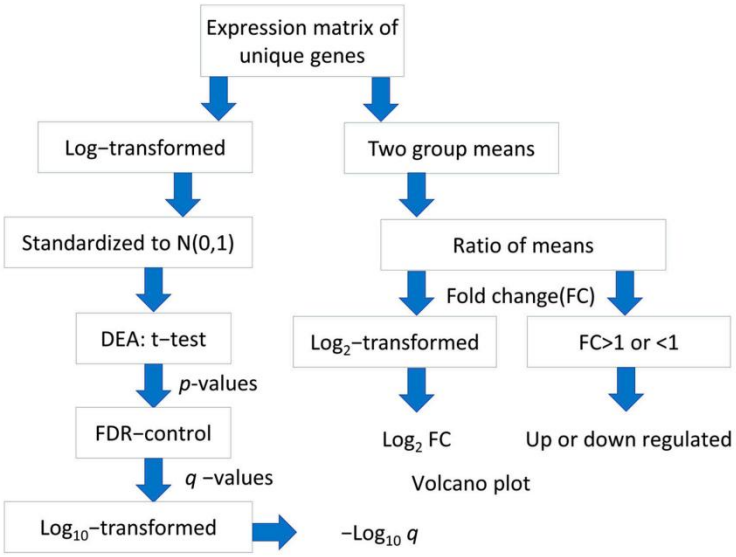

Figure 8. Flowchart of processing and analysis of microarray datasets.

4.3. GO Function and KEGG Pathway Enrichment Analysis of HSGs and HRGs

In this study, for the HSGs and HRGs, Gene Ontology (GO; http://geneontology.org, as of 29 November 2022) analysis was first performed by Python to obtain the results of HSGs and HRGs enrichment in Biological Process (BP), Cellular Component (CC), and Molecular Function (MF). The results of enrichment in Biological Process (BP), Cellular Component (CC), and Molecular Function (MF) were obtained. Then, the Kyoto Encyclopedia of Genes and Genomes (KEGG; https://www.kegg.jp/, as of 29 November 2022) signaling pathway enrichment analysis was performed, and the pathway enrichment results were obtained. The adjusted p-value < 0.05 and FDR adjusted p-value < 0.05 were statistically significant and were the thresholds for selecting the major enrichment functions and pathways of the HSGs and HRGs.

4.4. Gene Set Enrichment Analysis (GSEA) of HSGs and HRGs

GSEA is a computational method for analyzing and interpreting changes in gene pathway levels and association analysis in transcriptomics experiments, including genome-wide association studies and RNA-seq gene expression experiments. The random permutation procedure (permutation_num = 1000) using the gseapy-v1.0.0 python library was used to obtain the zero distribution. The Enrichr method in the gseapy-v1.0 python library was used to determine the signaling pathways regulated by hypoxia-related features of HCC (adjust p value < 0.05). The gseapy-v1.0.0 package currently supports a library of 202 databases.

4.5. PPI Network Construction and Identification of Hub Genes

STRING (Search Tool for the Retrieval of Interacting Genes, http://string-db.org/, as of 12 December 2022) is an online database for searching protein interactions. To further explore the interactions among HHOs, which represent the overlapping genes between HSGs and HRGs, the HHOs were imported into STRING to obtain the PPI network with a confidence score > 0.7 [42]. Among the HHOs, the PPI hub genes were identified with a degree threshold using the degree algorithm of cytoHubba, where the connectivity degree

of a gene is defined as its connected neighbors [43]. A threshold was selected to include 10 PPI hub genes with the top degree values for further analysis.

4.6. Multiple Regression Analysis of the Effect of HHOs on PD-L1

To examine the effect of HHO on PD-L1 expression, we used multiple regression analysis. RNAseq expressions of TCGA-LIHC were obtained from the UCSC xena website (https://xenabrowser.net/datapages/ as of 6 December 2022), including 371 HCC tissue samples, and RNAseq expressions of HHOs and PD-L1 were extracted and standardized. Compared with machine learning models, multiple regression could produce more stabilized and re-producible results without fixing a particular random seed. We adopted stepwise forward algorithm (p value < 0.05) to select the genes from HHO that significantly and substantially affect the PD-L1 expression level, denoted by Y in the following formula:

$$Y = b_0 + b_1X_1 + b_2X_2 + \ldots + b_nX_n,$$

where X_n represents the expression level of the nth selected gene and b_n represents the corresponding coefficient quantifying its effect on PD-L1 expression. The selected genes are denoted by PD-L1 regulator genes.

4.7. Survival Analysis and PD-L1 Inhibitor Response Prediction

Kaplan Meier plotter (KM plotter; http://kmplot.com/analysis/ as of 21 December 2022) is a survival analysis platform containing clinical data and gene expression data with survival information from GEO, EGA, and TCGA databases. We plotted survival curves and calculated risk ratios for log-rank p values and 95% confidence intervals for each of PPI hub genes and PD-L1 regulator genes in cancer patients. The patients were stratified into higher and lower expression groups based on the median expression level of each gene before PD-L1 inhibitor treatment.

The ROC plotter (https://www.rocplot.org/ as of 23 December 2022) is a tool that enables the identification of predictive biomarkers based on gene expression using transcriptomic data from many cancer patients. It was used to evaluate the ability of expression level of each of the PPI hub genes and PD-L1 regulator genes in predicting the response to the PD-L1 inhibitor based on 454 pan-cancer patients in the database.

In addition, we performed KEGG pathway enrichment analysis with the criteria of FDR < 0.05 for the union of PPI hub genes and PD-L1 regulator genes in the ShinyGo 0.76.3 platform (http://bioinformatics.sdstate.edu/go/ as of 1 January 2023).

5. Conclusions

Overall, a comprehensive bioinformatics analysis of hypoxia-induced PD-L1 inhibitor resistance in HCC was performed and revealed that genes such as *TPX2*, *NDC80*, *POLE2*, *GABARAPL1*, and *PIK3R1* may be involved in the PI3K-AKT signaling pathway and play an essential role in the pathological and physiological processes of hypoxia-induced PD-L1 inhibitor resistance. The results of this study may provide potential therapeutic targets and deepen the understanding of the underlying mechanisms of hypoxia-induced PD-L1 inhibitor resistance.

Supplementary Materials: The following supporting information can be downloaded at: https://www.mdpi.com/article/10.3390/ijms24108720/s1.

Author Contributions: Conceptualization, M.H. and L.W.C.C.; methodology, M.H. and L.W.C.C.; software, L.Z., Y.Z., M.H. and L.W.C.C.; validation, S.Y., W.C.S.T., W.C.S.C. and S.C.C.W.; formal analysis, M.H. and L.W.C.C.; investigation, M.H. and L.W.C.C.; data curation, L.Z., Y.Z. and M.H.; writing—original draft preparation, M.H. and L.W.C.C.; writing—review and editing, M.H., W.C.S.C., W.C.S.T. and L.W.C.C.; visualization, L.Z., Y.Z., M.H. and L.W.C.C.; supervision, L.W.C.C.; project administration, L.W.C.C. All authors have read and agreed to the published version of the manuscript.

Funding: The APC was funded by Faculty of Health and Social Sciences, Hong Kong Polytechnic University.

Institutional Review Board Statement: Ethical review and approval were waived for this study because only public datasets were used.

Informed Consent Statement: Patient consent was waived because only public datasets were used.

Data Availability Statement: https://www.ncbi.nlm.nih.gov/geo/query/acc.cgi?acc=gse14520; https://www.ncbi.nlm.nih.gov/geo/query/acc.cgi?acc=GSE41666; https://portal.gdc/cancer.gov/projects/TCGA-LIHC.

Conflicts of Interest: The authors declare no conflict of interest.

References

1. Yau, T.; Tai, D.; Chan, S.L.; Huang, Y.-H.; Choo, S.P.; Hsu, C.; Cheung, T.T.; Lin, S.-M.; Yong, W.P.; Lee, J.; et al. Systemic Treatment of Advanced Unresectable Hepatocellular Carcinoma after First-Line Therapy: Expert Recommendations from Hong Kong, Singapore, and Taiwan. *Liver Cancer* **2022**, *11*, 426–439. [CrossRef]
2. European Association for the Study of the Liver. European Association for the Study of the Liver. EASL Clinical Practice Guidelines: Management of hepatocellular carcinoma. *J. Hepatol.* **2018**, *69*, 182–236. [CrossRef] [PubMed]
3. Shek, D.; Read, S.A.; Nagrial, A.; Carlino, M.S.; Gao, B.; George, J.; Ahlenstiel, G. Immune-Checkpoint Inhibitors for Advanced Hepatocellular Carcinoma: A Synopsis of Response Rates. *Oncol.* **2021**, *26*, e1216–e1225. [CrossRef] [PubMed]
4. Shurin, M.R.; Umansky, V. Cross-talk between HIF and PD-1/PD-L1 pathways in carcinogenesis and therapy. *J. Clin. Invest.* **2022**, *132*, e159473. [CrossRef] [PubMed]
5. Guo, Y.; Xiao, Z.; Yang, L.; Gao, Y.; Zhu, Q.; Hu, L.; Huang, D.; Xu, Q. Hypoxia-inducible factors in hepatocellular carcinoma (Review). *Oncol. Rep.* **2020**, *43*, 3–15. [CrossRef]
6. Mo, Z.; Liu, D.; Rong, D.; Zhang, S. Hypoxic Characteristic in the Immunosuppressive Microenvironment of Hepatocellular Carcinoma. *Front. Immunol.* **2021**, *12*, 611058. [CrossRef]
7. Sadeghi, F.; Kardar, G.A.; Bolouri, M.R.; Nasri, F.; Sadri, M.; Falak, R. Overexpression of bHLH domain of HIF-1 failed to inhibit the HIF-1 transcriptional activity in hypoxia. *Biol. Res.* **2020**, *53*, 25. [CrossRef]
8. Sun, Y.; Tan, J.; Miao, Y.; Zhang, Q. The role of PD-L1 in the immune dysfunction that mediates hypoxia-induced multiple organ injury. *Cell Commun. Signal.* **2021**, *19*, 76. [CrossRef] [PubMed]
9. Ding, X.-C.; Wang, L.-L.; Zhang, X.-D.; Xu, J.-L.; Li, P.-F.; Liang, H.; Zhang, X.-B.; Xie, L.; Zhou, Z.-H.; Yang, J.; et al. The relationship between expression of PD-L1 and HIF-1α in glioma cells under hypoxia. *J. Hematol. Oncol.* **2021**, *14*, 1–5. [CrossRef] [PubMed]
10. Lee, C.K.; Chan, S.L.; Chon, H.J. Could We Predict the Response of Immune Checkpoint Inhibitor Treatment in Hepatocellular Carcinoma? *Cancers* **2022**, *14*, 3213. [CrossRef]
11. Bailey, C.M.; Liu, Y.; Liu, M.; Du, X.; Devenport, M.; Zheng, P.; Liu, Y.; Wang, Y. Targeting HIF-1α abrogates PD-L1–mediated immune evasion in tumor microenvironment but promotes tolerance in normal tissues. *J. Clin. Investig.* **2022**, *132*, e150846. [CrossRef] [PubMed]
12. Jin, X.; Ding, D.; Yan, Y.; Li, H.; Wang, B.; Ma, L.; Ye, Z.; Ma, T.; Wu, Q.; Rodrigues, D.N.; et al. Phosphorylated RB Promotes Cancer Immunity by Inhibiting NF-kappaB Activation and PD-L1 Expression. *Mol. Cell.* **2019**, *73*, 22–35.e6. [CrossRef] [PubMed]
13. Taniguchi, C.M.; Emanuelli, B.; Kahn, C.R. Critical nodes in signalling pathways: Insights into insulin action. *Nat. Rev. Mol. Cell Biol.* **2006**, *7*, 85–96. [CrossRef]
14. Taniguchi, C.M.; Winnay, J.; Kondo, T.; Bronson, R.T.; Guimaraes, A.R.; Aleman, J.O.; Luo, J.; Stephanopoulos, G.; Weissleder, R.; Cantley, L.C.; et al. The phosphoinositide 3-kinase regulatory subunit p85alpha can exert tumor suppressor properties through negative regulation of growth factor signaling. *Cancer Res.* **2010**, *70*, 5305–5315. [CrossRef] [PubMed]
15. Ai, X.; Xiang, L.; Huang, Z.; Zhou, S.; Zhang, S.; Zhang, T.; Jiang, T. Overexpression of PIK3R1 promotes hepatocellular carcinoma progression. *Biol. Res.* **2018**, *51*, 52. [CrossRef]
16. Fojtík, P.; Beckerová, D.; Holomková, K.; Šenfluk, M.; Rotrekl, V. Both Hypoxia-Inducible Factor 1 and MAPK Signaling Pathway Attenuate PI3K/AKT via Suppression of Reactive Oxygen Species in Human Pluripotent Stem Cells. *Front. Cell Dev. Biol.* **2021**, *8*, 607444. [CrossRef]
17. Chen, M.; Zhang, H.; Zhang, G.; Zhong, A.; Ma, Q.; Kai, J.; Tong, Y.; Xie, S.; Wang, Y.; Zheng, H.; et al. Targeting TPX2 suppresses proliferation and promotes apoptosis via repression of the PI3k/AKT/P21 signaling pathway and activation of p53 pathway in breast cancer. *Biochem. Biophys. Res. Commun.* **2018**, *507*, 74–82. [CrossRef]
18. Huang, D.H.; Jian, J.; Li, S.; Zhang, Y.; Liu, L.Z. TPX2 silencing exerts anti-tumor effects on hepatocellular carcinoma by regulating the PI3K/AKT signaling pathway. *Int. J. Mol. Med.* **2019**, *44*, 2113–2122. [CrossRef]
19. Scheiter, A.; Keil, F.; Lüke, F.; Grosse, J.; Verloh, N.; Opitz, S.; Schlosser, S.; Kandulski, A.; Pukrop, T.; Dietmaier, W.; et al. Identification and In-Depth Analysis of the Novel FGFR2-NDC80 Fusion in a Cholangiocarcinoma Patient: Implication for Therapy. *Curr. Oncol.* **2021**, *28*, 1161–1169. [CrossRef]
20. Rizvi, S.; Gores, G.J. Emerging molecular therapeutic targets for cholangiocarcinoma. *J. Hepatol.* **2017**, *67*, 632–644. [CrossRef]

21. Ju, L.-L.; Chen, L.; Li, J.-H.; Wang, Y.-F.; Lu, R.-J.; Bian, Z.-L.; Shao, J.-G. Effect of NDC80 in human hepatocellular carcinoma. *World J. Gastroenterol.* **2017**, *23*, 3675–3683. [CrossRef]
22. Zhou, J.; Pei, Y.; Chen, G.; Cao, C.; Liu, J.; Ding, C.; Wang, D.; Sun, L.; Xu, P.; Niu, G. SPC24 Regulates breast cancer progression by PI3K/AKT signaling. *Gene* **2018**, *675*, 272–277. [CrossRef] [PubMed]
23. Zhang, C.; Shen, Y.; Gao, L.; Wang, X.; Huang, D.; Xie, X.; Xu, D.; He, H. Targeting POLE2 Creates a Novel Vulnerability in Renal Cell Carcinoma via Modulating Stanniocalcin 1. *Front. Cell Dev. Biol.* **2021**, *9*, 622344. [CrossRef] [PubMed]
24. Su, W.; Li, S.; Chen, X.; Yin, L.; Ma, P.; Ma, Y.; Su, B. GABARAPL1 suppresses metastasis by counteracting PI3K/Akt pathway in prostate cancer. *Oncotarget* **2017**, *8*, 4449–4459. [CrossRef] [PubMed]
25. Jacquet, M.; Guittaut, M.; Fraichard, A.; Despouy, G. The functions of Atg8-family proteins in autophagy and cancer: Linked or unrelated? *Autophagy* **2021**, *17*, 599–611. [CrossRef] [PubMed]
26. Di-Luoffo, M.; Schmitter, C.; Barrere, E.C.; Therville, N.; Delarue, M.; Guillermet-Guibert, J. The biomechanical context influences the PI3K output signaling in breast and pancreatic cancer cells. *bioRxiv* **2022**. bioRxiv:2021.10.18.464825.
27. Zhuang, H.; Wang, S.; Chen, B.; Zhang, Z.; Ma, Z.; Li, Z.; Liu, C.; Zhou, Z.; Gong, Y.; Huang, S.; et al. Prognostic Stratification Based on HIF-1 Signaling for Evaluating Hypoxic Status and Immune Infiltration in Pancreatic Ductal Adenocarcinomas. *Front. Immunol.* **2021**, *12*, 790661. [CrossRef]
28. Meng, L.; Liu, B.; Ji, R.; Jiang, X.; Yan, X.; Xin, Y. Targeting the BDNF/TrkB pathway for the treatment of tumors. *Oncol. Lett.* **2018**, *17*, 2031–2039. [CrossRef]
29. Barsoum, I.B.; Smallwood, C.A.; Siemens, D.R.; Graham, C.H. A Mechanism of Hypoxia-Mediated Escape from Adaptive Immunity in Cancer Cells. *Cancer Res.* **2014**, *74*, 665–674. [CrossRef]
30. Lei, Q.; Wang, D.; Sun, K.; Wang, L.; Zhang, Y. Resistance Mechanisms of Anti-PD1/PDL1 Therapy in Solid Tumors. *Front. Cell Dev. Biol.* **2020**, *8*, 672. [CrossRef]
31. Ahn, A.; Rodger, E.J.; Motwani, J.; Gimenez, G.; Stockwell, P.A.; Parry, M.; Hersey, P.; Chatterjee, A.; Eccles, M.R. Transcriptional Reprogramming and Constitutive PD-L1 Expression in Melanoma Are Associated with Dedifferentiation and Activation of Interferon and Tumour Necrosis Factor Signalling Pathways. *Cancers* **2021**, *13*, 4250. [CrossRef] [PubMed]
32. Zalpoor, H.; Bakhtiyari, M.; Liaghat, M.; Nabi-Afjadi, M.; Ganjalikhani-Hakemi, M. Quercetin potential effects against SARS-CoV-2 infection and COVID-19-associated cancer progression by inhibiting mTOR and hypoxia-inducible factor-1alpha (HIF-1alpha). *Phytother Res.* **2022**, *36*, 2679–2682. [CrossRef] [PubMed]
33. Ye, L.-L.; Wei, X.-S.; Zhang, M.; Niu, Y.-R.; Zhou, Q. The Significance of Tumor Necrosis Factor Receptor Type II in CD8(+) Regulatory T Cells and CD8(+) Effector T Cells. *Front. Immunol.* **2018**, *9*, 583. [CrossRef] [PubMed]
34. Bulua, A.C.; Simon, A.; Maddipati, R.; Pelletier, M.; Park, H.; Kim, K.-Y.; Sack, M.N.; Kastner, D.L.; Siegel, R.M. Mitochondrial reactive oxygen species promote production of proinflammatory cytokines and are elevated in TNFR1-associated periodic syndrome (TRAPS). *J. Exp. Med.* **2011**, *208*, 519–533. [CrossRef]
35. Sebestyén, A.; Kopper, L.; Dankó, T.; Tímár, J. Hypoxia Signaling in Cancer: From Basics to Clinical Practice. *Pathol. Oncol. Res.* **2021**, *27*, 1609802. [CrossRef]
36. Schumacker, P.T. SIRT3 Controls Cancer Metabolic Reprogramming by Regulating ROS and HIF. *Cancer Cell* **2011**, *19*, 299–300. [CrossRef]
37. Hu, Z.Z.; Dong, N.; Lu, D.; Jiang, X.Q.; Xu, J.J.; Wu, Z.W.; Zheng, D.T.; Wechsler, D.S. A positive feedback loop between ROS and Mxi1-0 promotes hypoxia-induced VEGF expression in human hepatocellular carcinoma cells. *Cell. Signal.* **2017**, *31*, 79–86. [CrossRef]
38. Rohr-Udilova, N.; Sieghart, W.; Eferl, R.; Stoiber, D.; Björkhem-Bergman, L.; Eriksson, L.C.; Stolze, K.; Hayden, H.; Keppler, B.; Sagmeister, S.; et al. Antagonistic effects of selenium and lipid peroxides on growth control in early hepatocellular carcinoma. *Hepatology* **2011**, *55*, 1112–1121. [CrossRef]
39. Séhédic, D.; Roncali, L.; Djoudi, A.; Buchtova, N.; Avril, S.; Chérel, M.; Boury, F.; Lacoeuille, F.; Hindré, F.; Garcion, E. Rapamycin-Loaded Lipid Nanocapsules Induce Selective Inhibition of the mTORC1-Signaling Pathway in Glioblastoma Cells. *Front. Bioeng. Biotechnol.* **2020**, *8*, 602998. [CrossRef]
40. Salman, S.; Meyers, D.J.; Wicks, E.E.; Lee, S.N.; Datan, E.; Thomas, A.M.; Anders, N.M.; Hwang, Y.; Lyu, Y.; Yang, Y.; et al. HIF inhibitor 32-134D eradicates murine hepatocellular carcinoma in combination with anti-PD1 therapy. *J. Clin. Invest.* **2022**, *132*, e156774. [CrossRef]
41. Storey, J.D.; Tibshirani, R. Statistical significance for genomewide studies. *Proc. Natl. Acad. Sci. USA* **2003**, *100*, 9440–9445. [CrossRef] [PubMed]
42. Bozhilova, L.V.; Whitmore, A.V.; Wray, J.; Reinert, G.; Deane, C.M. Measuring rank robustness in scored protein interaction networks. *BMC Bioinform.* **2019**, *20*, 446. [CrossRef] [PubMed]
43. Wu, Q.; Ying, X.; Yu, W.; Li, H.; Wei, W.; Lin, X.; Zhang, X. Identification of ferroptosis-related genes in syncytiotrophoblast-derived extracellular vesicles of preeclampsia. *Medicine* **2022**, *101*, e31583. [CrossRef] [PubMed]

Supplementary materials

	Gene set	Overlap	Adjusted P-value	Genes	Databases
HSGs	Rb Immunity Downregulating Pd-L1 GSE109724 1	12/250	0.022	TPX2*; KIF20A*; CENPA*; DLGAP5*; LMNB1*; HILPDA; TM4SF1; GNAZ; CDK1; HMGB2; KDELR3; APOBEC3B	RNAseq_Automatic_GEO_Signatures_Human_Down
HSGs	Rb Immunity Downregulating Pd-L1 GSE109724 3	12/250	0.022	LMNB1*; HILPDA; TM4SF1; ZNF143; SERPINB1; CDCA4; PDGFA; SFN; EPPK1; SOX12; DKK1; SOX4	RNAseq_Automatic_GEO_Signatures_Human_Down
HRGs	Rb Immunity Downregulating Pd-L1 GSE109724 1	16/250	3.982×10^{-4}	CENPA*; LMNB1*; TPX2*; KIF20A*; DLGAP5*; KIFC1; TNFAIP8L1; RAD54L; CDCA3; DHCR24; PSRC1; PBK; NUSAP1; FAM64A; KIF2C; FAM72D	RNAseq_Automatic_GEO_Signatures_Human_Down
HRGs	Rb Immunity Downregulating Pd-L1	14/250	0.009	PRDM8; DUSP5; SEMA4B; PDGFB; NDRG1; VEGFA; FOSL1; ABTB1; GPRC5A; PLCH2; ARHGEF2; ITGA5; RIN2; EPHA2	RNAseq_Automatic_GEO_Signatures_Human_Down

	GSE109724 3				
HRGs	Tissue-Resident			PPP1R15A; USP36; CSRNP2; ANKRD37;	
	Pancreas Pd-1			PFKFB3; METRNL; HERPUD1; RND1;	
	Pd-L1			ZFP36; RASD1; SERTAD1; NAMPT; PMAIP1;	
	GSE135582 3			DNAJB9; PIM3; TSPYL2; EGR1; DUSP5;	RNAseq_Auto
				GABARAPL1; WSB1; FOS; TUBA4A; FOSL2;	matic_GEO_Signatures
		29/250	2.008×10^{-12}	VEGFA; PER1; DDIT3; MAFF; JMY; FOSB	_Human_Up
HRGs	Tissue-Resident				
	Pancreas Pd-1			TSPYL2; USP36; GABARAPL1; PFKFB3;	RNAseq_Auto
	Pd-L1			ARID5A; FOS; METRNL; NDRG1; FOSL2;	matic_GEO_Signatures
	GSE135582 1	14/250	0.004	PER1; ZFP36; NAMPT; IDS; PMAIP1	_Human_Up
HRGs	Rb Immunity				
	Downregulating			TSPYL2; ARRDC4; KLF10; PPP1R15A;	RNAseq_Auto
	Pd-L1			EGR1; PER1; USP36; DUSP1; MAFF; FOSB;	matic_GEO_Signatures
	GSE109724 1	12/250	0.023	FOS; ALOXE3	_Human_Up

Table S1. RNAseq GEO Signatures Human enrichment analysis of HSGs and HRGs.

[1] *Represents duplicate genes in HSGs and HRGs

Table S2. The multiple regression model identified 14 effector genes affecting the PD-L1 expression: Coefficient associated with the expression level of effector gene, the corresponding t-score and p-value.

Effector gene	Co-efficient, b	t	p
const	0.076	1.897	0.059
DLGAP5	0.443*	3.6	3.636×10^{-4}
NDC80	0.41*	3.292	0.001
LMNB1	0.317*	3.062	0.002
FAM13A	0.261	5.893	8.770×10^{-9}
FOS	0.24	5.369	1.434×10^{-7}
GABARAPL1	0.23	4.595	6.004×10^{-6}
PIK3R1	0.145	2.57	0.011
EPHA2	0.121	2.593	0.01
NEDD4L	−0.096	−2.008	0.045
CABYR	−0.123	−2.971	0.003
HGFAC	−0.15	−3.599	3.652×10^{-4}
ALDH5A1	−0.264	−5.006	8.740×10^{-7}
KIF20A	−0.418*	−3.472	5.803×10^{-4}
TPX2	−0.434*	−3.156	0.002

[1] *Represents PD-L1 regulator genes with the top five coefficient magnitudes

Table S3. Kaplan-Meier survival analysis and ROC of hub genes and PD-L1 regulator genes of hepatocellular carcinoma

Gene name	Hub gene	Regression	OS PD-L1	RFS	PFS	DSS	Respons PD-L1 inh
CCNB1	√		0.3	1.2×10^{-4}*	6.9×10^{-6}*	5.3×10^{-4}*	0.3
BUB1B	√		0.33	0.014*	1.1×10^{-4}*	1.2×10^{-4}*	0.33
KIF4A	√		0.85	0.005*	2.6×10^{-4}*	1.7×10^{-4}*	0.37
KIF11	√		0.51	6.8×10^{-4}*	2.6×10^{-5}*	4.0×10^{-4}*	0.24
CENPA*	√		0.094	0.009*	0.001*	4.1×10^{-4}*	0.22
POLE2*	√		0.081	0.77	0.087	0.029*	0.027
KIF20A*	√	√	0.14	2.7×10^{-4}*	1.8×10^{-5}*	1.6×10^{-4}*	0.22
NDC80*	√	√	0.024*	0.017*	0.003	0.004*	0.07
TPX2*	√	√	0.03*	0.001*	6.6×10^{-6}*	6.8×10^{-6}*	0.28
DLGAP5*	√	√	0.54	0.006*	1.0×10^{-4}*	1.4×10^{-4}*	0.38
FOS		√	0.2	0.47	0.67	0.71	0.26
FAM13A		√	0.92	0.8	0.87	0.77	0.08
ALDH5A1		√	0.35	0.13	0.033*	0.023*	0.31
GABARAPL1*		√	0.096	0.23	0.007*	0.002*	0.016
CABYR		√	0.17	0.07	0.089	0.1	0.15
PIK3R1*		√	0.74	0.05*	0.13	0.007*	0.04
HGFAC		√	0.52	0.023*	0.026*	0.14	0.26
LMNB1*		√	0.1	0.03*	0.002*	0.018*	0.5

EPHA2	√	0.88	0.12	0.051	0.22	0.12
NEDD4L	√	0.36	0.68	0.91	0.7	0.4

[1] *Represents hub genes and PD-L1 regulator genes with the top five coefficient magnitudes

RFS: Relapse-Free Survival; PFS: Progression-Free Survival; DSS: Disease-Specific Survival

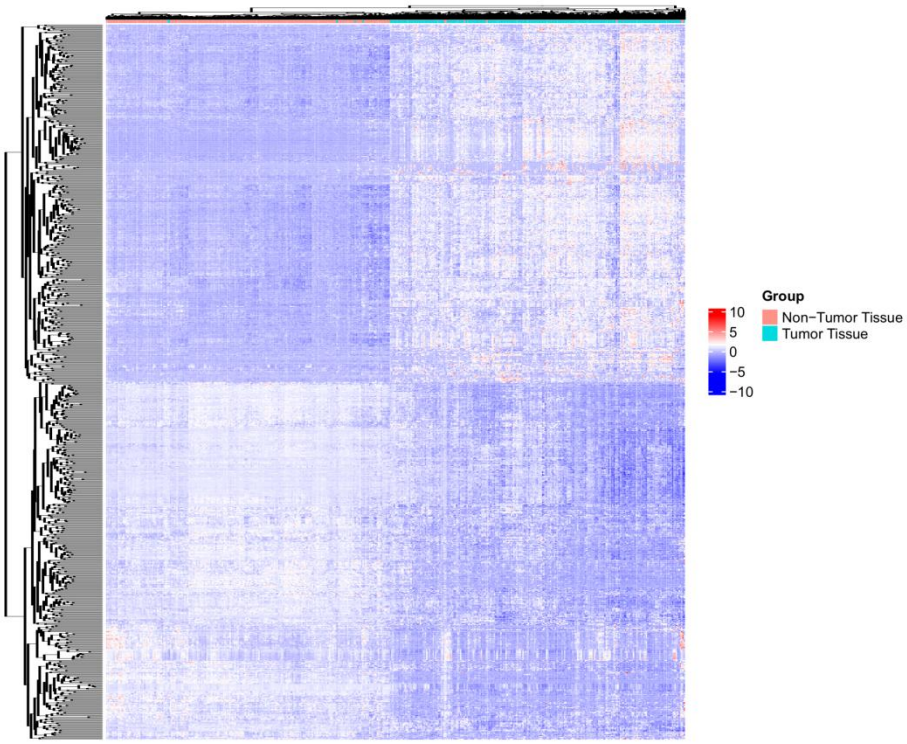

Figure S1a Heatmap for HSG expression levels

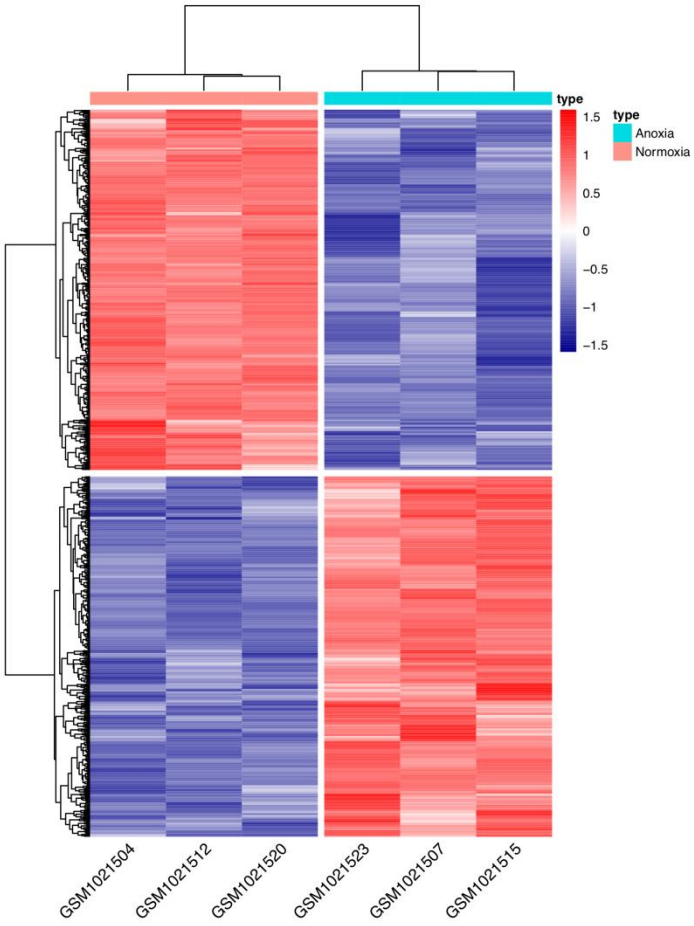

Figure S1b Heatmap for HRG expression levels

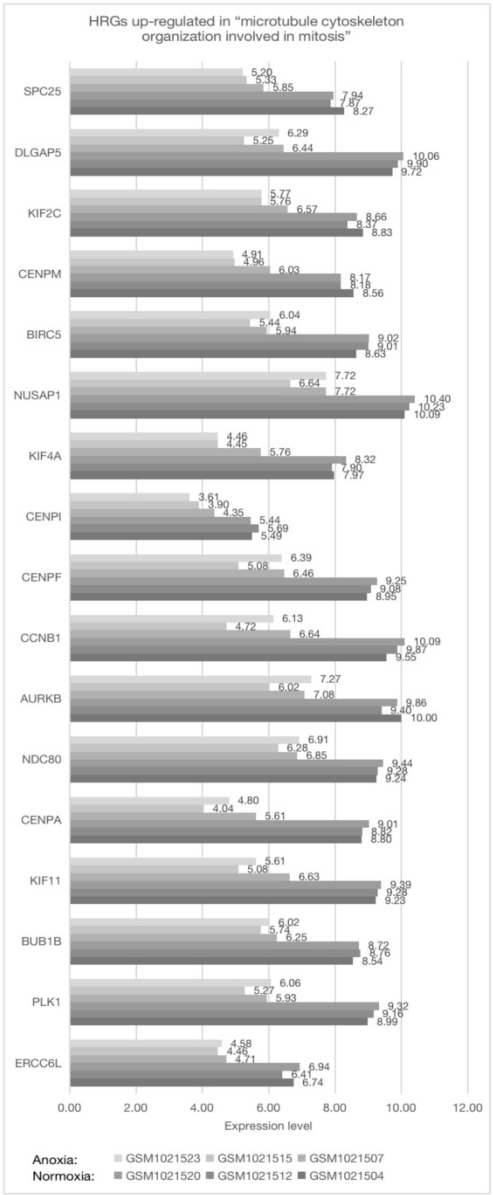

Figure S2 Bar chart of expression profiles of HRGs up-regulated in "microtubule cytoskeleton organization involved in mitosis"

Hypoxia-related genes and PD-L1 inhibitor resistance in hepatocellular carcinoma.

Huang Mohan, Wing Chi Chan; Health Technology and Informatics, Hong Kong, Hung Hom, Hong Kong; Health Technology and Informatics, Hong Kong, Hong Kong

Background: PD-L1 inhibitor in combination with anti-angiogenic drug has become the first-line treatment strategy for unresectable hepatocellular carcinoma (HCC). However, PD-L1 inhibitor resistance remains an essential issue in treating HCC. It has been proved in the tumor microenvironment that hypoxia-induced increase in PD-L1 expression makes a significant impact on drug resistance. **Methods:** Two public datasets of gene expression profiles (GSE 14520 and GSE 41666) from the Gene Expression Omnibus (GEO) database were analyzed using bioinformatics: (1) HCC tumor versus adjacent normal tissue (N = 214) and (2) normoxia versus anoxia of HepG2 cells (N = 6). HCC-signature and hypoxia-related genes were identified as the differentially expressed genes (DEGs). Gene set enrichment analyses (GSEA) were performed on the DEGs. Furthermore, multiple regression analysis on the TCGA-LIHC dataset (N=371) and construction of the protein-protein interaction (PPI) network were performed to investigate potential PD-L1 regulatory genes and hub genes. **Results:** A total of 52 genes overlapped in HCC-signature and hypoxia-related DEGs. Five genes were identified by GSEA as being concurrently associated with the PD-L1 expression pathways. Multiple regression analysis results showed 14 potential PD-L1 regulatory genes. Ten hub genes were identified in the PPI network. Finally, three genes (DLGAP5, KIF20A, and TPX2) were found in common and may be regulatory genes affecting PD-L1 expression. **Conclusions:** In conclusion, our study provides new insights into the potential hypoxia-related mechanisms of PD-L1 inhibitor resistance and contributes to exploring new therapeutic strategies for treating unresectable HCC. Research Sponsor: None.

e16261

Publication Only

Machine learning identification of hypoxia-related genes and prognostic risk-scoring model for effective survival stratification in hepatocellular carcinoma.

Huang Mohan, Wing Chi Chan; Department of Health Technology and Informatics, Hong Kong Polytechnic University, Hong Kong, Hung Hom, Hong Kong; Department of Health Technology and Informatics, Hong Kong Polytechnic University, Hong Kong, Hong Kong

Background: Hepatocellular carcinoma (HCC) is the fourth leading cause of cancer-related mortality globally, where treatment and prognostic assessment have important implications in clinical practice. Hypoxia, as a common feature within solid tumors, can directly change the tumor microenvironment, which affects the efficacy of cancer treatment and prognosis. In this study, we constructed and validated a hypoxia-based prognostic model using bioinformatics and machine learning. **Methods:** Two public datasets, GSE14520 and GSE41666, were collected from the Gene Expression Omnibus: (1) HCC tumor tissues compared to adjacent normal tissues (N = 214) and (2) HepG2 cells under normoxic and hypoxic conditions (N = 6). Differential expression analysis was performed to identify HCC characteristic genes and hypoxia-related genes, including their common genes (HCC-Hypoxia Overlap genes, HHOs). Using RNA-seq data of HCC patients (N = 367) from the TCGA Liver Cancer (LIHC) database, univariate Cox regression models were identified, and the Least Absolute Shrinkage and Selection Operator (LASSO) algorithm selected hypoxia-characteristic genes for the multivariate survival model. A hypoxia-related risk score was calculated based on the model of these characteristic genes and dichotomized cases into high-risk (HR) and low-risk (LR) groups. The model was validated using liver cancer cases (N = 232) from the International Cancer Genome Consortium database (ICGC-LIRI-JP). **Results:** Through differential expression analysis of the two datasets, we identified 52 HHOs. Univariate Cox analysis of these HHOs indicated that 21 genes were significantly associated with HCC patient survival. Through LASSO regression analysis, a total of 9 characteristic genes, including CENPA, KIF20A, DLGAP5, HMMR, UPB1, AFM, CABYR, PHLDA2, and N4BP2L1 were ultimately retained in the survival model. Based on these 9 genes, TCGA-LIHC samples were classified into HR and LR groups, and Kaplan-Meier (KM) analysis revealed significant differences in survival outcomes ($p < 0.032$). Risk scoring of the ICGC-LIRI-JP validation set classified samples into HR and LR. KM analysis showed that the survival times of patients in the HR group were significantly shorter than those in the LR group ($p < 0.0001$). Receiver Operating Characteristic Analysis analysis of the survival model showed area under the curve values of 0.815, 0.774, and 0.771 at 1, 2, and 3 years, respectively, demonstrating high performance in risk stratification. **Conclusions:** This study established a prognostic risk-scoring model based on 9 characteristic genes associated with hypoxia. This model can effectively stratify risks among HCC patients and demonstrate excellent performance in predicting survival. These findings may offer new biomarkers and therapeutic targets for the personalized treatment of HCC. Research Sponsor: None.

References

[1] Y.K. Sim, M.C. Chong, M. Gandhi, Y.M. Pokharkar, Y. Zhu, L. Shi, L. Lequn, C.H. Chen, M. Kudo, J.H. Lee, S.I. Strasser, R. Chanwat, P.K.H. Chow, G. Asia-Pacific Hepatocellular Carcinoma Trials, Real-World Data on the Diagnosis, Treatment, and Management of Hepatocellular Carcinoma in the Asia-Pacific: The INSIGHT Study, Liver Cancer 13(3) (2024) 298-313.

[2] Y. Liu, L. Liu, Changes in the Epidemiology of Hepatocellular Carcinoma in Asia, Cancers (Basel) 14(18) (2022).

[3] H. Rumgay, J. Ferlay, C. de Martel, D. Georges, A.S. Ibrahim, R. Zheng, W. Wei, V. Lemmens, I. Soerjomataram, Global, regional and national burden of primary liver cancer by subtype, Eur J Cancer 161 (2022) 108-118.

[4] G. Candita, S. Rossi, K. Cwiklinska, S.C. Fanni, D. Cioni, R. Lencioni, E. Neri, Imaging Diagnosis of Hepatocellular Carcinoma: A State-of-the-Art Review, Diagnostics (Basel) 13(4) (2023).

[5] T.A. Addissouky, I.E.T.E. Sayed, M.M.A. Ali, Y. Wang, A.E. Baz, A.A. Khalil, N. Elarabany, Latest advances in hepatocellular carcinoma management and prevention through advanced technologies, Egyptian Liver Journal 14(1) (2024) 2.

[6] Y. Pan, H. Chen, J. Yu, Biomarkers in Hepatocellular Carcinoma: Current Status and Future Perspectives, Biomedicines 8(12) (2020).

[7] T. Ren, X. Hou, X. Zhang, D. Chen, J. Li, Y. Zhu, Z. Liu, D. Yang, Validation of combined AFP, AFP-L3, and PIVKA II for diagnosis and monitoring of

hepatocellular carcinoma in Chinese patients, Heliyon 9(11) (2023) e21906.

[8] A. Forner, M. Reig, J. Bruix, Hepatocellular carcinoma, Lancet 391(10127) (2018) 1301-1314.

[9] K. Coffman-D'Annibale, C. Xie, D.M. Hrones, S. Ghabra, T.F. Greten, C. Monge, The current landscape of therapies for hepatocellular carcinoma, Carcinogenesis 44(7) (2023) 537-548.

[10] A. Della Corte, M. Rimini, S. Steidler, D. Palumbo, F. Ratti, L. Aldrighetti, S. Cascinu, A. Casadei-Gardini, F. De Cobelli, Combined Loco-Regional and Systemic Treatment Strategies for Hepatocellular Carcinoma: From Basics to New Developments, Cardiovasc Intervent Radiol 46(2) (2023) 175-186.

[11] R. Sun, C. Wu, Y. Gou, Y. Zhao, P. Huang, Advancements in second-line treatment research for hepatocellular carcinoma, Clinical and Translational Oncology (2024).

[12] A. Forner, M. Gilabert, J. Bruix, J.-L. Raoul, Treatment of intermediate-stage hepatocellular carcinoma, Nature Reviews Clinical Oncology 11(9) (2014) 525-535.

[13] C.G. Dalzell, A.C. Taylor, S.B. White, New Insights on Liver-Directed Therapies in Hepatocellular Carcinoma, Cancers (Basel) 15(24) (2023).

[14] D. Shek, S.A. Read, A. Nagrial, M.S. Carlino, B. Gao, J. George, G. Ahlenstiel, Immune-Checkpoint Inhibitors for Advanced Hepatocellular Carcinoma: A Synopsis of Response Rates, Oncologist 26(7) (2021) e1216-e1225.

[15] F. Jost-Brinkmann, M. Demir, A. Wree, T. Luedde, S.H. Loosen, T. Muller,

F. Tacke, C. Roderburg, R. Mohr, Atezolizumab plus bevacizumab in unresectable hepatocellular carcinoma: Results from a German real-world cohort, Aliment Pharmacol Ther (2023).

[16] J. Giraud, D. Chalopin, J.F. Blanc, M. Saleh, Hepatocellular Carcinoma Immune Landscape and the Potential of Immunotherapies, Front Immunol 12 (2021) 655697.

[17] B.P. Keenan, L. Fong, R.K. Kelley, Immunotherapy in hepatocellular carcinoma: the complex interface between inflammation, fibrosis, and the immune response, J Immunother Cancer 7(1) (2019) 267.

[18] J.H. Choi, S.N. Thung, Advances in Histological and Molecular Classification of Hepatocellular Carcinoma, Biomedicines 11(9) (2023).

[19] Y. Chen, Y. Zhou, Z. Yan, P. Tong, Q. Xia, K. He, Effect of infiltrating immune cells in tumor microenvironment on metastasis of hepatocellular carcinoma, Cell Oncol (Dordr) 46(6) (2023) 1595-1604.

[20] X. Gao, R. Zhao, H. Ma, S. Zuo, Efficacy and safety of atezolizumab plus bevacizumab treatment for advanced hepatocellular carcinoma in the real world: a single-arm meta-analysis, BMC Cancer 23(1) (2023) 635.

[21] A.X. Zhu, A.R. Abbas, M.R. de Galarreta, Y. Guan, S. Lu, H. Koeppen, W. Zhang, C.H. Hsu, A.R. He, B.Y. Ryoo, T. Yau, A.O. Kaseb, A.M. Burgoyne, F. Dayyani, J. Spahn, W. Verret, R.S. Finn, H.C. Toh, A. Lujambio, Y. Wang, Molecular correlates of clinical response and resistance to atezolizumab in combination with bevacizumab in advanced hepatocellular carcinoma, Nat Med

28(8) (2022) 1599-1611.

[22] E. Cariani, G. Missale, Immune landscape of hepatocellular carcinoma microenvironment: Implications for prognosis and therapeutic applications, Liver Int 39(9) (2019) 1608-1621.

[23] A.L. Cheng, S. Qin, M. Ikeda, P. Galle, M. Ducreux, A. Zhu, T.Y. Kim, M. Kudo, V. Breder, P. Merle, A. Kaseb, D. Li, W. Verret, Z. Xu, S. Hernandez, J. Liu, C. Huang, S. Mulla, H.Y. Lim, R. Finn, IMbrave150: Efficacy and safety results from a ph III study evaluating atezolizumab (atezo) + bevacizumab (bev) vs sorafenib (Sor) as first treatment (tx) for patients (pts) with unresectable hepatocellular carcinoma (HCC), Annals of Oncology 30 (2019) ix186-ix187.

[24] L. Kou, X. Xie, X. Chen, B. Li, J. Li, Y. Li, The progress of research on immune checkpoint inhibitor resistance and reversal strategies for hepatocellular carcinoma, Cancer Immunol Immunother 72(12) (2023) 3953-3969.

[25] Z. Wang, Y. Wang, P. Gao, J. Ding, Immune checkpoint inhibitor resistance in hepatocellular carcinoma, Cancer Lett 555 (2023) 216038.

[26] F. Chai, P. Li, X. Liu, Z. Zhou, H. Ren, Targeting the PD-L1 cytoplasmic domain and its regulatory pathways to enhance cancer immunotherapy, J Mol Cell Biol 15(11) (2024).

[27] J. Luo, K. Liu, Y. Wang, H. Li, Divergent roles of PD-L1 in immune regulation during ischemia-reperfusion injury, Front Immunol 13 (2022) 1021452.

[28] Z. Liu, X. Yu, L. Xu, Y. Li, C. Zeng, Current insight into the regulation of PD-L1 in cancer, Experimental Hematology & Oncology 11(1) (2022) 44.

[29] X. Jiang, J. Wang, X. Deng, F. Xiong, J. Ge, B. Xiang, X. Wu, J. Ma, M. Zhou, X. Li, Y. Li, G. Li, W. Xiong, C. Guo, Z. Zeng, Role of the tumor microenvironment in PD-L1/PD-1-mediated tumor immune escape, Mol Cancer 18(1) (2019) 10.

[30] M. Yi, M. Niu, L. Xu, S. Luo, K. Wu, Regulation of PD-L1 expression in the tumor microenvironment, J Hematol Oncol 14(1) (2021) 10.

[31] V. Atsaves, N. Tsesmetzis, D. Chioureas, L. Kis, V. Leventaki, E. Drakos, T. Panaretakis, D. Grander, L.J. Medeiros, K.H. Young, G.Z. Rassidakis, PD-L1 is commonly expressed and transcriptionally regulated by STAT3 and MYC in ALK-negative anaplastic large-cell lymphoma, Leukemia 31(7) (2017) 1633-1637.

[32] L. Ai, A. Xu, J. Xu, Roles of PD-1/PD-L1 Pathway: Signaling, Cancer, and Beyond, Adv Exp Med Biol 1248 (2020) 33-59.

[33] T. Doi, T. Ishikawa, T. Okayama, K. Oka, K. Mizushima, T. Yasuda, N. Sakamoto, K. Katada, K. Kamada, K. Uchiyama, O. Handa, T. Takagi, Y. Naito, Y. Itoh, The JAK/STAT pathway is involved in the upregulation of PD-L1 expression in pancreatic cancer cell lines, Oncol Rep 37(3) (2017) 1545-1554.

[34] S. Chen, G.A. Crabill, T.S. Pritchard, T.L. McMiller, P. Wei, D.M. Pardoll, F. Pan, S.L. Topalian, Mechanisms regulating PD-L1 expression on tumor and immune cells, J Immunother Cancer 7(1) (2019) 305.

[35] X. Zhang, Y. Zeng, Q. Qu, J. Zhu, Z. Liu, W. Ning, H. Zeng, N. Zhang, W. Du, C. Chen, J.A. Huang, PD-L1 induced by IFN-gamma from tumor-associated

macrophages via the JAK/STAT3 and PI3K/AKT signaling pathways promoted progression of lung cancer, Int J Clin Oncol 22(6) (2017) 1026-1033.

[36] X. Zheng, S. Li, H. Yang, Roles of Toll-Like Receptor 3 in Human Tumors, Front Immunol 12 (2021) 667454.

[37] A. Vidyarthi, N. Khan, T. Agnihotri, S. Negi, D.K. Das, M. Aqdas, D. Chatterjee, O.R. Colegio, M.K. Tewari, J.N. Agrewala, TLR-3 Stimulation Skews M2 Macrophages to M1 Through IFN-alphabeta Signaling and Restricts Tumor Progression, Front Immunol 9 (2018) 1650.

[38] Y. Chen, J. Lin, Y. Zhao, X. Ma, H. Yi, Toll-like receptor 3 (TLR3) regulation mechanisms and roles in antiviral innate immune responses, J Zhejiang Univ Sci B 22(8) (2021) 609-632.

[39] Z. Wang, X. Wu, Study and analysis of antitumor resistance mechanism of PD1/PD-L1 immune checkpoint blocker, Cancer Med 9(21) (2020) 8086-8121.

[40] K. Bardhan, T. Anagnostou, V.A. Boussiotis, The PD1:PD-L1/2 Pathway from Discovery to Clinical Implementation, Front Immunol 7 (2016) 550.

[41] S.T. Haile, S.P. Dalal, V. Clements, K. Tamada, S. Ostrand-Rosenberg, Soluble CD80 restores T cell activation and overcomes tumor cell programmed death ligand 1-mediated immune suppression, J Immunol 191(5) (2013) 2829-36.

[42] D. Sugiura, T. Maruhashi, I.M. Okazaki, K. Shimizu, T.K. Maeda, T. Takemoto, T. Okazaki, Restriction of PD-1 function by cis-PD-L1/CD80 interactions is required for optimal T cell responses, Science 364(6440) (2019) 558-566.

[43] M.Z. Noman, G. Desantis, B. Janji, M. Hasmim, S. Karray, P. Dessen, V. Bronte, S. Chouaib, PD-L1 is a novel direct target of HIF-1alpha, and its blockade under hypoxia enhanced MDSC-mediated T cell activation, J Exp Med 211(5) (2014) 781-90.

[44] G. Lamberti, M. Sisi, E. Andrini, A. Palladini, F. Giunchi, P.L. Lollini, A. Ardizzoni, F. Gelsomino, The Mechanisms of PD-L1 Regulation in Non-Small-Cell Lung Cancer (NSCLC): Which Are the Involved Players?, Cancers (Basel) 12(11) (2020).

[45] Y. Shi, Regulatory mechanisms of PD-L1 expression in cancer cells, Cancer Immunol Immunother 67(10) (2018) 1481-1489.

[46] K.W. Mouw, M.S. Goldberg, P.A. Konstantinopoulos, A.D. D'Andrea, DNA Damage and Repair Biomarkers of Immunotherapy Response, Cancer Discov 7(7) (2017) 675-693.

[47] F. Guo, W. Kong, D. Li, G. Zhao, M. Anwar, F. Xia, Y. Zhang, C. Ma, X. Ma, M2-type tumor-associated macrophages upregulated PD-L1 expression in cervical cancer via the PI3K/AKT pathway, Eur J Med Res 29(1) (2024) 357.

[48] Z. Wang, X. Wang, Y. Xu, J. Li, X. Zhang, Z. Peng, Y. Hu, X. Zhao, K. Dong, B. Zhang, C. Gao, X. Zhao, H. Chen, J. Cai, Y. Bai, Y. Sun, L. Shen, Mutations of PI3K-AKT-mTOR pathway as predictors for immune cell infiltration and immunotherapy efficacy in dMMR/MSI-H gastric adenocarcinoma, BMC Medicine 20(1) (2022) 133.

[49] M. Yang, M. Cui, Y. Sun, S. Liu, W. Jiang, Mechanisms, combination therapy,

and biomarkers in cancer immunotherapy resistance, Cell Commun Signal 22(1) (2024) 338.

[50] A. Puyalto, M. Rodriguez-Remirez, I. Lopez, I. Macaya, E. Guruceaga, M. Olmedo, A. Vilalta-Lacarra, C. Welch, S. Sandiego, S. Vicent, K. Valencia, A. Calvo, R. Pio, L.E. Raez, C. Rolfo, D. Ajona, I. Gil-Bazo, Trametinib sensitizes KRAS-mutant lung adenocarcinoma tumors to PD-1/PD-L1 axis blockade via Id1 downregulation, Mol Cancer 23(1) (2024) 78.

[51] M.H. Lee, J. Yanagawa, L. Tran, T.C. Walser, B. Bisht, E. Fung, S.J. Park, G. Zeng, K. Krysan, W.D. Wallace, M.K. Paul, L. Girard, B. Gao, J.D. Minna, S.M. Dubinett, J.M. Lee, FRA1 contributes to MEK-ERK pathway-dependent PD-L1 upregulation by KRAS mutation in premalignant human bronchial epithelial cells, Am J Transl Res 12(2) (2020) 409-427.

[52] B. Muz, P. de la Puente, F. Azab, A.K. Azab, The role of hypoxia in cancer progression, angiogenesis, metastasis, and resistance to therapy, Hypoxia (Auckl) 3 (2015) 83-92.

[53] J. Folkman, Tumor angiogenesis: therapeutic implications, N Engl J Med 285(21) (1971) 1182-6.

[54] G.L. Semenza, HIF-1 and tumor progression: pathophysiology and therapeutics, Trends Mol Med 8(4 Suppl) (2002) S62-7.

[55] G.L. Semenza, Hypoxia-inducible factors: mediators of cancer progression and targets for cancer therapy, Trends Pharmacol Sci 33(4) (2012) 207-14.

[56] G.L. Semenza, Hypoxia-inducible factors in physiology and medicine, Cell

148(3) (2012) 399-408.

[57] M. Ivan, K. Kondo, H. Yang, W. Kim, J. Valiando, M. Ohh, A. Salic, J.M. Asara, W.S. Lane, W.G. Kaelin, Jr., HIFalpha targeted for VHL-mediated destruction by proline hydroxylation: implications for O2 sensing, Science 292(5516) (2001) 464-8.

[58] G.L. Wang, B.H. Jiang, E.A. Rue, G.L. Semenza, Hypoxia-inducible factor 1 is a basic-helix-loop-helix-PAS heterodimer regulated by cellular O2 tension, Proc Natl Acad Sci U S A 92(12) (1995) 5510-4.

[59] P. Lee, N.S. Chandel, M.C. Simon, Cellular adaptation to hypoxia through hypoxia inducible factors and beyond, Nat Rev Mol Cell Biol 21(5) (2020) 268-283.

[60] Q. Chu, X. Gu, Q. Zheng, H. Zhu, Regulatory mechanism of HIF-1alpha and its role in liver diseases: a narrative review, Ann Transl Med 10(2) (2022) 109.

[61] M.R. Shurin, V. Umansky, Cross-talk between HIF and PD-1/PD-L1 pathways in carcinogenesis and therapy, J Clin Invest 132(9) (2022).

[62] H. Zhang, H. Lu, L. Xiang, J.W. Bullen, C. Zhang, D. Samanta, D.M. Gilkes, J. He, G.L. Semenza, HIF-1 regulates CD47 expression in breast cancer cells to promote evasion of phagocytosis and maintenance of cancer stem cells, Proc Natl Acad Sci U S A 112(45) (2015) E6215-23.

[63] J.C. Morote-Garcia, P. Rosenberger, J. Kuhlicke, H.K. Eltzschig, HIF-1-dependent repression of adenosine kinase attenuates hypoxia-induced vascular leak, Blood 111(12) (2008) 5571-80.

[64] V.J. Jasinghe, Z. Xie, J. Zhou, J. Khng, L.F. Poon, P. Senthilnathan, K.B. Glaser, D.H. Albert, S.K. Davidsen, C.S. Chen, ABT-869, a multi-targeted tyrosine kinase inhibitor, in combination with rapamycin is effective for subcutaneous hepatocellular carcinoma xenograft, J Hepatol 49(6) (2008) 985-97.

[65] W. Tang, G. Zhao, Small molecules targeting HIF-1alpha pathway for cancer therapy in recent years, Bioorg Med Chem 28(2) (2020) 115235.

[66] A. Sebestyen, L. Kopper, T. Danko, J. Timar, Hypoxia Signaling in Cancer: From Basics to Clinical Practice, Pathol Oncol Res 27 (2021) 1609802.

[67] P. Sharma, S. Hu-Lieskovan, J.A. Wargo, A. Ribas, Primary, Adaptive, and Acquired Resistance to Cancer Immunotherapy, Cell 168(4) (2017) 707-723.

[68] C. Liu, W. Peng, C. Xu, Y. Lou, M. Zhang, J.A. Wargo, J.Q. Chen, H.S. Li, S.S. Watowich, Y. Yang, D. Tompers Frederick, Z.A. Cooper, R.M. Mbofung, M. Whittington, K.T. Flaherty, S.E. Woodman, M.A. Davies, L.G. Radvanyi, W.W. Overwijk, G. Lizee, P. Hwu, BRAF inhibition increases tumor infiltration by T cells and enhances the antitumor activity of adoptive immunotherapy in mice, Clin Cancer Res 19(2) (2013) 393-403.

[69] W. Peng, J.Q. Chen, C. Liu, S. Malu, C. Creasy, M.T. Tetzlaff, C. Xu, J.A. McKenzie, C. Zhang, X. Liang, L.J. Williams, W. Deng, G. Chen, R. Mbofung, A.J. Lazar, C.A. Torres-Cabala, Z.A. Cooper, P.L. Chen, T.N. Tieu, S. Spranger, X. Yu, C. Bernatchez, M.A. Forget, C. Haymaker, R. Amaria, J.L. McQuade, I.C. Glitza, T. Cascone, H.S. Li, L.N. Kwong, T.P. Heffernan, J. Hu, R.L. Bassett, Jr., M.W. Bosenberg, S.E. Woodman, W.W. Overwijk, G. Lizee, J. Roszik, T.F.

Gajewski, J.A. Wargo, J.E. Gershenwald, L. Radvanyi, M.A. Davies, P. Hwu, Loss of PTEN Promotes Resistance to T Cell-Mediated Immunotherapy, Cancer Discov 6(2) (2016) 202-16.

[70] S.M. Ansell, A.M. Lesokhin, I. Borrello, A. Halwani, E.C. Scott, M. Gutierrez, S.J. Schuster, M.M. Millenson, D. Cattry, G.J. Freeman, S.J. Rodig, B. Chapuy, A.H. Ligon, L. Zhu, J.F. Grosso, S.Y. Kim, J.M. Timmerman, M.A. Shipp, P. Armand, PD-1 blockade with nivolumab in relapsed or refractory Hodgkin's lymphoma, N Engl J Med 372(4) (2015) 311-9.

[71] R.E. Green, J. Krause, A.W. Briggs, T. Maricic, U. Stenzel, M. Kircher, N. Patterson, H. Li, W. Zhai, M.H. Fritz, N.F. Hansen, E.Y. Durand, A.S. Malaspinas, J.D. Jensen, T. Marques-Bonet, C. Alkan, K. Prufer, M. Meyer, H.A. Burbano, J.M. Good, R. Schultz, A. Aximu-Petri, A. Butthof, B. Hober, B. Hoffner, M. Siegemund, A. Weihmann, C. Nusbaum, E.S. Lander, C. Russ, N. Novod, J. Affourtit, M. Egholm, C. Verna, P. Rudan, D. Brajkovic, Z. Kucan, I. Gusic, V.B. Doronichev, L.V. Golovanova, C. Lalueza-Fox, M. de la Rasilla, J. Fortea, A. Rosas, R.W. Schmitz, P.L.F. Johnson, E.E. Eichler, D. Falush, E. Birney, J.C. Mullikin, M. Slatkin, R. Nielsen, J. Kelso, M. Lachmann, D. Reich, S. Paabo, A draft sequence of the Neandertal genome, Science 328(5979) (2010) 710-722.

[72] M.S. Rooney, S.A. Shukla, C.J. Wu, G. Getz, N. Hacohen, Molecular and genetic properties of tumors associated with local immune cytolytic activity, Cell 160(1-2) (2015) 48-61.

[73] K.J. Lastwika, W. Wilson, 3rd, Q.K. Li, J. Norris, H. Xu, S.R. Ghazarian, H.

Kitagawa, S. Kawabata, J.M. Taube, S. Yao, L.N. Liu, J.J. Gills, P.A. Dennis, Control of PD-L1 Expression by Oncogenic Activation of the AKT-mTOR Pathway in Non-Small Cell Lung Cancer, Cancer Res 76(2) (2016) 227-38.

[74] E.A. Akbay, S. Koyama, J. Carretero, A. Altabef, J.H. Tchaicha, C.L. Christensen, O.R. Mikse, A.D. Cherniack, E.M. Beauchamp, T.J. Pugh, M.D. Wilkerson, P.E. Fecci, M. Butaney, J.B. Reibel, M. Soucheray, T.J. Cohoon, P.A. Janne, M. Meyerson, D.N. Hayes, G.I. Shapiro, T. Shimamura, L.M. Sholl, S.J. Rodig, G.J. Freeman, P.S. Hammerman, G. Dranoff, K.K. Wong, Activation of the PD-1 pathway contributes to immune escape in EGFR-driven lung tumors, Cancer Discov 3(12) (2013) 1355-63.

[75] M.K. Liszewski, M. Kolev, G. Le Friec, M. Leung, P.G. Bertram, A.F. Fara, M. Subias, M.C. Pickering, C. Drouet, S. Meri, T.P. Arstila, P.T. Pekkarinen, M. Ma, A. Cope, T. Reinheckel, S. Rodriguez de Cordoba, B. Afzali, J.P. Atkinson, C. Kemper, Intracellular complement activation sustains T cell homeostasis and mediates effector differentiation, Immunity 39(6) (2013) 1143-57.

[76] J.M. Zaretsky, A. Garcia-Diaz, D.S. Shin, H. Escuin-Ordinas, W. Hugo, S. Hu-Lieskovan, D.Y. Torrejon, G. Abril-Rodriguez, S. Sandoval, L. Barthly, J. Saco, B. Homet Moreno, R. Mezzadra, B. Chmielowski, K. Ruchalski, I.P. Shintaku, P.J. Sanchez, C. Puig-Saus, G. Cherry, E. Seja, X. Kong, J. Pang, B. Berent-Maoz, B. Comin-Anduix, T.G. Graeber, P.C. Tumeh, T.N. Schumacher, R.S. Lo, A. Ribas, Mutations Associated with Acquired Resistance to PD-1 Blockade in Melanoma, N Engl J Med 375(9) (2016) 819-29.

[77] T. Hato, A.X. Zhu, D.G. Duda, Rationally combining anti-VEGF therapy with checkpoint inhibitors in hepatocellular carcinoma, Immunotherapy 8(3) (2016) 299-313.

[78] J.D. Storey, R. Tibshirani, Statistical significance for genomewide studies, Proc Natl Acad Sci U S A 100(16) (2003) 9440-5.

[79] L.V. Bozhilova, A.V. Whitmore, J. Wray, G. Reinert, C.M. Deane, Measuring rank robustness in scored protein interaction networks, BMC Bioinformatics 20(1) (2019) 446.

[80] Q. Wu, X. Ying, W. Yu, H. Li, W. Wei, X. Lin, X. Zhang, Identification of ferroptosis-related genes in syncytiotrophoblast-derived extracellular vesicles of preeclampsia, Medicine (Baltimore) 101(44) (2022) e31583.

[81] X. Jin, D. Ding, Y. Yan, H. Li, B. Wang, L. Ma, Z. Ye, T. Ma, Q. Wu, D.N. Rodrigues, M. Kohli, R. Jimenez, L. Wang, D.W. Goodrich, J. de Bono, H. Dong, H. Wu, R. Zhu, H. Huang, Phosphorylated RB Promotes Cancer Immunity by Inhibiting NF-kappaB Activation and PD-L1 Expression, Mol Cell 73(1) (2019) 22-35 e6.

[82] C.M. Taniguchi, B. Emanuelli, C.R. Kahn, Critical nodes in signalling pathways: insights into insulin action, Nature Reviews Molecular Cell Biology 7(2) (2006) 85-96.

[83] C.M. Taniguchi, J. Winnay, T. Kondo, R.T. Bronson, A.R. Guimaraes, J.O. Aleman, J. Luo, G. Stephanopoulos, R. Weissleder, L.C. Cantley, C.R. Kahn, The phosphoinositide 3-kinase regulatory subunit p85alpha can exert tumor

suppressor properties through negative regulation of growth factor signaling, Cancer Res 70(13) (2010) 5305-15.

[84] X. Ai, L. Xiang, Z. Huang, S. Zhou, S. Zhang, T. Zhang, T. Jiang, Overexpression of PIK3R1 promotes hepatocellular carcinoma progression, Biol Res 51(1) (2018) 52.

[85] P. Fojtik, D. Beckerova, K. Holomkova, M. Senfluk, V. Rotrekl, Both Hypoxia-Inducible Factor 1 and MAPK Signaling Pathway Attenuate PI3K/AKT via Suppression of Reactive Oxygen Species in Human Pluripotent Stem Cells, Front Cell Dev Biol 8 (2020) 607444.

[86] M. Chen, H. Zhang, G. Zhang, A. Zhong, Q. Ma, J. Kai, Y. Tong, S. Xie, Y. Wang, H. Zheng, L. Guo, R. Lu, Targeting TPX2 suppresses proliferation and promotes apoptosis via repression of the PI3k/AKT/P21 signaling pathway and activation of p53 pathway in breast cancer, Biochem Biophys Res Commun 507(1-4) (2018) 74-82.

[87] D.H. Huang, J. Jian, S. Li, Y. Zhang, L.Z. Liu, TPX2 silencing exerts anti-tumor effects on hepatocellular carcinoma by regulating the PI3K/AKT signaling pathway, Int J Mol Med 44(6) (2019) 2113-2122.

[88] S.I. Ilyas, G.J. Gores, Emerging molecular therapeutic targets for cholangiocarcinoma, J Hepatol 67(3) (2017) 632-644.

[89] L.L. Ju, L. Chen, J.H. Li, Y.F. Wang, R.J. Lu, Z.L. Bian, J.G. Shao, Effect of NDC80 in human hepatocellular carcinoma, World J Gastroenterol 23(20) (2017) 3675-3683.

[90] C. Zhang, Y. Shen, L. Gao, X. Wang, D. Huang, X. Xie, D. Xu, H. He, Targeting POLE2 Creates a Novel Vulnerability in Renal Cell Carcinoma via Modulating Stanniocalcin 1, Front Cell Dev Biol 9 (2021) 622344.

[91] W. Su, S. Li, X. Chen, L. Yin, P. Ma, Y. Ma, B. Su, GABARAPL1 suppresses metastasis by counteracting PI3K/Akt pathway in prostate cancer, Oncotarget 8(3) (2017) 4449-4459.

[92] M. Jacquet, M. Guittaut, A. Fraichard, G. Despouy, The functions of Atg8-family proteins in autophagy and cancer: linked or unrelated?, Autophagy 17(3) (2021) 599-611.

[93] H. Zhuang, S. Wang, B. Chen, Z. Zhang, Z. Ma, Z. Li, C. Liu, Z. Zhou, Y. Gong, S. Huang, B. Hou, Y. Chen, C. Zhang, Prognostic Stratification Based on HIF-1 Signaling for Evaluating Hypoxic Status and Immune Infiltration in Pancreatic Ductal Adenocarcinomas, Front Immunol 12 (2021) 790661.

[94] L. Meng, B. Liu, R. Ji, X. Jiang, X. Yan, Y. Xin, Targeting the BDNF/TrkB pathway for the treatment of tumors, Oncol Lett 17(2) (2019) 2031-2039.

[95] I.B. Barsoum, C.A. Smallwood, D.R. Siemens, C.H. Graham, A mechanism of hypoxia-mediated escape from adaptive immunity in cancer cells, Cancer Res 74(3) (2014) 665-74.

[96] Z. Hu, N. Dong, D. Lu, X. Jiang, J. Xu, Z. Wu, D. Zheng, D.S. Wechsler, A positive feedback loop between ROS and Mxi1-0 promotes hypoxia-induced VEGF expression in human hepatocellular carcinoma cells, Cell Signal 31 (2017) 79-86.

[97] D. Sehedic, L. Roncali, A. Djoudi, N. Buchtova, S. Avril, M. Cherel, F. Boury, F. Lacoeuille, F. Hindre, E. Garcion, Rapamycin-Loaded Lipid Nanocapsules Induce Selective Inhibition of the mTORC1-Signaling Pathway in Glioblastoma Cells, Front Bioeng Biotechnol 8 (2020) 602998.

[98] M.I. Love, W. Huber, S. Anders, Moderated estimation of fold change and dispersion for RNA-seq data with DESeq2, Genome Biol 15(12) (2014) 550.

[99] L.L. Munn, R.K. Jain, Vascular regulation of antitumor immunity, Science 365(6453) (2019) 544-545.

[100] B.M. Walter, C. Nordhoff, G. Varga, G. Goncharenko, S.W. Schneider, S. Ludwig, V. Wixler, Mss4 protein is a regulator of stress response and apoptosis, Cell Death Dis 3(4) (2012) e297.

[101] S.I. Liochev, I. Fridovich, The effects of superoxide dismutase on H2O2 formation, Free Radic Biol Med 42(10) (2007) 1465-9.

[102] S. Seton-Rogers, Tumour metabolism: Functions of fumarate, Nat Rev Cancer 16(10) (2016) 617.

[103] M. Huang, X. Chen, Y. Jiang, L.W.C. Chan, Kolmogorov–Arnold Network Model Integrated with Hypoxia Risk for Predicting PD-L1 Inhibitor Responses in Hepatocellular Carcinoma, Bioengineering 12(3) (2025) 322.

[104] Yan, X., Chen, D., Wang, Y., Guo, Y., Tong, C., Wei, J., Zhang, Y., Wu, Z., Han, W., Identification of NOXA as a pivotal regulator of resistance to CAR T-cell therapy in B-cell malignancies, Sig Transduct Target Ther 7 (2022) 98.